NANYANG TECHNOLOGICAL UNIVERSITY

FUNDAMENTAL RELATIONS FOR RATIONAL CATALYST DESIGN IN OXYGEN ELECTROCATALYSIS

TAO HUABING

SCHOOL OF CHEMICAL AND BIOMEDICAL ENGINEERING

2017

2017

Fundamental Relations for Rational Catalyst Design in Oxygen Electrocatalysis

Tao Huabing

School of Chemical and Biomedical Engineering

A thesis submitted to the Nanyang Technological University
in fulfillment of the requirement for the degree of
Doctor of Philosophy

2017

Acknowledgements

Research is a complicated art. It requires a series philosophy to face endless challenges arise from anywhere. Therefore, long lasting interest in research is the only driving force to keep one alive in academic world. Luckily, my supervisor Prof. Liu Bin always gave me timely encouragement and good suggestions to help me overcome the difficulties in my research. I would like to sincerely thank Prof. Liu for culturing my interest in research. Thanks for the freedom given from Prof. Liu, I could spend a lot of time reading books and fundamental literatures to prepare for my mechanistic research. The habit of reading I developed during this period are great treasure to me for my whole life.

Next, I would like to specially thank Chen Jiazang, who was a post-doctor at the commencement of my PhD and became a professor in China Academy of Science last year. We have many common philosophies in research and solved many problems together. We're now good brothers and will keep close in touch in research.

I also learned a lot from our group members, Dr. Yang Hong Bin, Dr. Xiao Fang-Xing, Dr. Miao Jianwei, and Dr. Wang Hsin-Yi, and Chen Rong, with their kind help I quickly solve many technical problems encountered in my research. Thank them very much.

I'm grateful for the strong support from my family and my girlfriend, without their support I can't spend most of my time on the research work.

Lastly, I would also acknowledge the financial support of NTU research scholarship, with which I can concentrate on my research work. I also thank NTU and our School of Chemical and Biomedical Engineering @NTU for providing the facilities for my research and daily life.

Abstract

The rapid growth of economy brings about serious environmental and resources problems, which force human search for more efficient and environmental benign technologies for energy conversion. Among the various technologies, fuel cells and soar energy are most attractive. The wide application of the clean energy technologies heavily relies on the efficiency electrocatalytic reactions involved. However, the sluggish kinetics of oxygen electrocatalysis, including oxygen evolution reaction (OER) and oxygen reduction reaction (ORR), seriously limits the efficiency of the clean energy technologies.

The kinetics can't satisfy practical requirements even on the best catalysts of oxygen electrocatalysis, making them highly irreversible reactions. What's worse, the best catalysts are mainly consist of precious materials and their long-term stability is far below practical requirements, such as RuO_2 and IrO_2 in OER, Pt and Pd in ORR. On the other hand, earth abundant elements such as Fe, Co, Ni are more stable in oxygen electrocatalysis, but their activity is much lower than the precious catalysts. Therefore, detailed elementary processes in oxygen electrocatalysis and their origin should be identified so that one can rationally design new catalysts to fulfill the critical requirements from activity, stability and cost.

A number of important reactions such as the oxygen evolution reaction (OER) are catalyzed by transition metal oxides (TMOs), whereas surface reactivity of which is rather elusive. Therefore, rationally tailoring adsorption energy of intermediates on TMOs to achieve desirable catalytic performances still remains a great challenge. My first research work is the identification of a general and tunable surface structure, coordinatively unsaturated metal cation (M_{CUS}), as a good surface reactivity descriptor for TMOs in OER. Surface reactivity of a given TMO increases monotonically with the density of M_{CUS}, thus increase in M_{CUS} improves the catalytic activity for weak-binding TMOs but impairs that for strong-binding ones.

Then, I continued to identify the fundamental relations for catalyst design. The most challenging but critical research in the field of catalysis is to identify the rate determining step and associated with elementary thermodynamic origin. However, sophistication of electrified liquid/solid interface and complexity of catalyst's structure and composition make it incredibly difficult to derive the surface thermodynamics. Here for the first time, we developed a new kinetic model to give a quantitative description of the electrochemical kinetics of oxygen electrocatalysis with elementary surface thermodynamics. Based on the distinctive features in the kinetics for different surface thermodynamics, a straightforward methodology is developed to identify surface thermodynamics from simple electrochemical tests. Our results show that the mechanistic information derived from one reaction is a critical complement to the other, whereas individual study of either reaction could only provide incomplete mechanistic information. The predictive power of our method in developing better catalysts was successfully demonstrated on α-MnO_2.

Based on our model, we further answered several questions in oxygen electrocatalysis. For example, what's the origin of the inconsistence between exchange current density with overall catalytic activity? Exchange current density has been used to represent activity in hydrogen electrocatalysis. However, in oxygen electrocatalysis, exchange current density usually does not correlate with catalytic activity. Through comparison with kinetic behaviour of hydrogen electrocatalysis we prove that kinetics of oxygen electrocatalysis and other highly irreversible reactions are predominantly dependent on Tafel slope, instead of exchange current density. Low Tafel slope of good catalysts originates from the collective contribution from RDS and pre-adsorbed intermediates prior to RDS, which also causes orders decrease in exchange current density predicted from Tafel plots.

Table of contents

List of figures

Chapter 1. Introduction

1.1 Background

1.1.1 Background of clean and sustainable energy conversion technologies

Energy is the basis for human activities. In nature, the energy of our planet mainly comes from the solar energy, which can be harvested and stored in chemical bonds through photosynthesis. The energy carrier includes foods and fossil fuels. The processes utilization of the energy stored in the energy carriers usually include respiration and combustion. Human use combustion to get the energy needed for many activities such as industry and transportation. However, only certain kinds of fuels are suitable for industry and transportation. Among many kinds of energy carriers, hydrogen (H_2) is most preferable due to its cleanness and low activation barrier in utilization[1]. H_2 can be produced from water splitting when coupled to solar panels. The only waste of H_2 utilization is water. To get such kinds of fuels, researchers proposed artificial photosynthesis to convert solar energy into chemical energy. Natural energy storage processes-photosynthesis can be mimicked as artificial photosynthesis where the main products are fuels and O_2. Human activity need the energy stored in chemical bonds such as sugar or fuels.

$$2\ H_2O\ +\ 4.92\ eV\ \rightleftarrows\ 2\ H_2\ +\ O_2 \qquad (1\text{-}1)$$

The energy and environment conditions of our planet changes significantly since industrial revolution. The continues and vast consumption of fossil fuels not only result in energy crisis in the near future, but also bring about serious environmental problems such as air pollution and climate change. These increasingly serious challenges from energy and environment force human to search for sustainable solutions to save the planet and human themselves.

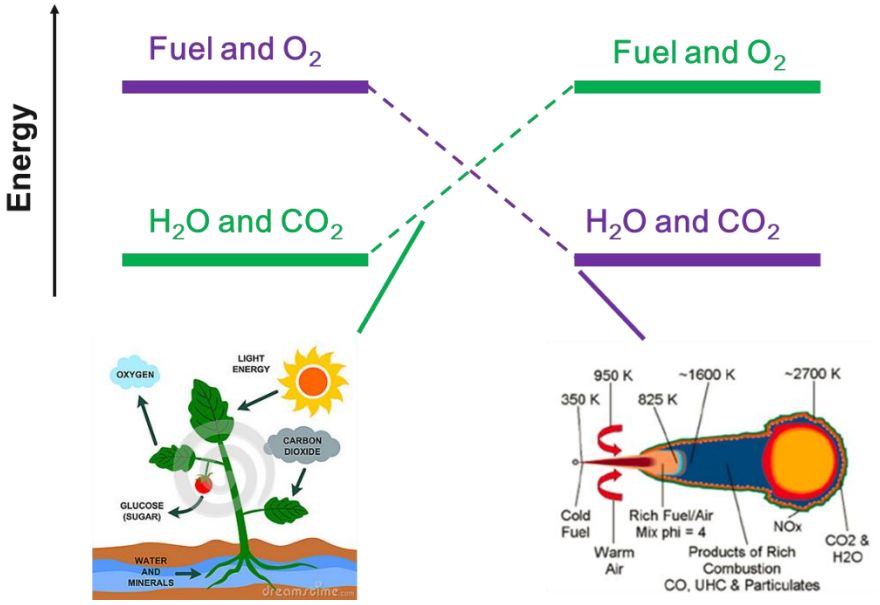

Figure 1-1. Diagram of energy conversion in nature and human activities. Energy storage and emission are reverse processes. Same species are involved in the conversion.

For example, utilization of clean and sustainable energies such as solar and wind energy, the storage of the intermittent energy usually coupled with water electrolysis. Besides, people should also reduce the waste emission from the combustion of fossil fuels. To accomplish this perspective, researchers designed various fuel cells. Irrespective of water electrolysis to store solar energy or convert chemical energy into electricity, oxygen electrocatalysis plays a central role because of large overpotential is responsible for the main efficiency loss.

1.1.2 Basic knowledge and history of catalysis

Catalysis is a fundamental technology that deeply influences the development of human society. For example, ammonia synthesis from its elements (H_2 and N_2) using Haber-Bosch process provides enough sources of fertilizers for food production, which directly supports population increase. Many clean and efficient chemical processes are strongly dependent on the catalytic reactions take place in specially designed reactors. As the increase in economics and human population, more and more clean and efficient catalytic processes are proposed to

replace conventional processes that usually cost too much resources, energy or generates serious pollution.

Efficient catalysis could make the chemical reactions that usually is kinetically slow or unselective happen in a faster reaction rate and through desired pathway. As illustrated in Figure 1-2, the increased reaction rate in catalytic reaction originates from reduced activation energy, which is caused by the interaction between catalyst surface with the intermediates involved in the reaction. The interaction is also referred as activation. Many reactions need extreme conditions because of high activation energy of reactants. For example, the activation of N_2 is rate determining step in ammonia synthesis[2] and activation of O_2 is rate determining step in combustion[3].

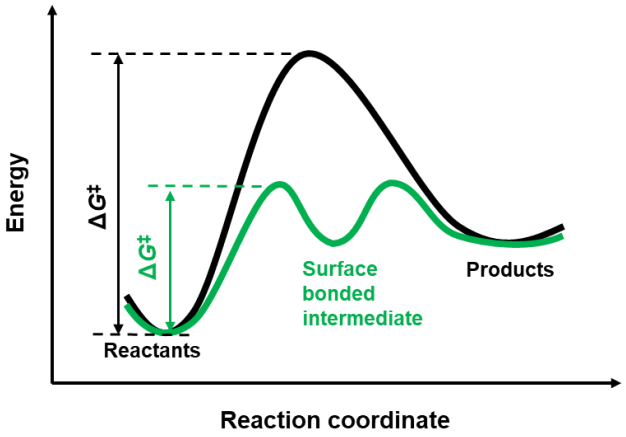

Figure 1-2. Schematic illustration of activation energy difference between catalytic reaction and un-catalytic reaction. The catalytic reaction pathway has lower activation energy, $\Delta G^{\ddagger}$, because of a new surface bonded intermediate created by catalyst surface. Therefore, the mechanism of catalytic reaction is different from that of un-catalytic reaction. Usually, the elementary steps involved in catalytic pathway should be more than that of un-catalytic pathway.

The beginning of intended catalysis by human could date back to as early as the 19th century. Interestingly, the first catalytic reaction involves the activation of H_2 and O_2 by platinum (Pt),

which was developed as a portable lighter source by Dobereiner in 1823[4]. Many catalytic processes had been developed in the period of 1860-1912. The most notable achievements include ammonia synthesis by Haber (Nobel prize 1918), the relation between catalytic activity with adsorbate-surface interaction by Sabatier (Nobel prize 1912), and adsorption principles on surface by Langmuir (Nobel prize 1932). Since 1960s, many surface science techniques are available to probe surface structure and interaction in molecular or atomic level. This makes surface science and chemistry a new subject which attracts lots of researchers. The development of surface science and surface chemistry greatly promotes the understanding of catalysis. Moreover, the development of accurate density functional theory (DFT) calculation since 1990 enable detailed study of surface interaction and exploration of reaction pathways[5]. Nowadays, most insightful research in catalysis combines surface chemistry techniques and DFT to reveal reaction mechanisms. The above pioneering set solid foundation for the rational design or development of better catalysts.

1.2 Oxygen electrocatalysis

The importance of oxygen electrocatalysis originates from its much slower kinetics compared to its counterpart half reactions in energy conversion devices[6]. Specifically, OER is the limiting half reaction in many energy storage devices such as water splitting and rechargeable metal air batteries, while ORR is the determining half reaction in various kinds of fuel cells. The comparison of the kinetics of oxygen electrocatalysis with hydrogen electrocatalysis is visualized in Figure 1-3. Although oxygen electrocatalysis has been extensively studied for over a half century, many problems with reaction mechanisms still remain elusive. The design or development of efficient oxygen electrocatalysts is seriously hindered by the weak understanding of the detailed processes involved in the catalytic reactions. Experimental screening of catalysts has been completed decades ago. Unfortunately, as most cases in catalysis, good catalysts for oxygen electrocatalysis are usually composed of precious

and scarce elements such as Ru, Ir, Pt and Pd. Even the precious catalysts catalyse the oxygen electrocatalysis with a substantial overpotential, which severely reduces the theoretical efficiency that could be achieved. What's worse, the long-term durability of these catalysts is far less satisfy technical demands. Therefore, a further step to develop better catalysts to meet for practical demands is urgently needed. The success of this perspective is heavily dependent on the understanding of elementary steps involved in oxygen electrocatalysis.

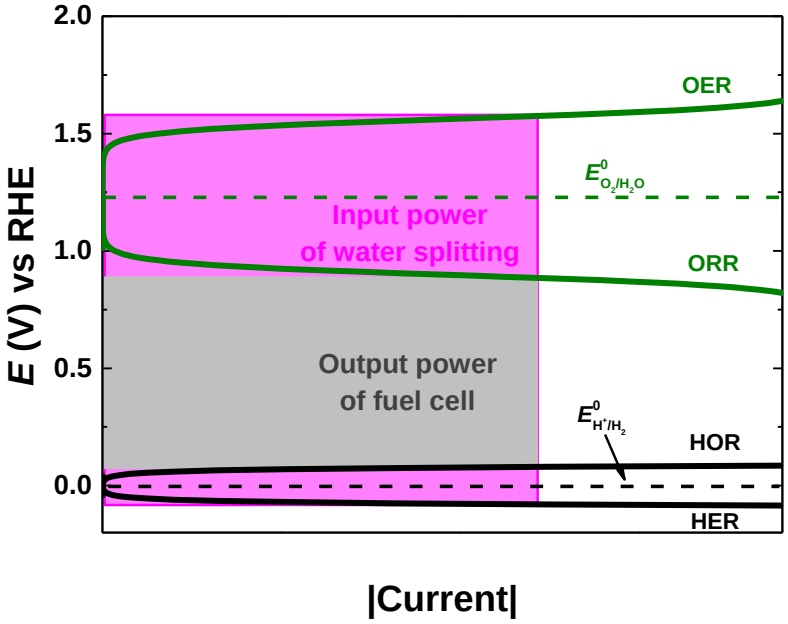

Figure 1-3. Comparison of kinetics of oxygen and hydrogen electrocatalysis. The kinetics of hydrogen electrocatalysis (hydrogen evolution (HER) and oxidation reaction (HOR)) on noble metals such as Pt is very fast that approaches reversible. Therefore, the overpotential of HER and HOR is usually very low (less than 100 mV) on good catalysts. However, for oxygen electrocatalysis, the at least 300 mV overpotential is needed to drive the reaction with a significant rate even on the state of the art catalysts.

However, electrocatalysis is a relatively immature subject whose development greatly benefits from other subjects. For example, without the surface science techniques and single crystals preparation techniques the surface chemistry of electrocatalysis can't be understood.

Since the catalysts are usually buried in liquid electrolytes, the study of electrocatalysis becomes more difficult than heteoregeneous catalysis that takes places at solid-gas interfaces. Many surface science techniques that involve the scattering, absorption or emission of electrons, atoms, and ions can't be used in electrocatalysis occurs at electrified solid-liquid interfaces.

1.2.1 Oxygen evolution reaction (OER)

OER is a critical half reaction that is widely involved in energy storage reactions such as solar water splitting, metal air batteries and CO_2 electrochemical reduction[7]. Solar water splitting is a very promising strategy for large scale production of high purity H_2, an ideal clean energy carrier which could be used in fuel cells for vehicles. Nowadays, 95% of the H_2 produced in the United States is made by natural gas reforming in large central plants[4]. However, natural gas reforming not only bring about large amount of CO_2 emmision, the H_2 production from this technology also suffers from the subsequent difficult gas purification process, which requires eliminating carbon monoxide (CO) to an extremely low level as only trace amount of CO could poison fuel cell anode catalysts. Due to its high irreversibility, OER always behaves as limiting reaction in the overall reactions.

The overall reaction of OER in alkaline solution is:

$$4\ OH^- \rightarrow O_2 + 2\ H_2O + 4\ e^- \qquad (1\text{-}2)$$

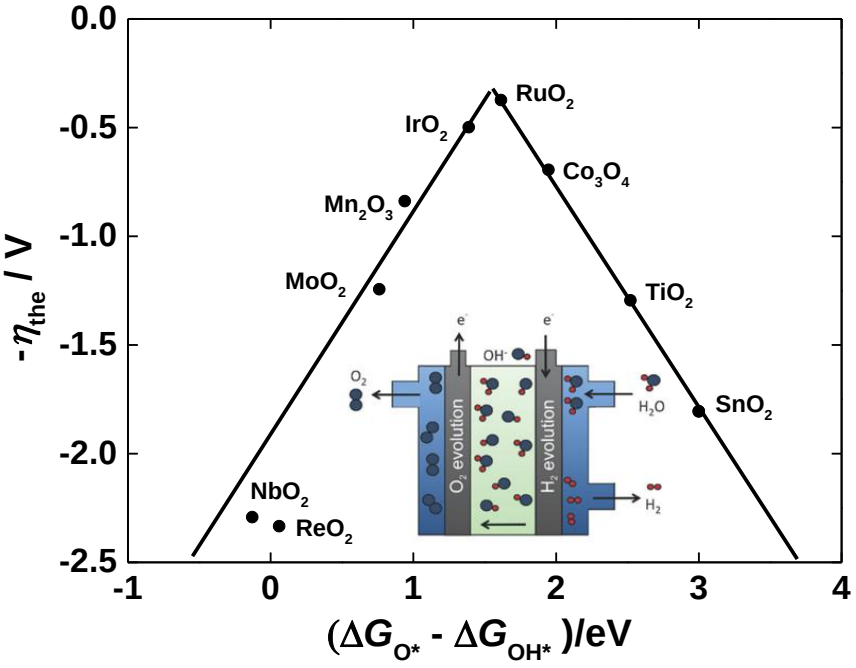

Figure 1-4. Activity volcano plot OER[8,9]. Inset figure Schematic illustrations of anion-exchange membrane electrolyzer used with alkaline electrolytes[10].

1.2.2 Oxygen reduction reaction (ORR)

Fuel cells that involve ORR electrocatalysis as cathodic reaction is one of the most efficient artificial way in the combustion of fuels. Due to its wide availability and environmental compatibility, O_2 has been choose as the ideal oxidant in fuel cells. The chemical energy stored in chemical bonds is directly converted into electricity at relatively low temperature compared to traditional combustion in internal combustion engine (ICE). Therefore, it is usually termed as "cold combustion" to distinguish from the combustion takes place in ICE. The low temperature reaction avoids the many toxic waste production such as NOx, CO and particulates that released from ICE. Moreover, the energy conversion efficiency could be achieved by fuel cells is much higher than that by state-of-the-art ICE as no intermediate step of heat-mechanical work transfer involved in fuel cells. The efficiency of fuel cells thus is not limited by Carnot efficiency. Therefore, ORR is widely used as cathodic half reaction in many energy conversion technologies, ranging from various kinds of fuel cells to metal-air batteries. Moreover, chlor-

alkali industry is also developing oxygen cathodes to replace HER to save energy and avoid the subsequent treatment of H_2 produced in current technologies[11].

The overall reaction of ORR in alkaline solution is:

$$O_2 + 2\,H_2O + 4\,e^- \rightarrow 4\,OH^- \quad (3)$$

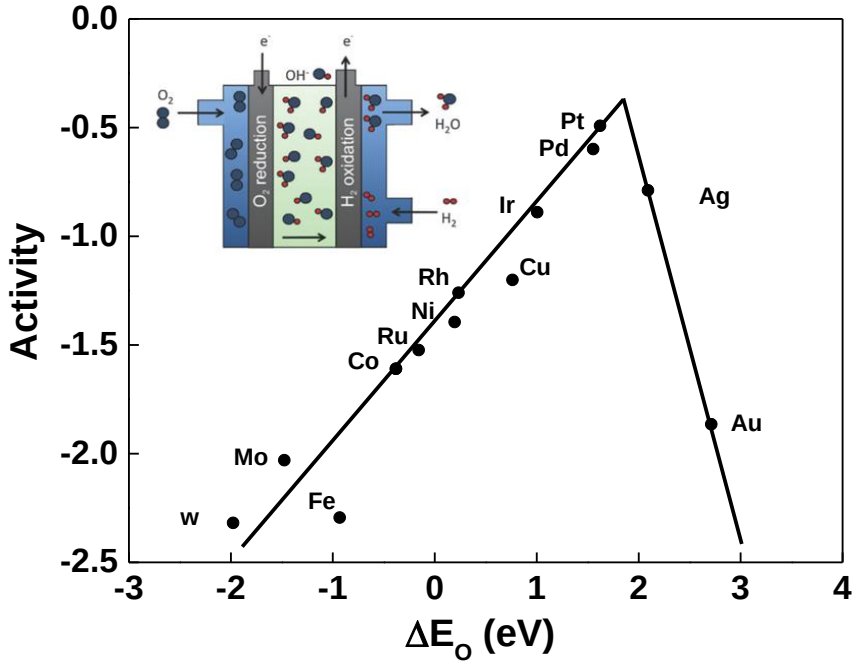

Figure 1-5. Trends in ORR activity of transition metals plotted as a function of the oxygen binding energy[12]. The most active catalyst predicted from the volcano plot is Pt, a precious metal. Inset figure schematically illustrates fuel cell used with alkaline electrolytes[10].

A key elementary step in ORR is the O_2 activation. Since the oxygen atoms are bonded by a double bond with a relatively strong bond energy (498 kJ/mol)[13], O_2 could stably exist in nature although oxygen atom is very reactive oxidant. The double bond in O_2 means that suitable ORR catalysts should be easily activate O_2, which requires surface reactivity high enough.

To have an overview of ORR activity of common materials, we present here the classical activity volcano plot of ORR. The transition metals that fall on the left line of the volcano plot

means their surface reactivity is too high for ORR. The activity is limited by the OH* desorption to generate final product H_2O. As Pt and Pd all belong this category, their catalytic activity could be, in principle, improved by reducing their surface reactivity slightly. This strategy has been proved a significant success, which will be discussed in section 1.3.3.

1.3 Closely related disciplines

The history of electrocatalysis is about 60 years[14]. Impressive progress has been achieved in this field. But the development of electrocatalysis intimately connected to many disciplines. In this section I'll briefly describe the closely related disciplines which influences greatly in my following research work.

1.3.1 Surface chemistry

Surface chemistry deals with the physical and chemical phenomena occurs at the interfaces at two phases and the influence of surface structure, composition and chemical state on various properties. The development of surface chemistry, especially after the emerging of modern surface science techniques from 1960s, greatly promotes the understanding of catalysis[15]. Here, we mostly concern the interfaces of solid-gas and solid-liquid and briefly present the basic concepts and characterization techniques that will be frequently used in the thesis.

Surface structure. One of the most notable characters of surface is that the atoms at surfaces have a different bonding environment. Specifically, the coordination number of the surface atoms is lower than the atoms in the bulk. The unsaturated valence of the surface atoms results in very different chemical reactivity from bulk atoms. Usually, undercoordinated atoms tend to bind adsorbates stronger and the bonding strength increases with the decrease in coordination number. Different crystal faces feature different chemical reactivity and thus different catalytic activity[16,17]. Identifying the relationship between surface structure, both in geometrical and

electronic structure, with chemical reactivity to adsorbates is a critical theme in the field of surface chemistry, heterogeneous catalysis, electrocatalysis, etc.

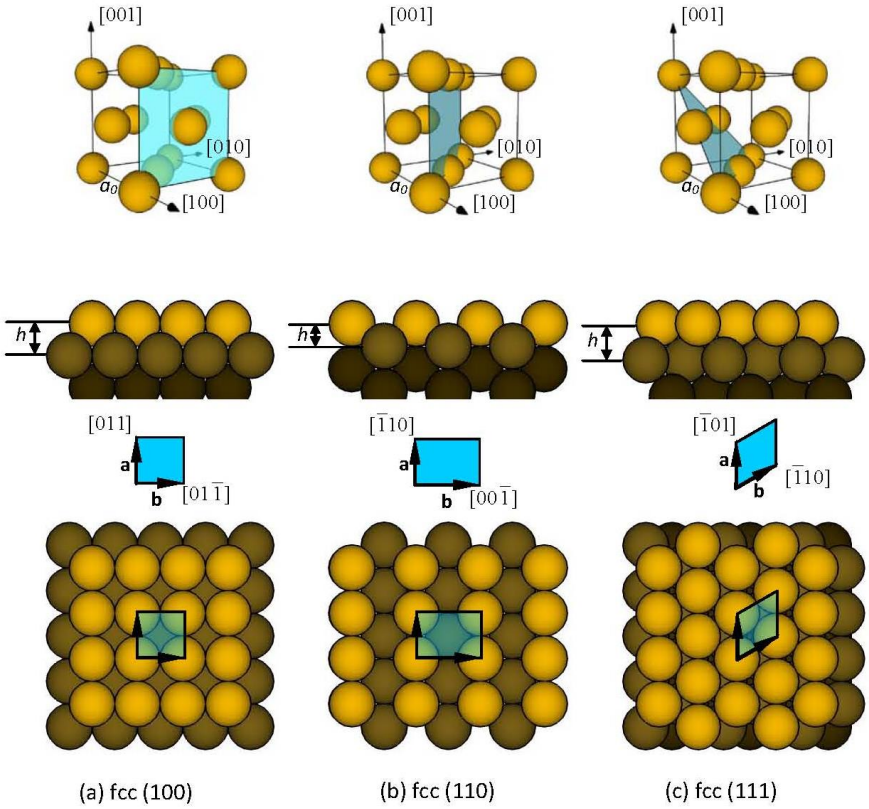

Figure 1-6. Unreconstructed surface of fcc crystal surface. Reproduced from ref[4].

Adsorption. The adsorption of adsorbates on surfaces can be classified into physisorption and chemisorption according to the difference in adsorption energy. Physisorption is mostly contributed by van der Waals interaction. Hence, the adsorption energy of physisorption is relatively low. Whereas, chemisorption involves chemical bond formation between surface with adsorbates and thus the adsorption energy is relatively high. The chemical bond between surface with adsorbates is critical as it determines the bond breaking and formation in catalytic cycle. The adsorption energy of an adsorbate may change as the coverage of the adsorbate changes due to the interaction of adsorbate-adsorbate and adsorbate-surface[18,19]. The adsorption energy for some gases can be evaluated by temperature programmed desorption

(TPD). Conventionally, scientists use heat of adsorption (ΔH_{ads}) to express adsorption energy. The surface coverage of adsorbates is determined by the following equation[4]:

$$\theta = F\tau_0 \exp(\frac{\Delta H_{\mathrm{ads}}}{RT}) \qquad (1\text{-}2)$$

Where F is the gas flux, τ_0 is correlated with the surface vibration times, T is temperature, R is gas constant. According to its definition, the higher ΔH_{ads}, the stronger adsorption and the higher surface coverage of adsorbates. Equation (1-2) is very useful in evaluating the surface reactivity of a catalyst as adsorption energy for many cases can't be directly measured. On the other hand, the coverages of adsorbates could be detected many techniques.

Surface reactivity. Surface reactivity is the most critical property that determines the adsorption energy of adsorbates to surfaces, which finally determines catalytic activity. Sabatier principle can be formulated with regard to surface reactivity: the best catalyst should have optimal surface reactivity for a particular reaction, adsorption of reactants is difficult for a catalyst with relative low surface reactivity, whereas desorption becomes difficult for catalysts with relatively too high surface reactivity.

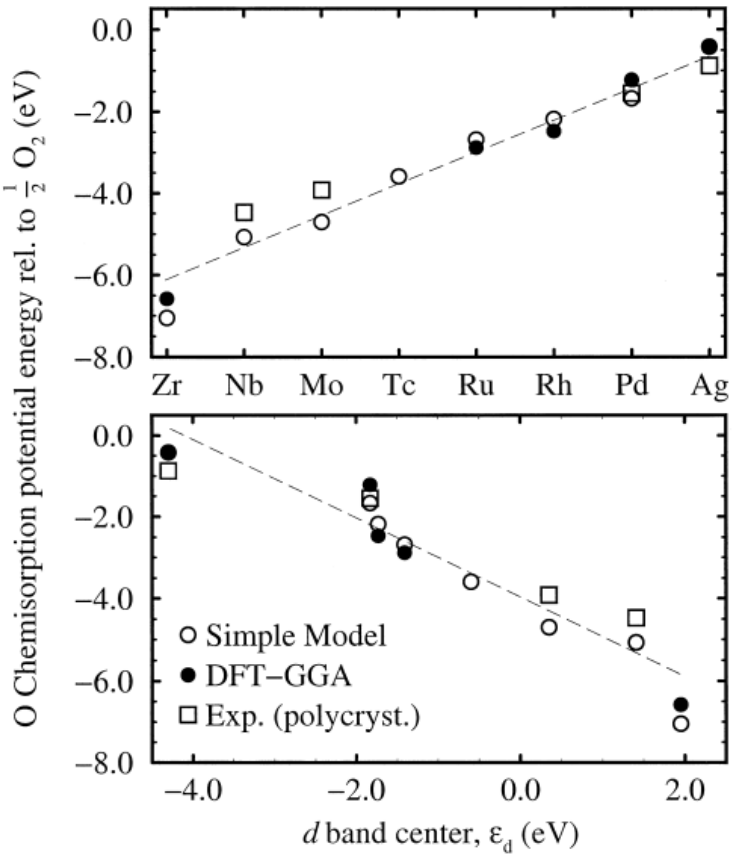

Figure 1-7. Comparison of DFT-based oxygen chemisorption energies with experimental values, and model estimates of the bond strengths for the various close-packed transition and noble metal surfaces. Data represented by open circles were determined by using the Newns–Anderson model. The experimental values are from Toyoshima and Somorjai. (Bottom) The calculated adsorption energies correlate well with the d band center. Reproduced from ref[20].

Although surface reactivity is a very useful concept, it is not easily tuned. So far, the difficulty in controlling and measuring surface reactivity badly limits the rational catalyst design. In many cases, the surface reactivity of catalysts can be indirectly evaluated by the adsorption energy of probing molecules. Because of such importance, many research focuses on the accurate assessment, calculation and the origin of surface reactivity.s

Temperature programmed desorption/reaction (TPD/R). As the adsorption energy or surface reactivity is so important to catalysis, the measurement or evaluation of such property for catalysts becomes one of the fundamental characterization. Due to its simple instrumentation and operation, temperature programmed desorption/reaction becomes one of most widely used fundamental techniques. As the bond strength of adsorbates on surfaces determines the temperature of desorption and coverage of adsorbates, surface reactivity information could be resolved from TPD spectra by analyzing temperature and the amount of adsorbates[4].

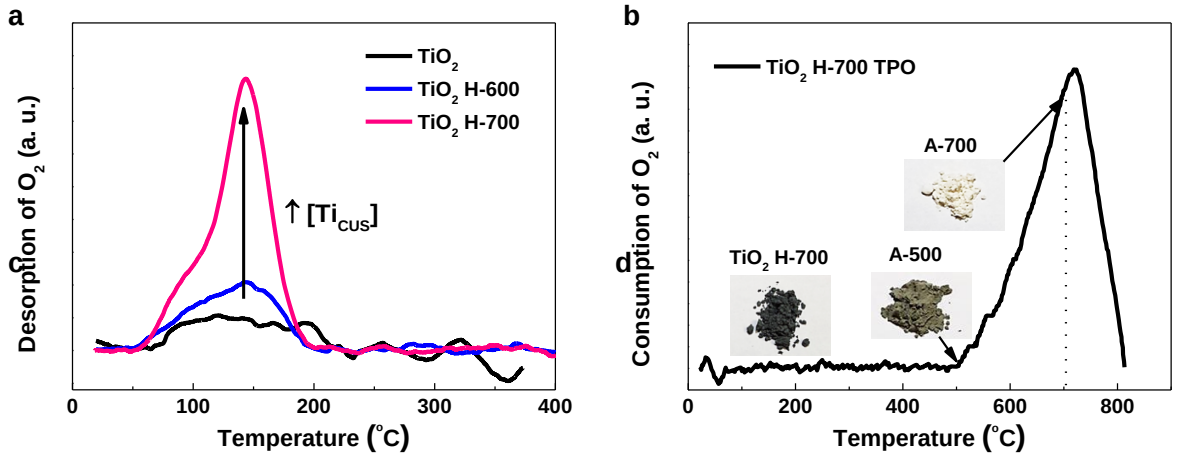

Figure 1-8. Surface reactivity of TiO_2 with varying density of surface Ti_{CUS}. (a) O_2 TPD spectra for TiO_2 with varying density of surface Ti_{CUS}. (b) TPO spectrum of TiO_2 H-700. Insets show the color of original TiO_2 H-700, after calcination at 500 °C and 700 °C in air for 1 h, respectively. The ramping temperature of both TPD and TPO is 20 °C/min. The samples are named with treatment environment and temperature. Specifically, A and H represent the samples annealed in air and 5% H_2/Ar, respectively, and numbers are the treatment temperature. Reproduced from ref[21].

1.3.2 Heterogeneous catalysis

Heterogeneous catalysis is a subject that affects human society deeply as it makes it possible to produce large amounts of desired products in economic way. About 85-90% of all chemical processes are catalyzed by different kinds of catalysts. Among different kinds of catalysts, heterogeneous catalysis amounts to 80-85%[22]. For example, the development of Fe-based catalysts for Haber-Bosh process make it possible to synthesize ammonia in a large scale. Ammonia could be used to produce fertilizers and explosives. Therefore, the catalyst not only directly contributed to the growth of human population by greatly promoting the production of foods, but also "contributed" to wars by providing more powerful weapons. Heterogeneous catalysis itself is already an interdisciplinary field that requires cooperation of experts from different subjects such as solid-state chemistry and physics, materials science, surface science, theoretical chemistry and chemical reaction engineering.

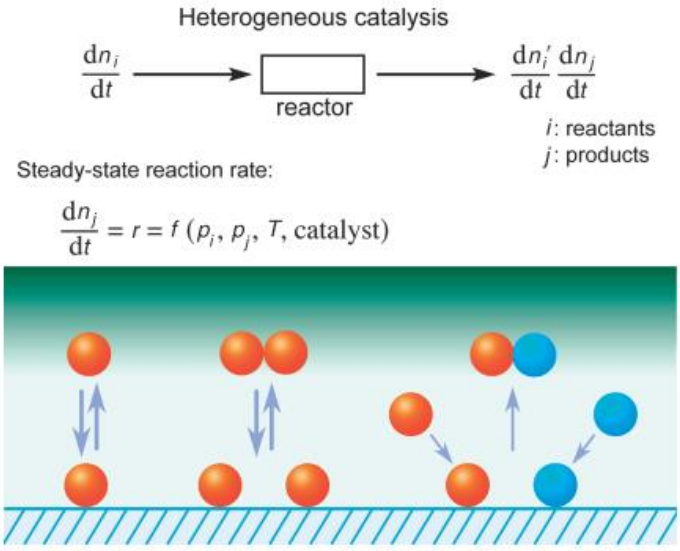

Figure 1-9. The principle of heterogeneous catalysis. Reproduced from ref[23].

The development of electrocatalysis benefits greatly from that of heterogeneous catalysis. Many theories, concepts, methods and technologies formulated in heterogeneous catalysis could be introduced to electrocatalysis and has been proved to be helpful in the development

of this relatively immature discipline. Here we specially discuss some basic concepts in heterogeneous catalysis because it is a relatively mature field that closely related with electrocatalysis.

Sabatier principle. Sabatier principle is one of the most important principle in heterogeneous catalysis. It provides a basic criterion for identifying optimal catalysts, which should bind to intermediates neither too strong, nor too weak. An optimal adsorption energy is required for highest activity. As illustrated in Scheme 1-1, the activity of a catalyst that binds intermediates too weakly is limited by the activation of reactants, whereas activity of a catalyst that binds to intermediates too strongly is limited by the desorption of products. As Sabatier principle gives a conceptual description of catalytic activity based on adsorption property, it is also called activity map or activity descriptor.

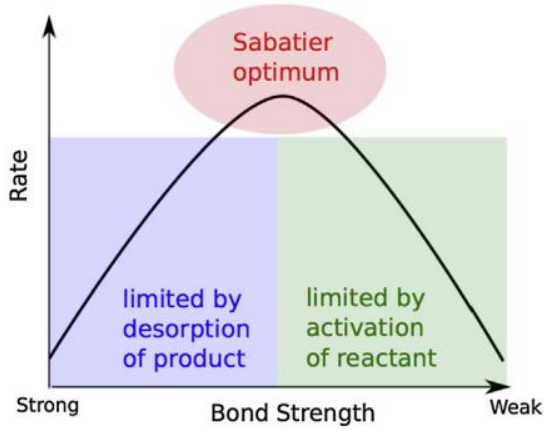

Scheme 1-1. Schematic representation of the qualitative Sabatier principle. Reproduced from ref[24].

The theory qualitatively rationalizes activity trends for most reactions and serves as a basic guidance in catalyst design until today. However, it does not specialize which quantity could be used for describing activity trends in a certain reaction as multiple intermediates may be involved. Moreover, bond strength of many intermediates in most reactions can't be measured experimentally, at least at early years of research. Therefore, even for the most intensively

studied reactions such as ammonia synthesis, quantitative activity volcano plots have only been developed recently, after the work by several generation of scientists.

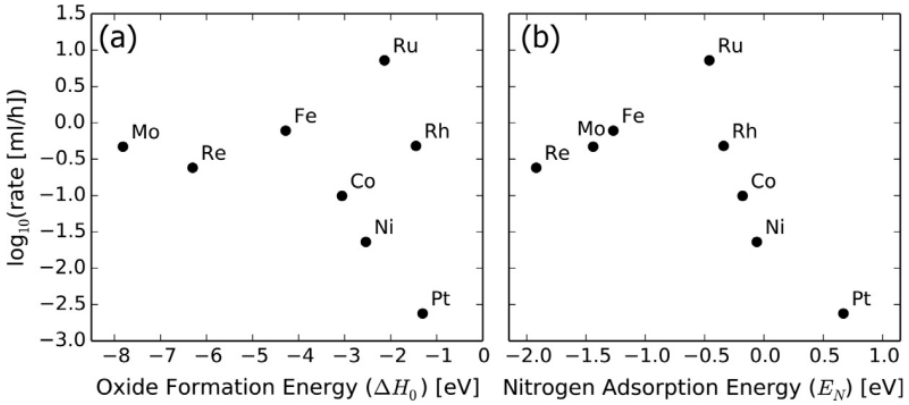

Figure 1-10. Activity volcano plots for ammonia synthesis using different parameters as descriptor. (a) Volcano plot for the ammonia synthesis reaction over K-promoted transition-metal catalysts at 523 K and 0.8 bar using oxide heat of formation as a bond strength descriptor. (b) Volcano plot of the same rates with the nitrogen adsorption energy at stepped metal surfaces as determined by DFT calculations using the RPBE functional as a descriptor. Reproduced from ref[24].

The activity trends could be described by more than one descriptors, which should in principle correlate with the bond strength between catalyst surface with intermediates. For example, as shown in Fig. 1-10, the catalytic activity of metals in ammonia synthesis can be well described by oxide formation energy and nitrogen adsorption energy. As direct information of adsorption energy of intermediates in early studies is not available, scientists at that time usually use bulk properties to correlate activity trends[25]. Such descriptors give rise to a volcano shaped activity trend, which could rationalize Sabatier principle. However, such kinds of descriptors can't provide insights into reaction mechanisms and have been gradually replaced by better and more direct descriptors such as first principle calculated adsorption energy.

Active sites and turnover frequency (TOF)[26]. Active site hypothesis provides a very good method in analyzing complex catalysts as not all sites directly contribute to the catalytic cycle. The concept originates from the biology where biologists use it analyze enzyme catalysis. It provides insights into the reaction mechanism and predicts how to control the overall activity of a catalyst. However, identifying the active sites is not an easy task as it usually requires the combination of different technologies such as *in-situ* methods[27-30]. For example, Fe and Ru based catalysts were identified as best catalysts for ammonia synthesis by Haber and Bosch at the early years of 20th century[31,32], but the active site (edge of Ru nanocrystals) was conclusively identified until 21st century by combining latest surface science techniques, theoretical simulation and kinetic study[2]. TOF is defined as the number of revolution of catalytic cycles per unit time. Compared with normal parameters in assessing catalytic activity, TOF is more a direct parameter that reflects intrinsic activity of a catalyst. Calculation of TOF requires quantification of active sites, which is very difficult. Many reports use different approaches to approximate the number of active sites and make the comparison seems arbitrary. Based on my knowledge, active site and TOF could rationalize many experimental phenomena for the catalysts that composed of distinct sites that have very different chemical property. The catalytic cycle only take place at a certain kind of sites. But for catalysts that carry out the overall reaction by the cooperation of different sites, the hypothesis no longer applies.

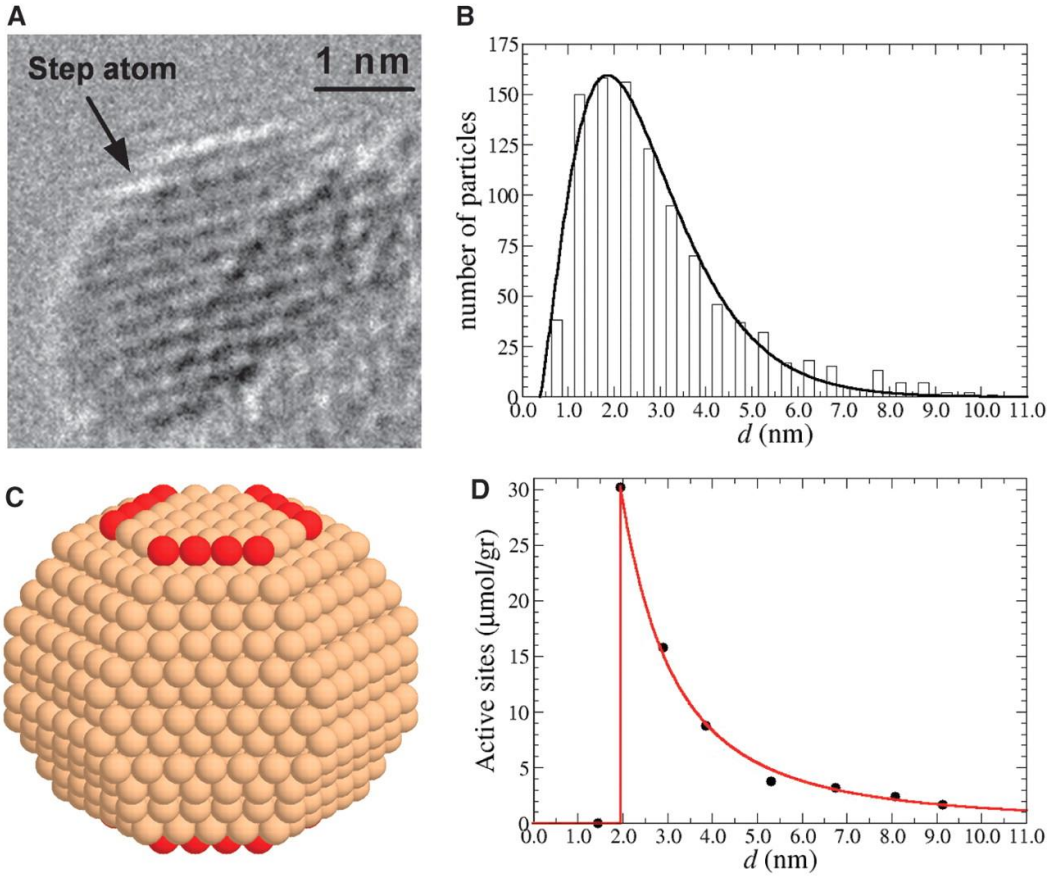

Figure 1-11. Identification and quantification of edge active sites of Ru/MgO catalyst for ammonia synthesis. (A) TEM image of a supported Ru particle with a step. (B) Particle size distribution function obtained from the TEM experiments. d, diameter. (C) A typical calculated Ru particle, with an average diameter of 2.9 nm. Atoms that belong to active B5 sites are shown in red. (D) Density of active sites as a function of particle diameter, as calculated through analysis of the atomistic Wulff construction. Reproduced from ref[2].

Rate determining step (RDS). A catalytic cycle is usually composed of several elementary steps which have distinct kinetic barrier or activation energy. Among the elementary steps, usually only one of them limits the overall reaction rate. The step is called rater determining step (RDS). RDS is a very useful concept in catalysis research as it greatly reduced the difficulty in describing kinetics. Moreover, RDS really provides deep insights into reaction mechanism and thus could be used to predict how to improve catalytic activity or design better

catalysts. Since catalytic processes are generally complicated, the simplification by RDS could help researchers concentrate on the bottleneck step, which is effective in tuning overall catalytic activity. For example, it has been identified that RDS in ammonia synthesis is N_2 activation due to the strong triple bond in the molecule[4]. Therefore, a good catalyst should be able to break the initial bond in N_2 molecule but also not bind to nitrogen atom too strongly according to Sabatier principle.

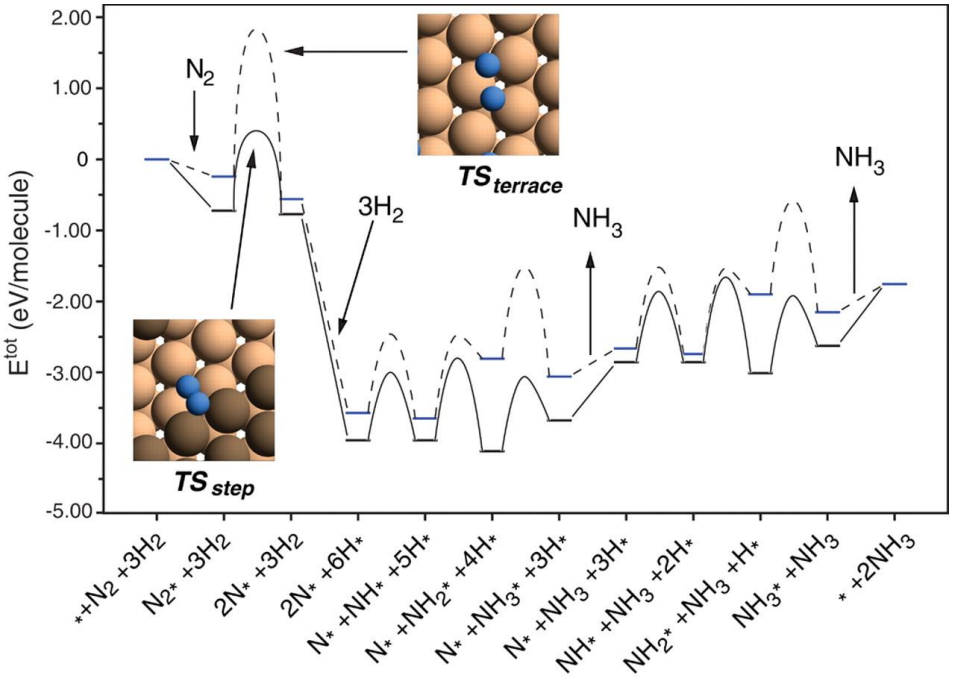

Figure 1-12. The DFT calculated potential energy (E_{tot}) diagram for NH_3 synthesis from N_2 and H_2 over close-packed (001) and stepped Ru surfaces. Reproduced from ref[33].

Therefore, a good catalyst should be able to break the initial bond in N_2 molecule, meanwhile it also not binds to nitrogen atom too strongly according to Sabatier principle. Individually tuning the energy barrier of each step is impossible because of scaling relationship. Working on all the steps to optimize kinetics is difficult.

1.3.3 Electrochemistry and electrocatalysis

Electrochemistry itself is a very disciplinary subject. Typically, the investigated region is the solid-liquid interfaces. One side of the interfaces is electronic conductor called electrode, usually in solid phase, while the other side is ionic conductor called electrolyte, typically in liquid phase. Sometimes solid electrolytes are preferred in application such as solid oxide fuel cells (SOFC). The overall reaction in electrochemistry is divided into two half reactions that take place at anodes and cathodes respectively. But the two half reactions take place simultaneously at the identical rate (in current). Therefore, the charge passed in every part of the circuit should be identical.

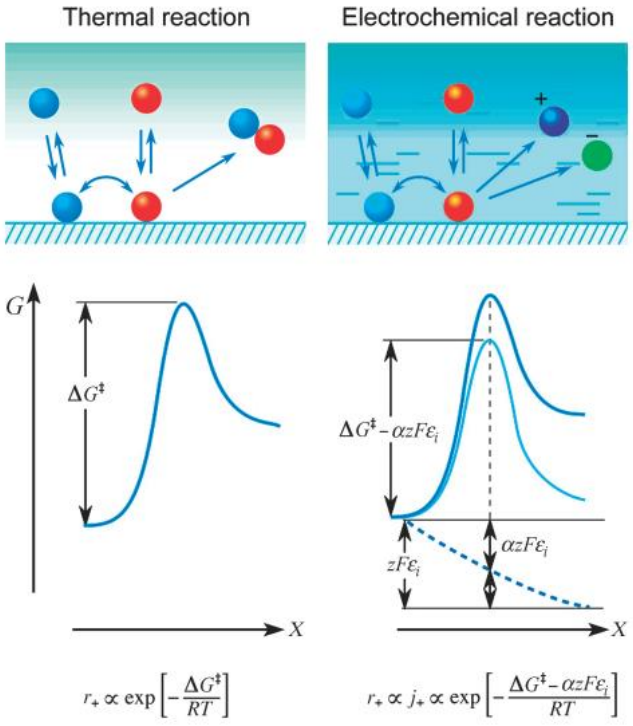

Figure 1-13. Energetics and kinetics of a thermal and an electrochemical reaction. Reproduced from ref[34].

In heterogeneous catalysis, the reactants meet at catalyst surface where old bond breaks and new bond forms. Different from heterogeneous catalysis, the reactants in electrocatalysis do not meet at a same catalyst surface. And hence the products generated from different electrodes

could be easily separated, which is an inherent advantage of electrocatalysis compared to heterogeneous catalysis. In electrocatalysis, membranes are widely used to separate reactants and products. For example, in polymer electrolyte membrane (PEM) water electrolyzer high purity H_2 is directly collected from cathodes. The mix of reactants is very dangerous. Another significant difference between the two category reactions is the driving force. Temperate and concentration in heterogeneous catalysis used in heterogeneous catalysis to control reaction rate, whereas applied potential in electrocatalysis is used to control reaction rate. Moreover, the reaction rate of heterogeneous catalysis could only be measured by detecting the concentration of reactants and products. The reaction rate of electrocatalysis, however, could be easily evaluated by current at any time providing the Faradaic efficiency is constant. The sensitivity in measuring reaction rate in electrocatalysis is higher in electrocatalysis. And also because electrocatalysis controls potential to get current or control current to measure potential, the electrode materials should be electronic conductive. Therefore, isolators such as SiO_2 in electrocatalysis can't be used but widely employed in heterogeneous catalysis.

1.3.4 Theoretical simulation

Thanks to the rapid development of computation technologies and theories, the theoretical simulation could be used to interpret and sometimes predicts experimental trends. Since theoretical simulation could get thermodynamic information straightforwardly, many conceptual theories are formulated to give valuable instruction of research.

The d-band model developed by Hammer and Norskov (20, 21) has proven particularly useful in understanding bond formation and trends in reactivity among the transition metals. The d-band model is an approximate description of the bond formation at a transition-metal surface, as illustrated in Fig. 1-14. It describes the interaction between adsorbate valence states and the s and d states of a transition-metal surface. Coupling to the itinerant s states gives rise to a shift and broadening of the adsorbate states, but this contributes to a first approximation

equal to the bond energy for all transition metals (they all have half-filled, very broad s bands). The differences between transition metals are due to the formation of bonding and antibonding states between the (renormalized) valence states and the metal d states. The strength of the bond is given by the filling of the antibonding states but, unlike gas-phase chemistry, where this is determined by the number of electrons in the system, at a metal surface the filling is given by the energy of the antibonding states relative to the Fermi level. Because the antibonding states are always above the d states, the energy of the d states (the center of the d states) relative to the Fermi level is a good first indicator of the bond strength. The higher the d states are in energy relative to the Fermi level, the higher in energy the antibonding states are and the stronger the bond.

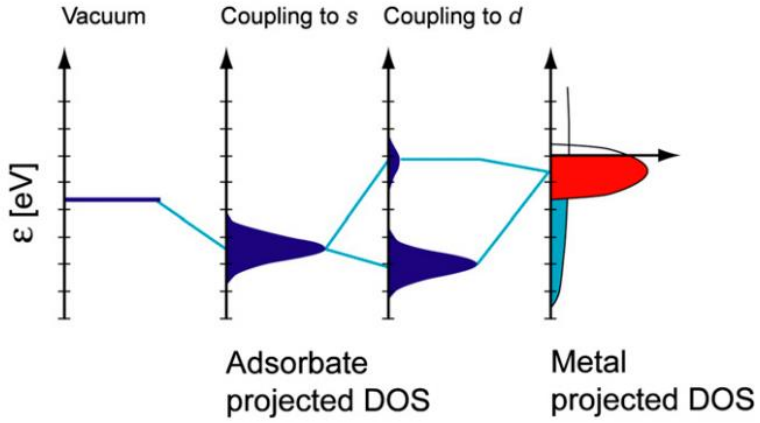

Figure 1-14. Bond formation at a transition-metal surface. Schematic illustration of the formation of a chemical bond between an adsorbate valence level and the s and d states of a transition-metal surface. The bond is characterized by the degree to which the antibonding state between the adsorbate state and the metal d states is occupied. The higher the d states are in energy relative to the Fermi level, the more empty the antibonding states and the stronger the adsorption bond. DOS, density of states. Reproduced from ref[35].

1.4 Rational catalyst design

The rapid development of economics and human society urgently require rational catalyst design principles so as to meet for the demands of human activities. Traditional trail-and-error strategy in developing catalysts is not afforded to face the serious challenges from energy and environment. Rational catalyst design provide an efficient way to develop practical catalysts to satisfy the requirements of industries. However, rational catalyst design is a highly knowledge-intensive activity which could only be performed by very expert scientists. Here, we present some examples in rational catalyst design to highlight the philosophy used in the excellent research. Inspiring strategies can be learned from these classical examples in catalyst design.

1.4.1 Design of a steam reforming catalyst with slow graphite formation

Besenbacher *et al* designed a Au-Ni surface alloy catalyst for steam reforming to reduce the graphite formation by reducing surface reactivity[36]. The authors firstly identified that the main problem in Ni catalyst deactivation is Ni catalysed graphite formation, which blocks the catalytic sites. Graphite formation is caused by the strong bonding between carbon atoms with surface Ni atoms. To reduce the poison, the surface reactivity of Ni should be reduced. The authors proposed introducing Au atoms on Ni surface may possibly reduce surface reactivity and thus improve the resistance to graphite formation. This prediction was well proved on model catalysts both on experimental and DFT calculation as shown in Figure 1-3-1. The methods employed in the work is not so complicated but very convincing as direct evidences are provided for their arguments. Another interesting data is that they examine graphite formation not directly in natural gas steam reforming. Instead, they tested the catalysts' stability in n-butane reforming because n-butane gives rise to the most severe graphite formation problems. The success of this Au-Ni catalyst design benefits from the solid understanding of the key elementary reaction that give rise to main problem. Based on this critical knowledge,

they specially designed strategies to change the thermodynamic origin of the key elementary reaction and finally solved the main problem.

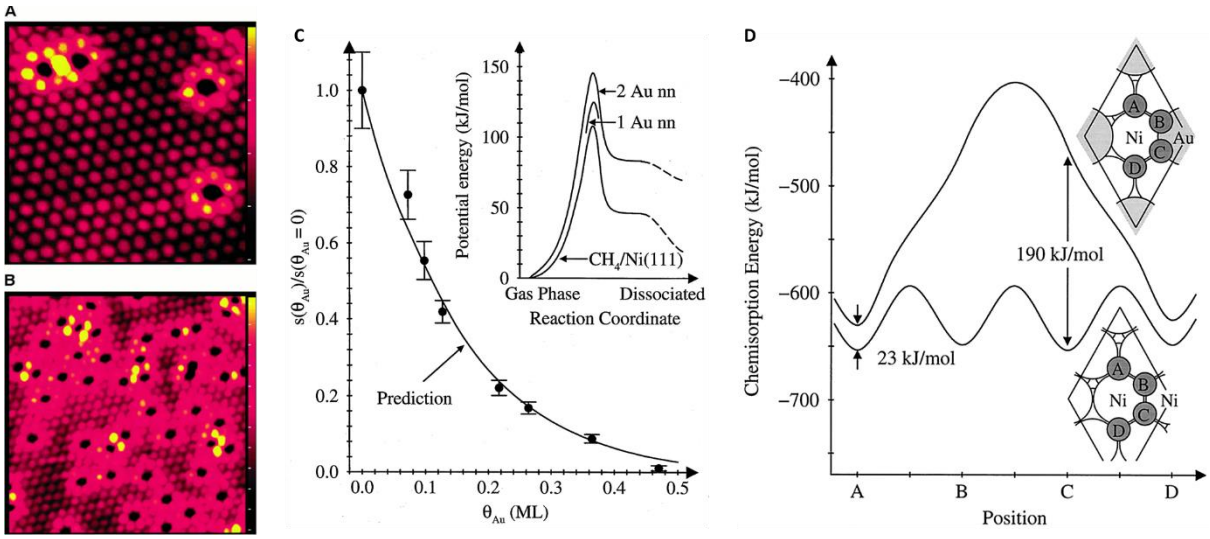

Figure 1-15. Two STM images of a Ni(111) surface with 2% (A) and 7% (B) of a monolayer of Au. The Au atoms appear black in the images. C, The measured dissociation probabilitys(θ_{Au}) for CH_4 on Ni(111) as a function of the Au coverage θ_{Au}. D, The calculated adsorption energy of a C atom on a Ni(111) surface as a function of position along the surface. Reproduced from ref[36].

1.4.2 Design of efficient electrocatalysts for HER/HOR in alkaline media

It is widely known that Pt is a very active catalyst in HER. The activity is so high that the reaction in acid electrolytes almost approach reversibility. Therefore, very few catalysts can be found with a higher activity than Pt. However, the HER activity of Pt in alkaline media is ~2 to 3 orders of magnitude lower than that in acid solution. The low activity seriously impedes the development of alkali-water splitting technologies to produce high purity H_2 for fuel cells and also chlor-alkali electrolyzers. Markovic *et al*[37] suggest that, in alkaline media, the adsorption and recombination of the reactive hydrogen intermediates (H_{ad}) are no longer RDS. Instead, the prior step of water dissociation should be RDS for Pt and Pt-group metals. To reduce the barrier of RDS, the authors deposited $Ni(OH)_2$ clusters on Pt surfaces to promote

water dissociation. The designed $Ni(OH)_2$/Pt shows much better activity than bard Pt surface. Moreover, the activity of $Ni(OH)_2$/Pt approaches that of Pt in acid media, which conclusively supports their fundamental understanding. This catalyst design has been accepted by research community as a new design principle.

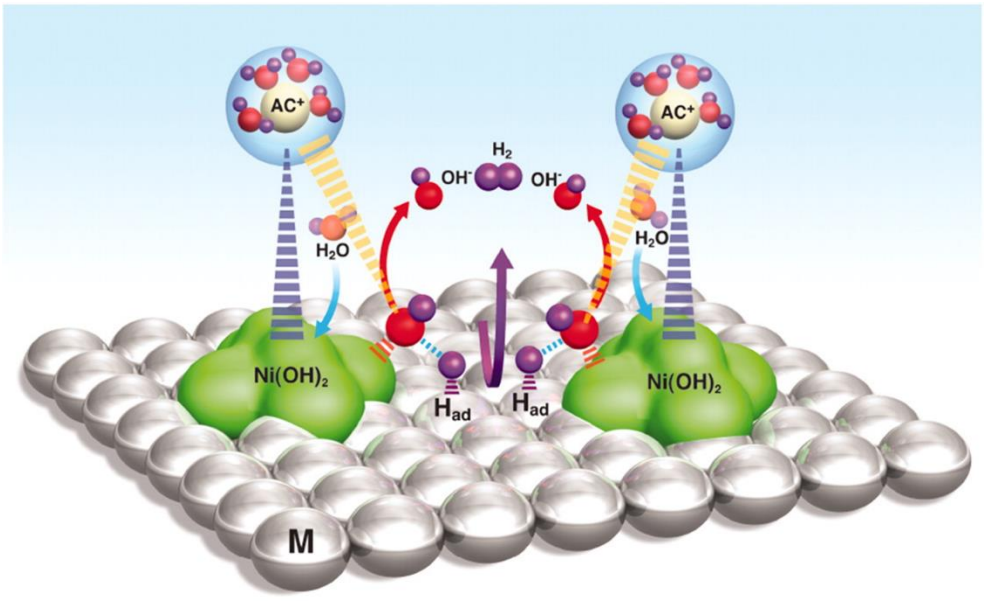

Figure 1-16. Schematic representation of water dissociation, formation of M-H_{ad} intermediates, and subsequent recombination of two H_{ad} atoms to form H_2 (magenta arrow) as well as OH^- desorption from the $Ni(OH)_2$ domains (red arrows) followed by adsorption of another water molecule on the same site (blue arrows). Reproduced from ref [38].

1.4.3 Rational design of Pt alloys for ORR guided by *d*-band theory

Perhaps one biggest success of rational catalyst design in ORR recently is the development of Pt skin alloys guided by *d*-band theory. As discussed in section 1.2.4, *d*-band theory provide an excellent description of surface reactivity of transition metals. It not only rationalizes experimental trends very well, but also successfully predicted the development of better catalysts by changing *d*-band center of transition metals or alloys.

As shown in the activity volcano plot, Pt is the best metal catalysts in ORR. But the surface reactivity of Pt is still too high, which means reducing its surface reactivity could improve its

activity a step further. This prediction is well verified by rationally designing new catalysts with lower d-band center of Pt alloys.

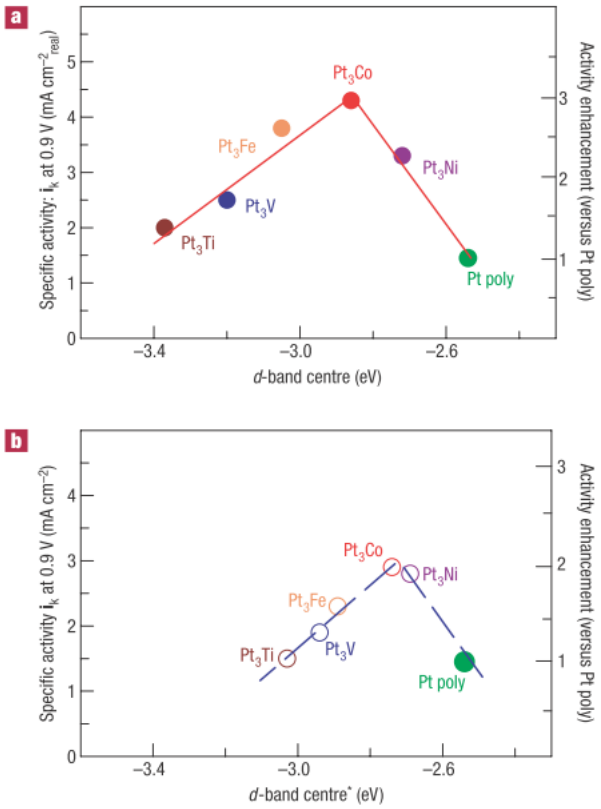

Figure 1-17. a,**b**, Relationships between experimentally measured specific activity for the ORR on Pt_3M surfaces in 0.1 M $HClO_4$ at 333 K versus the *d*-band centre position for the Pt-skin (**a**) and Pt-skeleton (**b**) surfaces. **b** shows the *d*-band centre values* established in UHV, which may deviate in the electrochemical environment due to dissolution of non-Pt atoms. Reproduced from ref[39].

1.5 Research motivation

Choosing an appropriate research topic for PhD period is very important. Since my first project in electrocatalysis, I noticed that the most meaningful but challenging research in electrocatalysis is rational catalyst design, which is the ultimate goal of the fundamental research in catalysis. However, many fundamental relations remain unclear and thus seriously impede the development of catalyst design principles. For example, Sabatier principle indicates the catalytic activity is determined by the adsorption of energy of intermediates. But what determines adsorption energy has not been clearly identified. Since the adsorption energy is

governed by the surface reactivity of catalysts, my first project is to identify the surface reactivity descriptor of transition metal oxides, a major group of catalysts in OER and ORR. After identification of coordinatively coordinated unsaturated metal (M_{CUS}) cations as a good surface reactivity descriptor on transition metal oxides, I continued exploring more fundamental relations between kinetics with thermodynamics of elementary steps involved in oxygen electrocatalysis. Only clearly understanding this relation one can conclusively predict how tune the surface reactivity of a catalyst to improve its catalytic activity. Through developing the model to describe the relation between electrochemical kinetics and thermodynamics of elementary steps, I found some basic questions that remain unanswered. For example, why better catalysts in oxygen electrocatalysis have lower exchange current density? This trend is in contrast with that in hydrogen electrocatalysis. Many problems in catalysis research could only be solved after knowing the fundamental relations, and all these fundamental relations are the key to rational catalyst design.

Chapter 2. Surface reactivity origin of transition metal oxides

A number of important reactions such as the oxygen evolution reaction (OER) are catalyzed by transition metal oxides (TMOs), whereas surface reactivity of which is rather elusive. Therefore, rationally tailoring adsorption energy of intermediates on TMOs to achieve desirable catalytic performances still remains a great challenge. Here we show the identification of a general and tunable surface structure, coordinatively unsaturated metal cation (M_{CUS}), as a good surface reactivity descriptor for TMOs in OER. Surface reactivity of a given TMO increases monotonically with the density of M_{CUS}, thus increase in M_{CUS} improves the catalytic activity for weak-binding TMOs but impairs that for strong-binding ones. The electronic origin of the surface reactivity can be well explained by a new model proposed in this work, wherein the energy of the highest occupied *d*-states relative to the Fermi level determines the intermediates bonding strength by affecting the filling of the antibonding states. Our model for the first time well describes the reactivity trends among TMOs, and would initiate viable design principles for, but not limit to, OER catalysts.

2.1 Introduction

Many electrochemical processes involve OER as the anodic reaction, some desire efficient OER catalysis (e.g., water electrolysis)[40,41], while the others need to suppress this reaction (e.g., Chlor-Alkali process)[42]. Owing to the mismatch in adsorption energy of the multi-intermediates involved in the reaction[43], OER is highly irreversible and thus usually manifests high overpotential (visualized in Figure S1). Because of the high working potential, OER takes place at oxidized surfaces and typical good OER catalysts are transition metal oxides (TMOs) and oxyhydroxides. Unraveling the behavior of OER catalysis on TMOs is of critical

importance for both practical application and fundamental understanding of the interfacial chemistry.

Although intermediates adsorption energy (corresponding to surface reactivity) well describes the activity trend of OER on well-studied TMOs[8,9], the factors that govern the adsorption property or surface reactivity of TMOs still remain elusive. Besides, the critical working condition of OER makes it extremely difficult to directly measure the intermediates adsorption property[10]. Therefore, effectively tailoring the adsorption energy of intermediates to achieve desirable OER activity is highly challenging. This frustrating outcome is in stark contrast with the oxygen reduction reaction (ORR), the reverse reaction to OER, despite the same intermediates (OH*, O*, and OOH*) involve in these two reactions. Unlike OER, ORR can be efficiently catalyzed by transition metals (TMs), whose surface reactivity can be well described by the *d*-band model[20,44], which leads to successful catalyst design[39,45]. On the contrary, no general model exists to well describe the surface reactivity of TMOs[5,46].

The deduction of surface reactivity descriptor for TMOs is primarily prohibited by the extreme divergence in structure and property of these materials[47], in contrast to the relatively continuous variation in electronic structure and property of TMs. Nonetheless, several attempts have been tried to correlate adsorption property with several features in electronic structure of oxides, including e_g filling for perovskites (AMO_3)[48,49] and the states near Fermi level for TiO_2[50] and 4*d* and 5*d* late TMOs[51]. Although the correlations well describe the trends for the investigated materials, no descriptor proves predictability in well-studied group of OER catalysts such as Co_3O_4 and MnO_2. However, if we could avoid the complexity of TMOs and tune the surface electronic structure continuously, it could be possible to identify the surface reactivity descriptor for TMOs.

Here, we demonstrate that surface reactivity of a TMO for OER can be well-described by a general and tunable surface structure, coordinatively unsaturated metal cation (M_{CUS}). Surface

reactivity increases monotonically with the density of M_{CUS} (denoted as [M_{CUS}]), hence weak-binding TMOs benefit from higher [M_{CUS}] while strong-binding TMOs favor lower [M_{CUS}] to achieve good OER catalytic activity. In our study, [M_{CUS}] was carefully tuned by slight oxidation or reduction to prevent bulk structure or phase transition, which results in continuous variation in surface electronic structure. We then propose that the energy of the highest occupied *d*-states of a TMO relative to its Fermi level describes the intermediates-surface bonding strength, which can be established as a universal descriptor for surface reactivity of TMOs.

2.2 Experimental Section

2.2.1 Chemicals

Semiconductor grade potassium hydroxide (KOH) (99.99% trace metal basis, Sigma-Aldrich) was used as supporting electrolyte in all electrochemical tests. The electrolyte solution of 1 M KOH was prepared by dissolving the semiconductor grade KOH with 18.2 MΩ • cm deionized (DI) water. The high purity electrolyte could eliminate the influence of impurity on the intrinsic activity and properties of the catalysts studied in this work by showing no observable change during many cycles of cyclic voltammetry.

2.2.2 Materials preparation

Rutile TiO_2 nanorods with exposed facets were synthesized by a modified hydrothermal method[52]. In a typical synthesis, 1 ml of titanium butoxide (97% Aldrich) was added into a mixed solution containing 30 ml of deionized (DI) water and 30 ml of hydrochloric acid (37 wt%). 20 mg of P25 nanoparticles were added as seeds and dispersed in the growth solution by ultrasonication. The hydrothermal reaction was conducted in a 100 ml autoclave at 170 ℃ for 5 h. After reaction, the product was washed several times with DI water and harvested by centrifugation.

The as-prepared TiO_2 nanorods were oxidized and reduced in air and hydrogen (5% H_2 mixed with Ar) to remove and create coordinatively unsaturated Ti cation sites (Ti_{CUS}) at the surface, respectively, denoted as TiO_2 A-700, H-600, and H-700, where A and H represent the air and hydrogen environment, and numbers are the treatment temperature. Structure and surface reactivity characterization of TiO_2 can be found in Figure S3 & Figure 2.

Single-crystalline Co_3O_4 nanocubes, α-Fe_2O_3 nanorhombohedrons and α-MnO_2 nanorods were synthesized via the methods reported in literature with slight modifications[53-55]. NiO was obtained from Sigma Aldrich (size < 50 nm, 99.8%) showing black color, indicating much excess oxygen at the surface. The density of Ni_{CUS} can be increased by calcination at high temperature to remove excess oxygen at the surface. The surface reduction and oxidation conditions (e.g., temperature) were carefully chosen to only induce the atomic structure changes at the surface. As a representative of relative reducible TMOs, Co_3O_4 was treated in much lower temperature to tune the density of Co_{CUS} (structure and surface reactivity characterization are provided in Figure S4 & S5).

2.2.3 Materials characterization.

The crystal structure of as-prepared TMOs was analyzed by X-ray powder diffraction (Cu Kα radiation, Bruker D2 Phaser). Transmission electron microscopy (TEM) and high-resolution transmission electron microscopy (HRTEM) images were obtained on a JEOL model JEM 3010 TEM equipped with a Gatan camera. X-ray photoelectron spectroscopy (XPS) measurements were conducted on an ESCALAB 250 photoelectron spectrometer (Thermo Fisher Scientific) at 2.4×10^{-10} mbar using a monochromatic Al Kα X-ray beam (1486.60 eV). Binding energy (BE) of the element was calibrated to the BE of carbon (284.60 eV).

2.2.4 TPX measurements.

All measurements were carried out at a heating rate of 20 °C/min and ambient pressure on ChemBET Pulsar (ITS Science & Medical Pte Ltd). Temperature-programmed reduction (TPR) was performed in 5% H_2/Ar (v/v) to determine the suitable temperature to create surface M_{CUS}. Temperature-programmed oxidation (TPO) was carried out in 5% O_2/He (v/v). Prior to O_2-TPD (temperature-programmed

desorption) test, the samples were exposed to high purity O_2 (99.9995%) for half an hour to let the samples reach saturated adsorption of O_2.

2.2.5 Electrochemical studies.

Electrochemical tests were conducted on an Autolab PGSTAT 30 with a three-electrode configuration. Saturated calomel electrode (SCE, 0.241 V vs. SHE (standard hydrogen electrode)) and Pt plate (~1 cm^2) were used as the reference and counter electrode, respectively. To prepare a working electrode, the TMO samples were firstly dispersed in an isopropyl alcohol/water (v: v = 1: 1) solution with a concentration of 2 mg/ml. The mixture was sonicated for 3 h to form a well-dispersed solution. Subsequently, 10 μl of this solution was drop-casted onto a pre-cleaned glassy carbon (GC) rotating disk electrode (0.196 cm^2). Finally, 5 μl of 0.5 wt% Nafion solution was drop-casted onto the TMOs to fix the material. The electrodes were dried in atmosphere overnight before electrochemical tests. The electrochemical testing was conducted at a rotating speed of 1600 rpm in 1 M KOH electrolyte (pH = 13.72) to minimize mass transport limit. To reduce the effects of impurities, plastic cell and high purity KOH (semiconductor grade, 99.99% trace metals basis) were used during the electrochemical testing. In particular, for the electrochemical characterization of NiO, the KOH solution was purified to remove trace amount of Fe impurity, which has been reported to sensitively influence the electrocatalytic performance of NiO[56].[47] All polarization curves in this work were corrected by eliminating *iR* drop in the electrical circuit. Relatively low scan rate (5 mV s^{-1}) was employed to diminish the contribution of non-faradic current to the current of polarization curves. The series resistance (R_s), mainly originating from ionic conduction in the electrolyte, is in the range of 5.5 to 7.0 Ω. The potentials of polarization curves were compensated based on the following equation: $V_{RHE} = V_{SCE} + 0.241 + 0.059 * pH - R_s * i$.

Electrochemical impedance spectroscopy (EIS) measurements were conducted on Solartron 1287A potentiostat coupled with 1260 FRA (Frequency Response Analysis). EIS were collected in the same dc potential range as that of electrochemical tests. 10 mV sinusoidal wave potential perturbations were applied to the dc potential. Polarization curve was collected prior to and after sequential ac impedance tests to evaluate the reliability of the electrodes. EIS data was collected only if there was no observable change for the two curves. Polarization of

working electrodes at each dc potential for one minute was conducted to allow the system to reach steady state.

2.3 DFT simulation and kinetic analysis

2.3.1 Theoretical background

The analysis and interpretation of theoretical and experimental data in this work are based on two general assumptions: first, the activation energy scales with adsorption energy in a Brønsted–Evans–Polanyi relation, which is valid for most of the cases[45]. Therefore, potential determining step (PDS) will be identical to the rate determining step (RDS). With this assumption, we can directly correlate r_{OER} with adsorption energy. Second, since OER is a four-electron transfer reaction that involves multiple intermediates, the scaling relation of adsorption energy among these intermediates is assumed to be applicable in our case studies[2-4]. Thus, we can employ adsorption energy of a key intermediate such as *O as an activity descriptor to get the trend of kinetics determined by adsorption energy.[2]

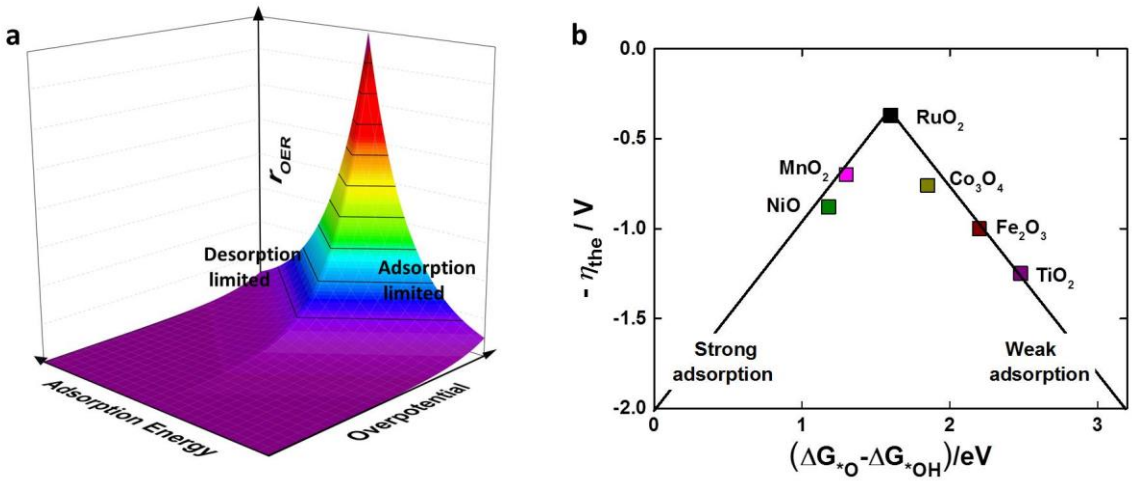

Figure 2-1. Theoretical dependence of OER rate and overpotential (η_{the}) on intermediates adsorption energy. (a) Schematic illustration of kinetics determined by overpotential and intermediates adsorption energy. Only charge transfer limitation in OER was taken into consideration; thus the reaction rate (r_{OER}) is exponentially dependent on applied overpotential

for a catalyst with a given adsorption energy. (b) A general activity volcano plot for TMOs in OER derived from literatures. Results of TMOs from literature: TiO_2, RuO_2 and MnO_2,[3] Co_3O_4,[5] Fe_2O_3,[6] NiO.[7] The oxides fall on the right leg are weakly binding catalysts, whereas those on the left leg are strongly binding ones.

Based on the above assumptions, it can be found that r_{OER} decreases exponentially with the discrepancy in adsorption energy from the optimal value at a given overpotential (Figure S1a). Thus, a volcano relation between overpotential and adsorption energy appears (solid black lines). A general OER activity volcano plot is shown in Figure S1b. RuO_2 adsorbs oxygen intermediates at near optimal binding energy, while non-precious TMOs either bind to the intermediates too weakly (TiO_2, Fe_2O_3, Co_3O_4, and etc.) or too strongly (NiO, MnO_2, and etc.). As a result, the non-precious TMOs show inferior OER activities. Figure S1 clearly shows the role of adsorption energy in defining a good OER catalyst. Our work is thus focused on the identification of surface reactivity descriptor for TMOs, with which we can tailor the adsorption energy and in turn make OER catalytic activity under control.

2.3.2 Computational details

We studied the adsorption of oxygenated intermediates on rutile TiO_2 (110) surfaces by first-principles DFT calculations, which were performed using PWSCF code in the Quantum ESPRESSO package.[8] In the simulation, we applied the generalized gradient approximation (GGA) of the Perdew-Burke-Ernzerhof (PBE) functional and carried out the spin-polarized calculations. Ultra-soft pseudo-potentials were used to deal with the ion cores. Periodically repeating 4-layer slabs with different density of Ti_{CUS} were used to model the rutile TiO_2 materials, with a vacuum layer of 20 Å placed above the surface. The oxygenated adsorbates and the two top Ti layers were allowed to relax, whereas the lower layers were kept frozen at the bulk position. The plane wave cutoff energy was 30 Ry. For the surface model with 3/4 ML, 1 ML, 5/8 ML, and 9/16 ML of Ti_{CUS}, we used the 2×2, 2×2, 2×4, and 4×4 surface unit

cells, and 4×4×1, 4×2×1, 2×2×1 Monkhorst–Pack type of k-point sampling meshes respectively. Various possible adsorption sites for oxygenated adsorbates were considered to determine stable adsorption sites for different adsorbates. The overpotentials for OER were calculated using the theoretical model developed by Norskov *et. a.l*[2] Since the absolute adsorption energy calculated for a given species varies somewhat with different computation software, we shifted the calculated adsorption energies for pristine TiO_2 to that obtained by Norskov *et al,*[2] so that the model activity volcano given by them can be used to analyze the activity-adsorption energy relation. The values required for this shift for various intermediate were then applied for TiO_2 with surface vacancies.

2.3.3 Kinetic analysis

Surface coverage of an adsorbate is determined by adsorption energy according to the following equation:[9,10]

$$\theta = \frac{F}{\sigma} * \tau_0 * \exp(\frac{\Delta H_{\text{ads}}}{RT}) \qquad (2\text{-}1)$$

where F is the flux of adsorbate, σ is the number of adsorbates per surface area for monolayer coverage, τ_0 is the residence time for the adsorbate binding to the catalyst surface, R is the gas constant and T is the temperature. From conventional definition ΔH_{ads} is always positive: larger ΔH_{ads} corresponds to stronger adsorption.

Equation (1) is very useful as it provides a method to directly evaluate adsorption energy of adsorbates on surface. Surface coverage of OER intermediates could be obtained from EIS measurements, from which low frequency dominated specific adsorption of oxygen intermediates (C_{ads}) could be distinguished from double layer charging (C_{dl}). The physical models (the electrical equivalent circuit, EEC) employed in this work to simulate the electrode process is shown Figure S6.[11,12] Harrington and Conway gave the definition of C_{ads} as:[13]

$$C_{\mathrm{ads}}(E) = q\,(^{\mathrm{d}\theta(E)}/_{\mathrm{d}E}) \qquad (2\text{-}2)$$

where q is the charge density for a monolayer coverage, which can be assumed as constant for each TMO in our study as slight surface structure modification exerts little influence on the total number of adsorption sites. By numerical integrating equation (2), we can roughly get the dependence of surface coverage (in arbitrary scale) on applied potential E.

$$\theta(E) = \frac{1}{\sigma}\int_{E0}^{E} C_{ads}(E)\mathrm{d}E \qquad (2\text{-}3)$$

where the starting point $E0$ refers to the potential under which no obvious adsorption occurs, the ending point E is the potential that gives rise to $\theta(E)$. Specifically, the $E0$ for Co_3O_4 and MnO_2 are 1.2 and 1.15 V vs. RHE, respectively. Under these potentials the adsorption of intermediates is not significant. The variation of θ for Co_3O_4 and MnO_2 along with E are shown in Figure S6 e & f, while its integration results can be found in Figure 4 e & f.

2.4 Results and Discussion

2.4.1 Structure modification and characterization

To make the study simple and convincing, all of the TMOs used in this work are structurally well-defined nanostructured single crystals. Moreover, gentle modification of the surface structure only results in relatively continuous variation in surface electronic structure; hence it would be much easier and conclusive to identify the descriptor for surface reactivity. Structural characterization of TiO_2 in Figure 2-2 demonstrates that surface reduction of TiO_2 (110) did not induce any obvious changes in the bulk structure, thus the change in surface reactivity should originate from the variation in surface electronic structure.

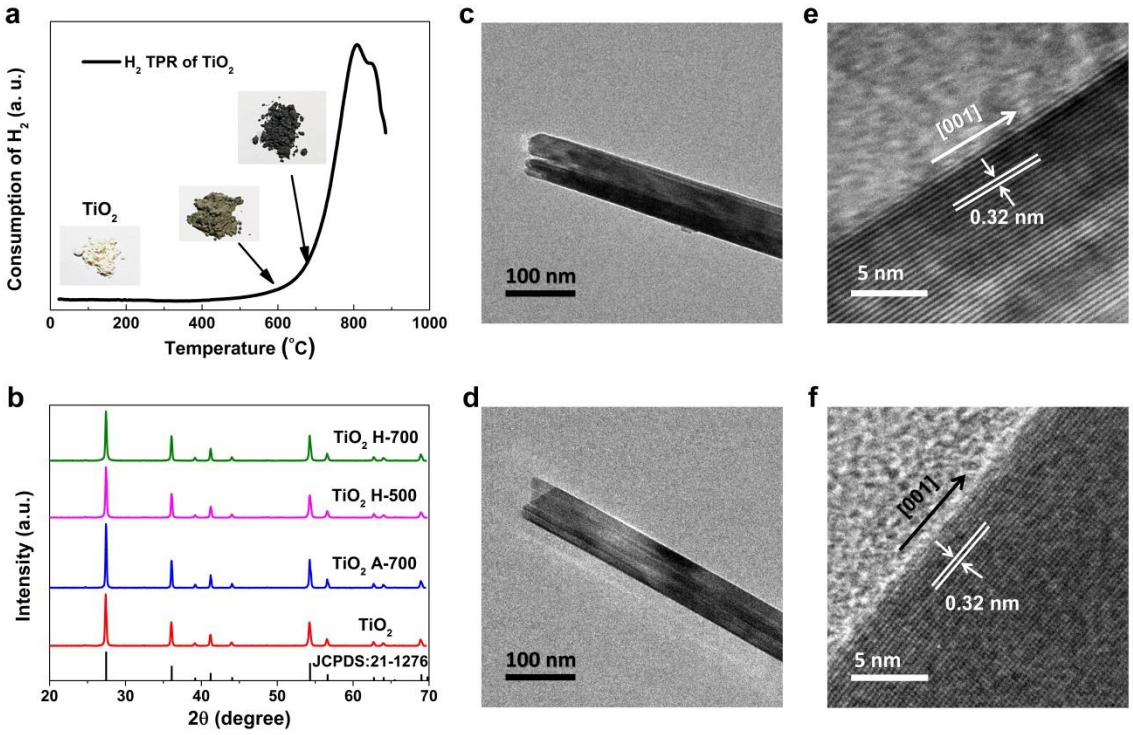

Figure 2-2. Structural characterization of TiO_2 with varying density of surface Ti_{CUS}. (a) Temperature programmed reduction (TPR) spectrum of TiO_2 in H_2/Ar (5%, v/v). (b) XRD patterns of TiO_2 with varying density of surface Ti_{CUS}. (c, e) TEM and HRTEM images of as prepared TiO_2. (d, f) TEM and HRTEM images of TiO_2 H-700 (with higher density of Ti_{CUS}).

Compared with TiO_2, many other TMOs such as Co_3O_4 are more reducible. Therefore, the surface treatment condition for other TMOs used in this work was examined with great care. For example, in terms of Co_3O_4, firstly, temperature programmed reduction (TPR) was performed to determine the reduction temperature for the creation of surface Co_{CUS}. As shown in Figure 2-3 a, reduction of Co_3O_4 to CoO becomes significant above 280 °C. So the reduction temperature we chose is 250 °C, which should not cause any significant changes in the bulk structure. Instead, the reduction mainly took place at the surface, which can be verified by a collection of XRD, TEM and HRTEM measurements (Figure 2-3 and Figure 2-4). Besides, the mild oxidation of Co_3O_4 in air (300 °C) also did not induce any significant bulk structure variations.

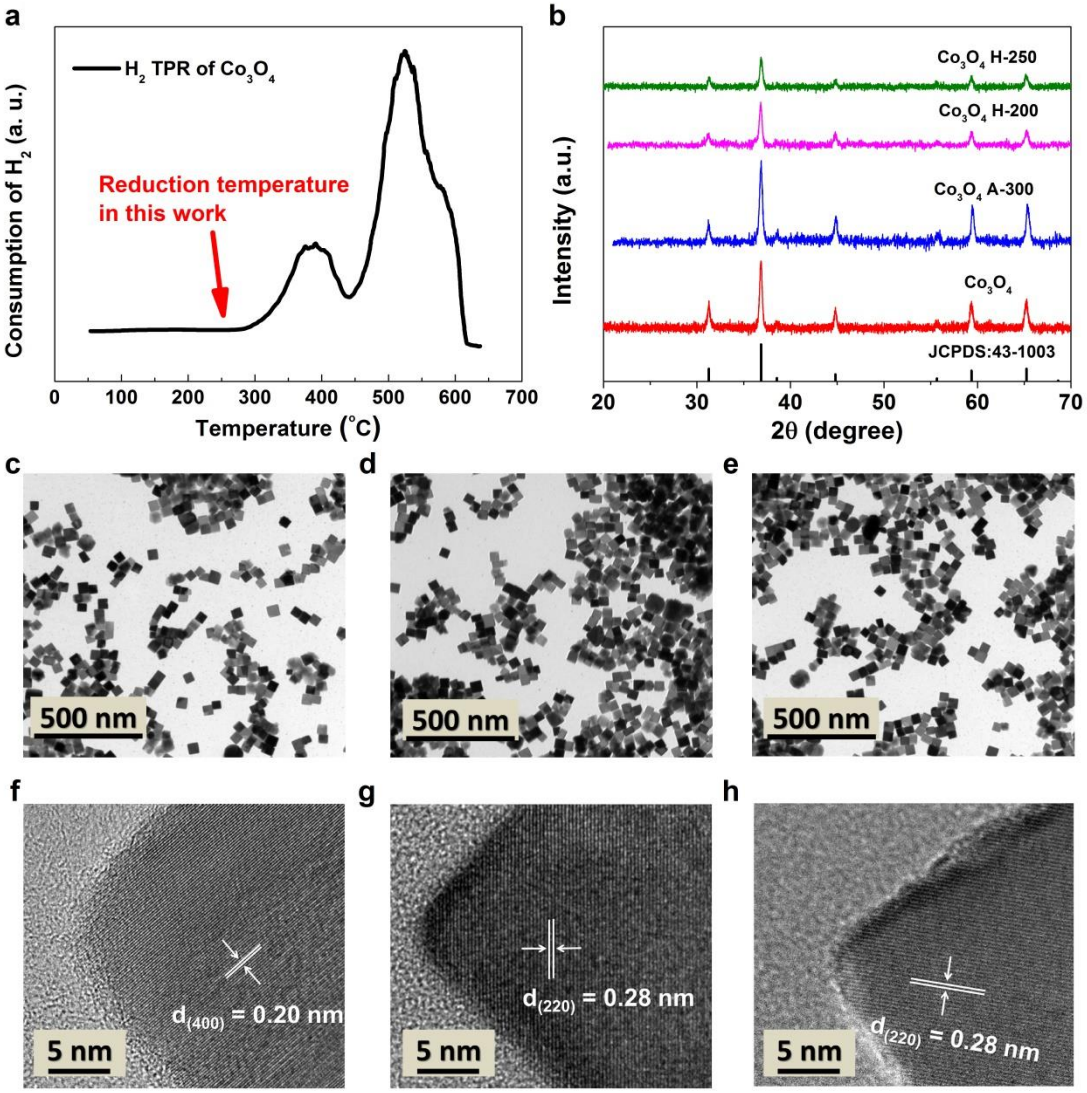

Figure 2-3. Structural characterization of Co_3O_4 with varying density of Co_{cus}. (a) TPR spectrum of Co_3O_4 in H_2/Ar (5%, v/v). (b) XRD patterns for Co_3O_4 with varying density of Co_{cus}. (c, d, e) TEM images of Co_3O_4 A-300, pristine Co_3O_4, and Co_3O_4 H-250, respectively. (f, g, h) HRTEM images of Co_3O_4 A-300, pristine Co_3O_4, and Co_3O_4 H-250, respectively.

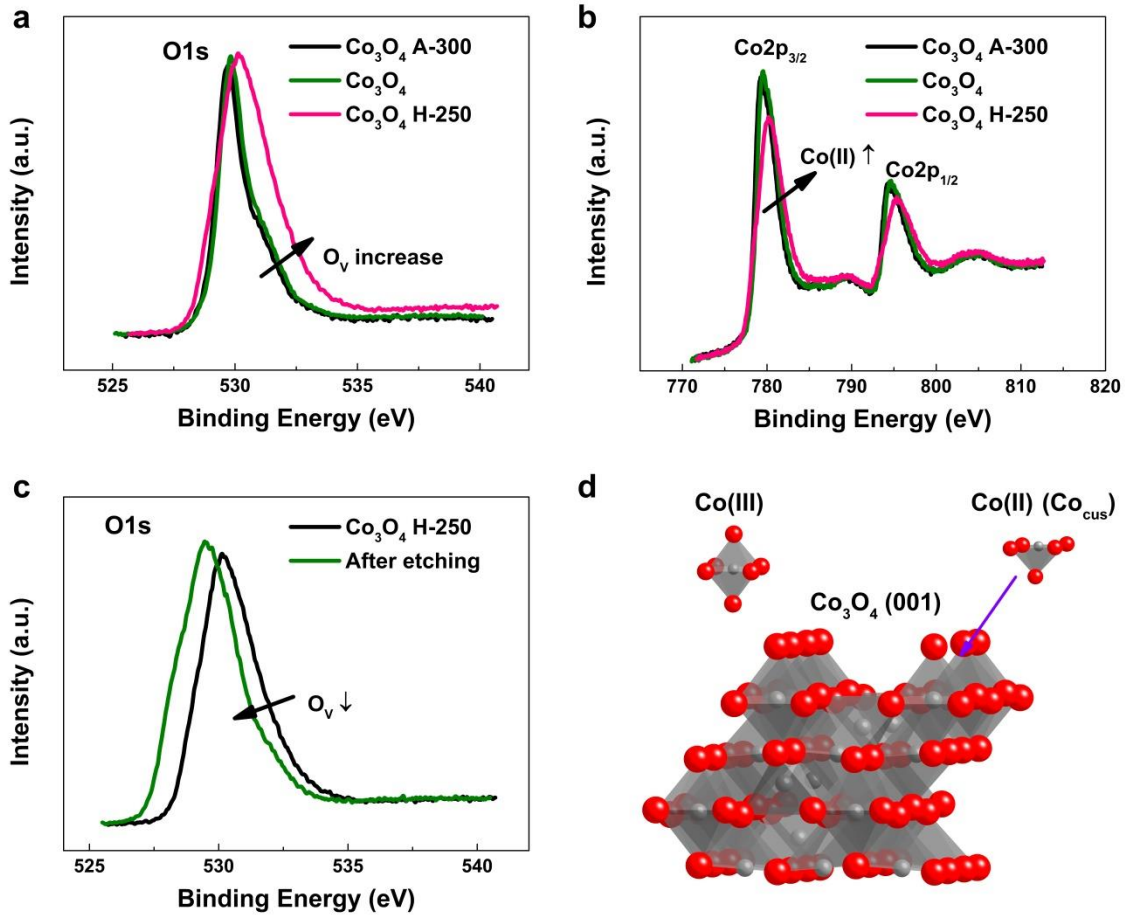

Figure 2-4. Change of surface states in Co_3O_4. (a, b) O 1s and Co 2p XPS spectra for Co_3O_4 after different treatments. The reduction of Co(III) to Co(II) gives rise to peak shift of Co 2p spectrum towards higher binding energy. (c) Comparison of O1s XPS spectra for Co_3O_4 H-250 and the same sample after surface etching (Ar plasma), showing that O_v at the surface of Co_3O_4 can be removed by Ar plasma etching, which indicates that O_v could only be created at the surface of Co_3O_4 at 250 °C in hydrogen. (d) Schematic structure of Co(III) and Co(II) (Co_{cus}) in the octahedral site.

2.4.2 Surface reactivity and catalytic performance of TiO_2 with varying [Ti_{CUS}].

We first performed density functional theory (DFT) calculations to explore the correlation between adsorption energy with [M_{CUS}] on rutile TiO_2 (110), a prototype model TMO for application in energy conversion. Rutile TiO_2 usually behaves as an n-type semiconductor and

its extremely low surface reactivity could be improved by surface oxygen vacancy (O_V, corresponding to higher [Ti_{CUS}] relative to the stoichiometric surface)[57,58]. Herein, we systematically examined the influence of varying [Ti_{CUS}] on the overall surface reactivity and OER activity. Owing to its inert surface, perfect rutile TiO_2 (110) adsorbs oxygen intermediates very weakly and features high OER overpotential, whereas creating more Ti_{CUS} monotonically enhances the intermediates adsorption and thus effectively changes the OER activity (Figure 2-5 & Figure 2-6). This trend is consistent with previous theoretical and experimental studies that oxygen deficient surface showed higher reactivity with adsorbates (e.g., O_2 and H_2O)[59] and the enhanced reactivity is not constraint to O_V sites but delocalized[60,61]. The strong dependence of adsorption energy on [Ti_{CUS}] indicates that Ti_{CUS} can be used as a descriptor for adsorption energy of OER intermediates on TiO_2.

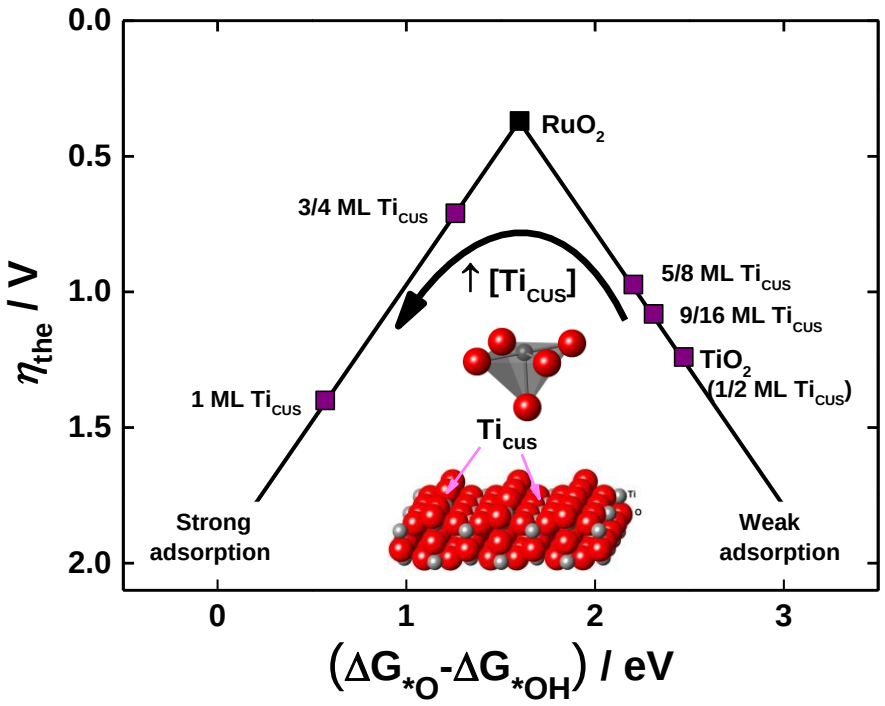

Figure 2-5. Dependence of theoretical overpotential (η_{the}) of rutile TiO_2 (110) in OER catalysis on [Ti_{CUS}]. η_{the} for RuO_2 is shown for comparison. Inset shows the molecular structure of rutile TiO_2 (110) surface, which is characterized by alternate rows of five-fold coordinated Ti (Ti_{5c})

and bridging O atoms (O_b). Underneath O_b rows are the six-fold coordinated Ti (Ti_{6c}) rows. Ti_{6c} is fully coordinated by oxygen in a typical octahedral site, whereas the Ti_{5c} row and the O_V created Ti_{CUS} (denoted as O_v-Ti_{CUS}) in Ti_{6c} row are coordinatively unsaturated and thus denoted as Ti_{CUS}. Different from Ti_{CUS} on stoichiometric surface, O_v-Ti_{CUS} and Ti_{CUS} neighboring to O_v are more reactive due to excess *d*-electrons[60,61]. The density of Ti_{CUS} is defined as the ratio of Ti_{CUS} to the sum of Ti_{5c} and Ti_{6c} rows. According to this definition, perfect TiO_2 surface contains 1/2 ML (monolayer) Ti_{CUS}.

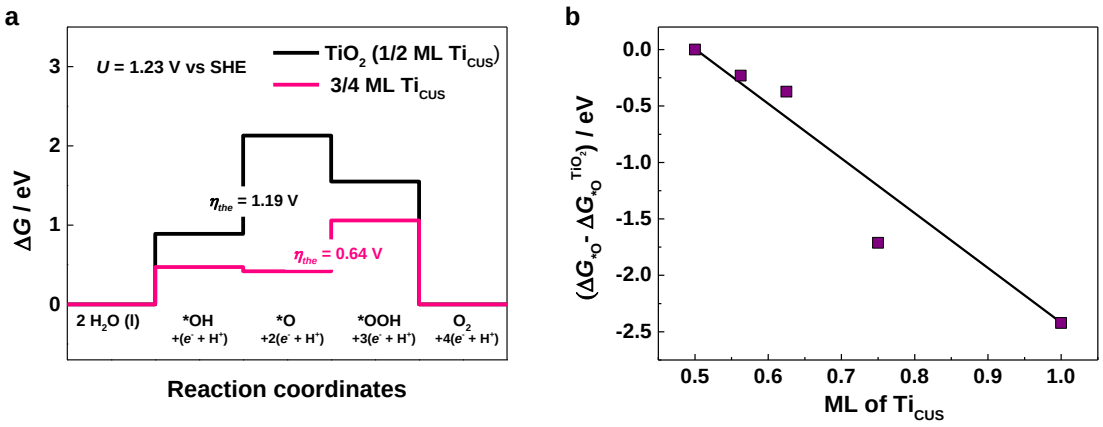

Figure 2-6. DFT calculation results of TiO_2 (110) with varying [Ti_{CUS}] in water oxidation catalysis. (a) Standard free energy diagram of OER at 1.23 V vs. SHE. The theoretical overpotential (η_{the}) was derived from the free energy change of the potential determining step. Striking reduction of η_{the} from 1.19 V for perfect TiO_2 (110) (1/2 ML Ti_{CUS}) to 0.64 V for TiO_2 (110) with 3/4 ML Ti_{CUS} can be clearly observed, highlighting the decisive role of Ti_{CUS} in OER electrocatalysis. (b) Dependence of *O adsorption free energy on the density of Ti_{CUS}. The bonding strength of *O increases linearly with the density of Ti_{CUS}.

To examine our theoretical prediction, we studied single-crystalline rutile TiO_2 nanorods with exposed (110) facets – the same ones used in our simulation. To increase [Ti_{CUS}], the TiO_2 nanorods were slightly reduced to partially remove surface bridging oxygen. As shown in

Figure 2-2, the bulk composition and structure of TiO_2 nanorods are well preserved after creation of additional Ti_{CUS}, whereas, the surface structure and reactivity have been obviously modified (Figure 2-7). By ruling out bulk influence we could safely conclude that any difference in surface reactivity and catalytic performance should originate from Ti_{CUS}.

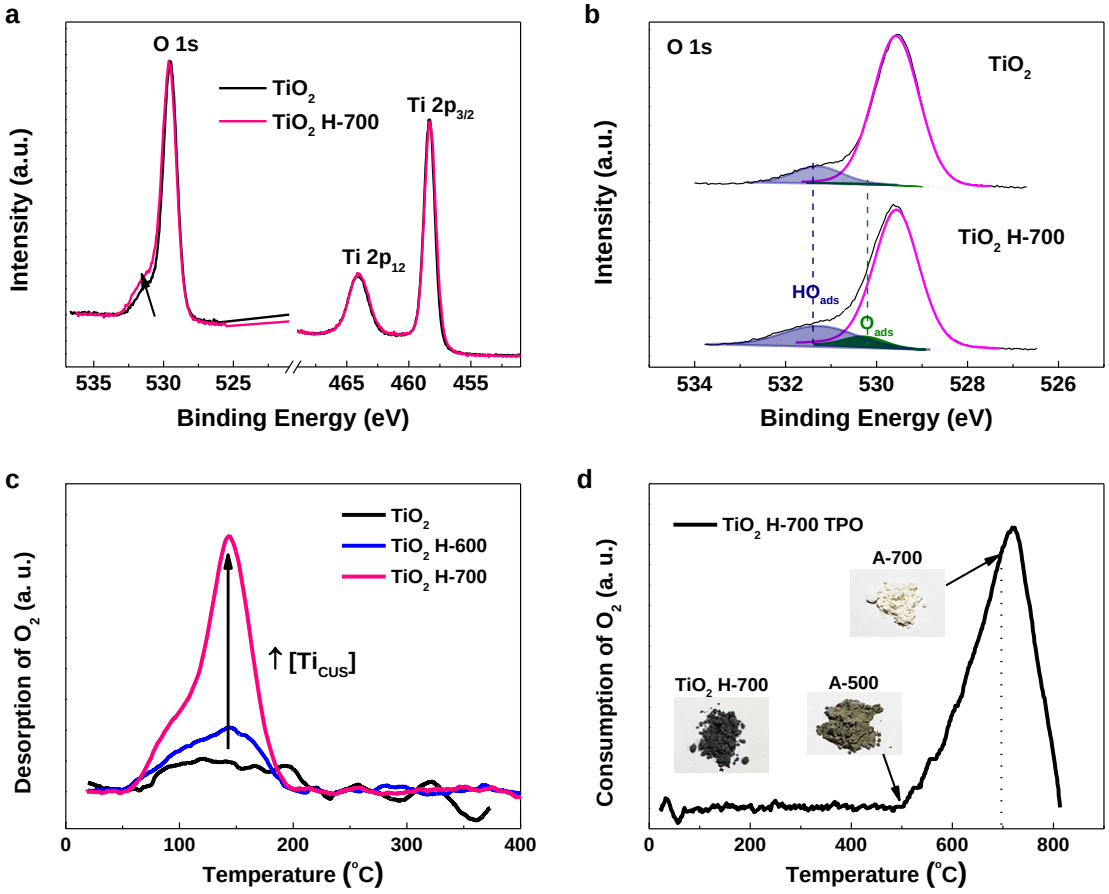

Figure 2-7. Surface reactivity of TiO_2 with varying density of surface Ti_{CUS}. (a) O 1*s* and Ti 2*p* XPS spectra for TiO_2 with different [Ti_{CUS}]. TiO_2 H-700 (with higher [Ti_{CUS}]) shows a more intense shoulder than that of pristine TiO_2, whereas no obvious change is observed in Ti 2*p* spectra. (b) Detailed O 1*s* spectra of pristine TiO_2 and TiO_2 H-700. A new peak, which can be assigned to dissociative adsorbed O_2 (O_{ads}), arises at about 530.2 eV (about 0.9 eV higher than lattice O) for TiO_2 H-700 together with increase in peak intensity of dissociative adsorbed water (OH_{ads}). (c) O_2 TPD spectra for TiO_2 with varying density of surface Ti_{CUS}. (d) TPO spectrum of TiO_2 H-700. Insets show the color of original TiO_2 H-700, after calcination at

500 °C and 700 °C in air for 1 h, respectively. The ramping temperature of both TPD and TPO is 20 °C/min. The samples are named with treatment environment and temperature. Specifically, A and H represent the samples annealed in air and 5% H_2/Ar, respectively, and numbers are the treatment temperature.

Both X-ray photoelectron spectroscopy (XPS) and O_2 temperature programed desorption (TPD) suggest the surface reactivity increases with [Ti_{CUS}] (Figure 2-7 a, b & c), well in line with our DFT calculation results. O 1*s* spectrum (Figure 2-7 a & b) suggests that dissociative O_2 adsorption (O_{ads}) on TiO_2 H-700 is significantly enhanced compared to pristine TiO_2. O_{ads} brings two effects: i) the dissociative adsorption of water (OH_{ads}) is enhanced through the interaction between adsorbed water and O_{ads}[62,63] and ii) electron transfer from Ti_{CUS} to O_{ads} makes the Ti 2*p* spectrum of TiO_2 H-700 invariant from that of TiO_2. That's why we observe enhanced OH_{ads} intensity in the O 1*s* spectrum but overlapped Ti 2*p* spectrum for TiO_2 H-700 as compared to pristine TiO_2. O_2-TPD directly reveals the correlation between surface reactivity and [Ti_{CUS}]. The higher amount of desorbed O_2 from surfaces with higher [Ti_{CUS}] indicates stronger adsorption. Moreover, the slightly reduced TiO_2 surface e.g., TiO_2 H-700 could only be re-oxidized at temperatures as high as 500 °C (Figure 2-7 d). Such a good stability can be attributed to the delocalization of unpaired *d*-electrons (which form band gap states slightly below the Fermi level),[22] which improves the overall surface reactivity and stability of O_V sites[64].

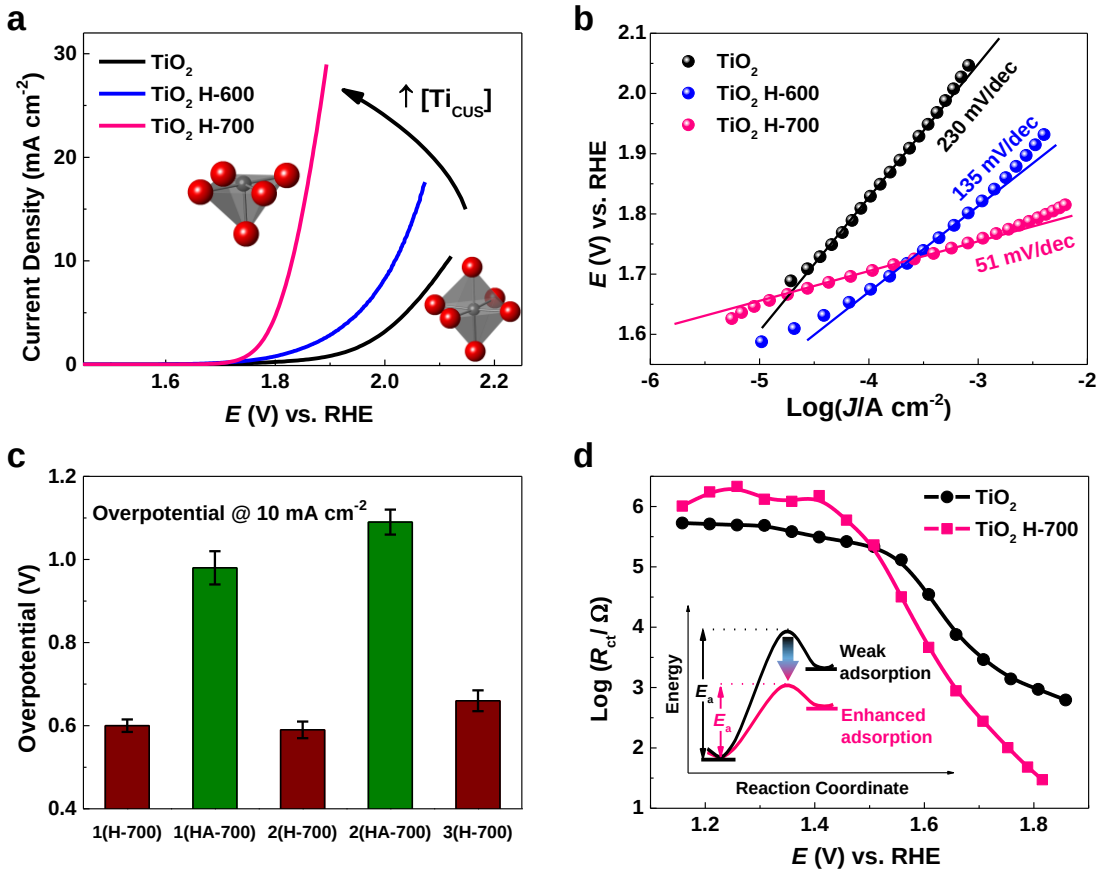

Figure 2-8. Electrocatalytic kinetics of TiO_2 with varying [Ti_{CUS}] in OER. (a, b) Polarization curves and Tafel plots. Inset in (a) illustrates the structure transition that is responsible for activity variation. (c) Overpotential of TiO_2 after alternate reduction and oxidation treatments to tune [Ti_{CUS}]. Here we define the reduction and subsequent oxidation (all at 700 °C) as a cycle, and the sequence of each circle is numbered by 1, 2 and 3, respectively. For example, 2(HA-700) refers to the reduced TiO_2 sample after surface oxidation in the second circle. (d) Response of charge transfer resistance (R_{ct}) to applied potential. At potential > 1.6 V, R_{ct} for TiO_2 H-700 is more than one order of magnitude smaller than that for pristine TiO_2. Inset shows the mechanistic illustration of reduced activation energy (E_a) by enhancing intermediates adsorption. Scan rate: 5 mV s^{-1} and 1 mV s^{-1} for polarization curves and Tafel plots, respectively.

Catalytic OER performances were evaluated using a thin-film rotating-disk electrode (RDE) with well-defined mass transport. It is well-known that TiO_2 is a very poor OER catalyst owing to its weak binding to oxygen intermediates, which is reflected by the large onset potential (~1.9 V vs. RHE) and extremely high Tafel slope 230 mV/dec (Figure 2-8 a & b). However, the OER activity of TiO_2 is sharply improved by increasing [Ti_{CUS}], characterized by the much lower onset potentials and smaller Tafel slopes. In particular, TiO_2 H-700 shows good kinetics with Tafel slope as low as 51 mV/dec, which is almost comparable to that of good OER catalysts such as Co_3O_4. Besides, TiO_2 H-700 also shows stable OER electrocatalysis with nearly 100% Faradaic efficiency (Figure 2-9), suggesting that the Ti_{CUS}-rich surface could work sustainably in OER catalysis. The good stability implies that the surface of TiO_2 H-700 is not easy to be blocked by intermediates, in line with the previous prediction from the surface reactivity characterization. Besides, alternately increasing or decreasing [Ti_{CUS}] on TiO_2 results in opposite changes in OER activity (Figure 2-8 c), emphasizing the decisive role played by Ti_{CUS} in OER catalysis. Electrochemical impedance spectroscopy (EIS) analysis demonstrates that the OER activity is mainly determined by interfacial charge transfer resistance (R_{ct}) (Figure 3d). R_{ct} is controlled by activation energy (E_a), which is very high for pristine TiO_2 due to its weak adsorption of intermediates. Inset in Figure 2-8 d schematically describes the mechanism of reduced E_a and thus R_{ct} by increasing [Ti_{CUS}] through enhancing the adsorption of intermediates[65].[27] Based on these experimental results, we could confidently conclude that Ti_{CUS} could effectively alter the surface reactivity of TiO_2 and thus change its catalytic activity in OER.

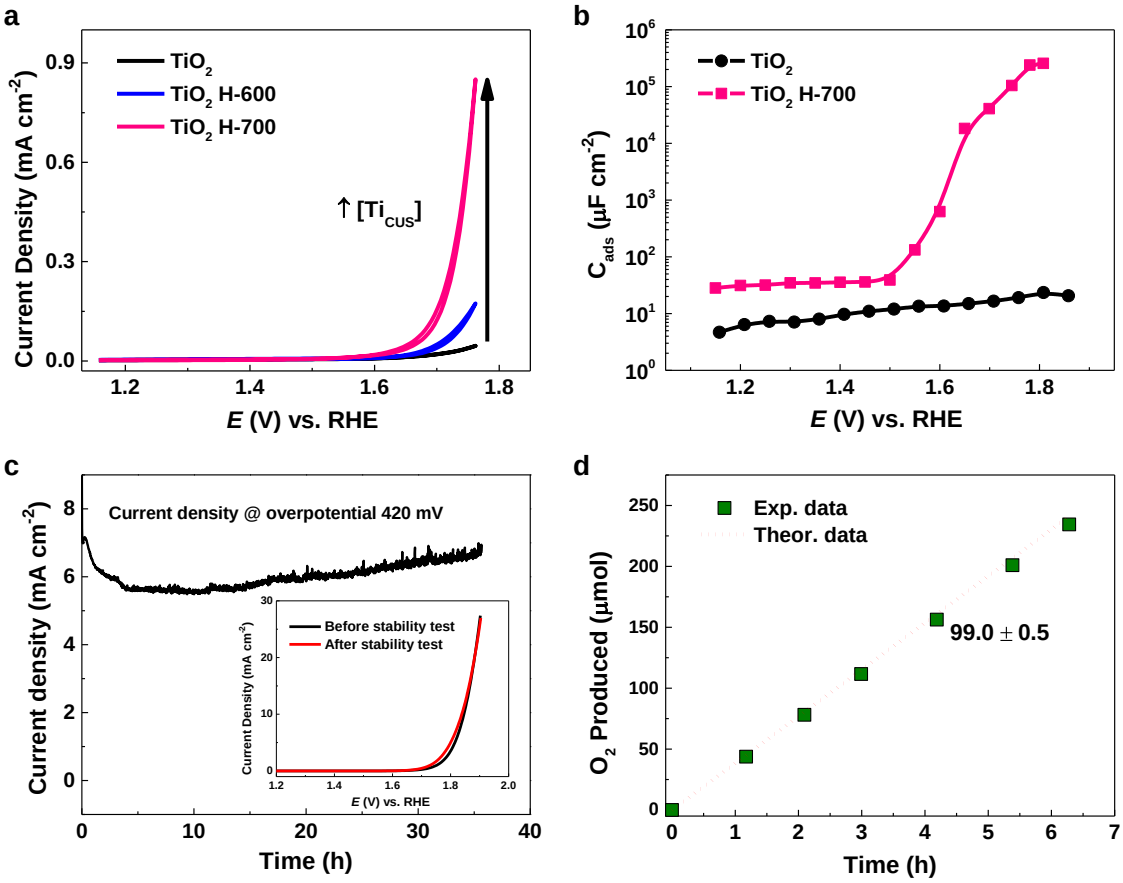

Figure 2-9. Detailed electrochemical characterization of TiO_2 H-700 in OER electrocatalysis. (a) Cyclic voltammetry (CV) of TiO_2 with different densities of surface Ti_{CUS}. The CV curves are obtained from the second cycle of CV scan in the electrochemical tests. (b) The response of C_{ads} to E for TiO_2 and TiO_2 H-700. The sharp increase in C_{ads} for TiO_2 H-700 demonstrates its good reactivity in oxygen intermediates adsorption, whereas inert surface of TiO_2 results in sluggish response to E. (c) Electrocatalytic stability test of TiO_2 H-700, inset shows the linear sweep voltammetry of TiO_2 H-700 before and after the longtime stability test. (d) Faradaic efficiency test. The excellent stability and near 100% Faradaic efficiency of TiO_2 H-700 imply that Ti_{CUS}-rich TiO_2 can act as potent electrocatalyst for the OER.

2.4.3 Effects of [M_{CUS}] on the catalytic performance of the TMOs with different surface reactivity.

The strong correlation between [M_{CUS}] and surface reactivity stimulates us to examine the generality of M_{CUS} as a surface reactivity descriptor for more TMOs. We studied Co_3O_4 and α-MnO_2 as they are typical TMOs whose activities are limited by weak and strong adsorption of oxygen intermediates, respectively (Figure 2-1 b)[25]. Theoretically, we expect to observe opposite influence of M_{CUS} on OER activities for the TMOs that bind oxygen intermediates too strongly or too weakly. We found that increase in [Co_{CUS}] could significantly improve the OER activity (Figure 2-10 a & c). The Co_{CUS}-rich surface shows the best OER activity and good stability (Figure 2-11) ever reported for pure crystalline Co_3O_4,[66,67] whereas, the Co_3O_4 oxidized in air displays poor OER activity due to reduction of [Co_{CUS}] at the surface. On the contrary, for α-MnO_2, increase of [Mn_{CUS}] diminishes the OER activity, while decrease in [Mn_{CUS}] results in significantly better activity (Figure 2-10 b & d). This trend of activity with [M_{CUS}] for α-MnO_2 is totally opposite to that of Co_3O_4, but well demonstrates the M_{CUS} as a surface reactivity descriptor. Similar to TiO_2, Co_3O_4 binds to intermediates too weakly so that enhancing surface reactivity can improve its OER activity. However, the activity of α-MnO_2 can only be improved by reducing [Mn_{CUS}] at the catalyst surface to weaken the strong adsorption of intermediates.

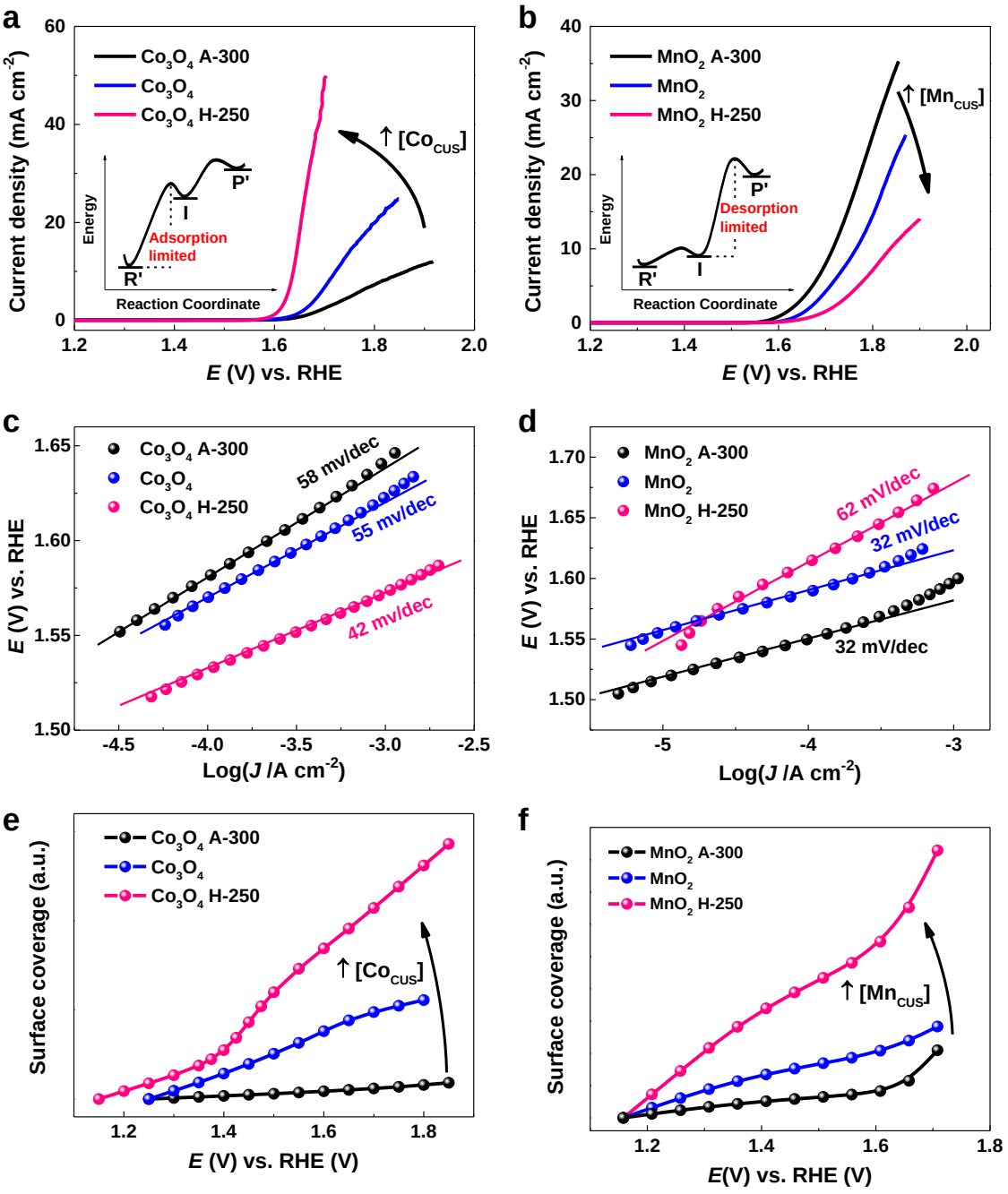

Figure 2-10. Electrochemical characterization of Co_3O_4 and α-MnO_2 with varying density of M_{CUS}. (a, b) OER polarization curves of Co_3O_4 (a weak-binding catalyst) and α-MnO_2 (a strong-binding catalyst). Insets show the simplified energy diagram to illustrate the rate-determining step (RDS) associated with key intermediate (I), wherein only two critical steps of adsorption and desorption of intermediate (I) are shown. Here we use R' and P' to represent reactant equivalent and product equivalent, respectively. The equivalent means that the

transition from reactant to R' and from P' to product are fast. (c, d) Tafel plots for Co_3O_4 and α-MnO_2. (e, f) Variation in the surface coverage of intermediates on Co_3O_4 and α-MnO_2. Scan rate: 5 mV s^{-1} and 1 mV s^{-1} for polarization curves and Tafel plots, respectively. The naming rules of the samples are the same as that of TiO_2.

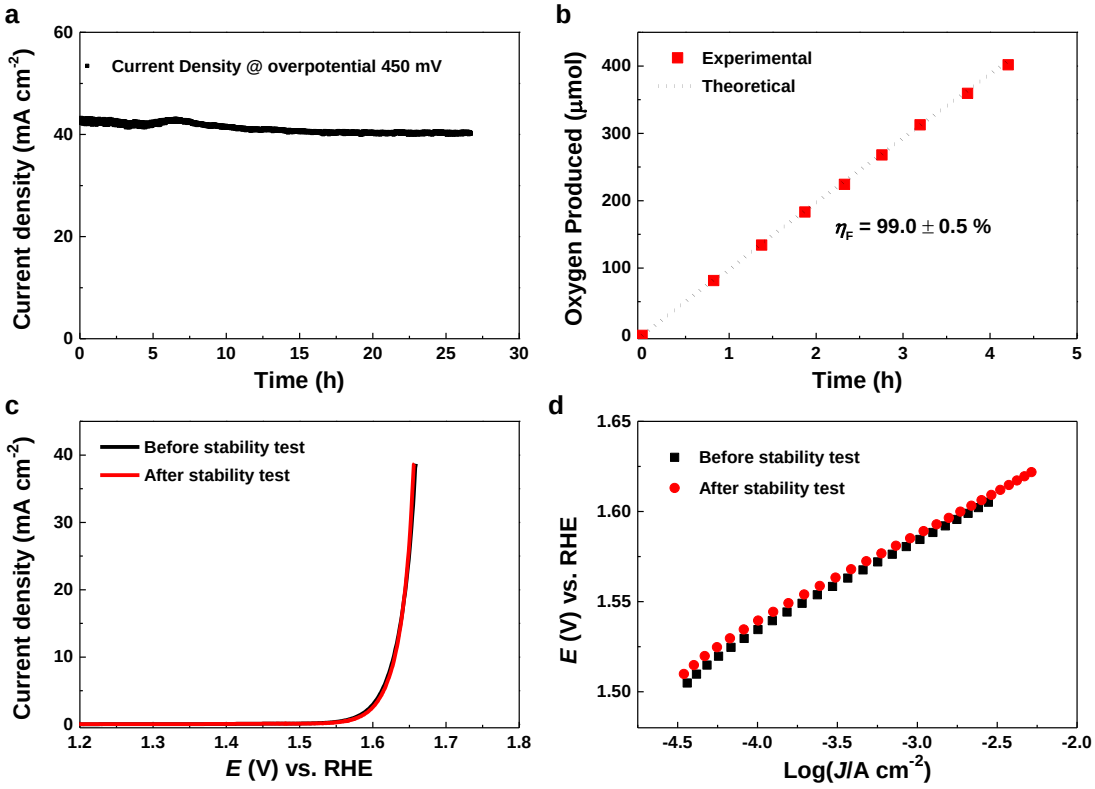

Figure 2-11. Stability and Faradaic efficiency test of Co_3O_4 H-250. (a) Stability test only less than 5% decrease in current density can be observed after 27 hours of continuous electrolysis, highlighting the excellent durability of Co_{cus}-rich surface in OER catalysis. (b) Faradic efficiency test. (c, d) Electrocatalytic kinetics before and after stability test. The good stability indicates the slightly modified Co_3O_4 surface with higher density of Co_{CUS} could work stably in OER catalysis.

Despite the opposite trend of OER activity for Co_3O_4 and α-MnO_2 with [M_{CUS}], we found that the capacitance prior to the onset of OER varies with [M_{CUS}] along the same trend for both

Co_3O_4 and α-MnO_2 (Figure 2-12 c & d). Through in-depth EIS studies, we found that this variation originates from the capacitance associated with intermediates adsorption (C_{ads}) (detailed analysis can be found in the *Kinetic analysis* part of *section 2.3*). C_{ads} can be used to estimate the fractional surface coverage of intermediates (θ), which reflects the adsorption energy (ΔH_{ads}) of intermediates as described by equation (1)[19,68].

$$\theta \propto \exp\left(\frac{\Delta H_{ads}}{RT}\right) \quad (2\text{-}4)$$

Equation (1) indicates that higher ΔH_{ads} (stronger adsorption) gives rise to higher θ. Figure 2-10 e & f show that θ on both Co_3O_4 and α-MnO_2 increase with increasing [M_{CUS}], indicating that higher [M_{CUS}] results in stronger adsorption, which agrees well with the trend of OER activity. Since experimentally evaluating the adsorption of OER intermediates is very difficult, the θ obtained from C_{ads} could be used as an indication of adsorption energy for OER intermediates.

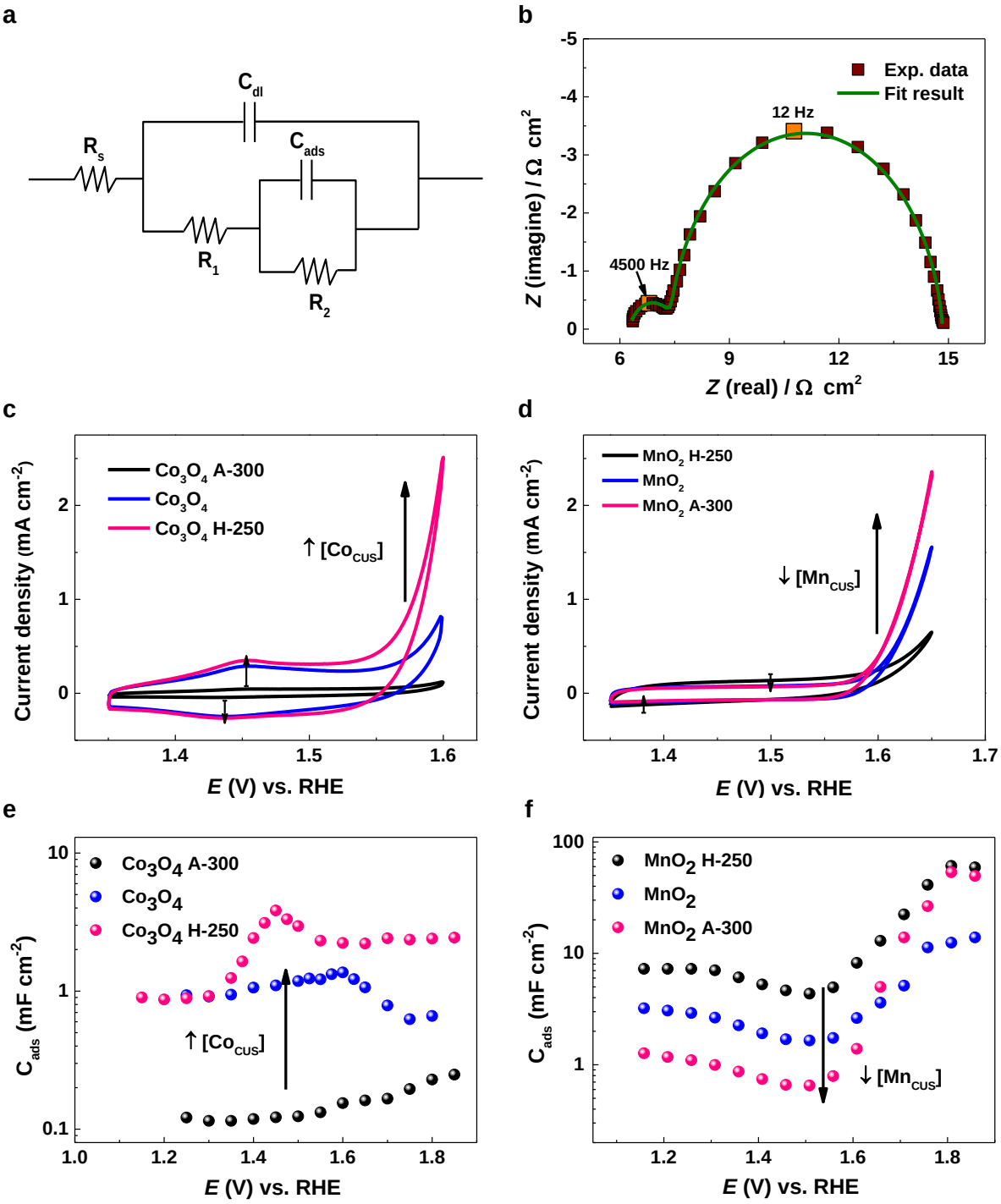

Figure 2-12. Electrochemical characterization of oxygenated intermediates adsorption. (a) Electrical equivalent circuit (EEC) for adsorption. R_s refers to the series resistance in the circuit. C_{dl} and C_{ads} are the capacitance from double layer and intermediates adsorption, respectively, whereas the physical significance of R_1 and R_2 are still under debate but with a general

viewpoint that overall charge transfer resistance $R_{ct} = R_1 + R_2$[12]. To account for the deviation of capacitance from ideal capacitive behavior, constant phase elements are adopted in the specific fitting to replace pure capacitors in the equivalent circuit. (b) A typical comparison between the fitting result and the experimental data (Co_3O_4), which shows an excellent match. (c, d) Cyclic voltammetry (CV) of Co_3O_4 and α-MnO_2 with varying density of M_{CUS}. The CV curves are obtained from the second cycle of CV scan in the electrochemical tests. The capacitance charging current prior to the onset of OER for both Co_3O_4 and α-MnO_2 is positively dependent on the density of M_{CUS}. The activity for Co_3O_4 varies in the same trend with the capacitance charging current, whereas the activity for α-MnO_2 changes oppositely with the variation of the capacitance charging current. (e, f) Trend of C_{ads} decoupled from EIS results. The variation of C_{ads} contributes the change in capacitance charging current prior to the onset of OER with density of M_{CUS}.

Moreover, the universality of M_{CUS} as a surface reactivity descriptor was further verified on α-Fe_2O_3 and NiO (Figure 2-13), whose activities are positively and negatively dependent on [M_{CUS}], respectively. The trends are consistent with their surface reactivities (as shown in Figure 2-1 b, activities of α-Fe_2O_3 and NiO are limited by low and high surface reactivity, respectively). So far, we have demonstrated M_{CUS} as an effective surface reactivity descriptor for five TMOs that are well studied in OER. The OER overpotential difference for each TMO with lowest to highest [M_{CUS}] summarized in Figure 2-14 indicates that M_{CUS} leads to vast difference in OER kinetics. Such a strong dependence of surface reactivity and OER catalytic activity on [M_{CUS}] suggests that M_{CUS} could serve as an effective surface reactivity descriptor for TMOs in OER.

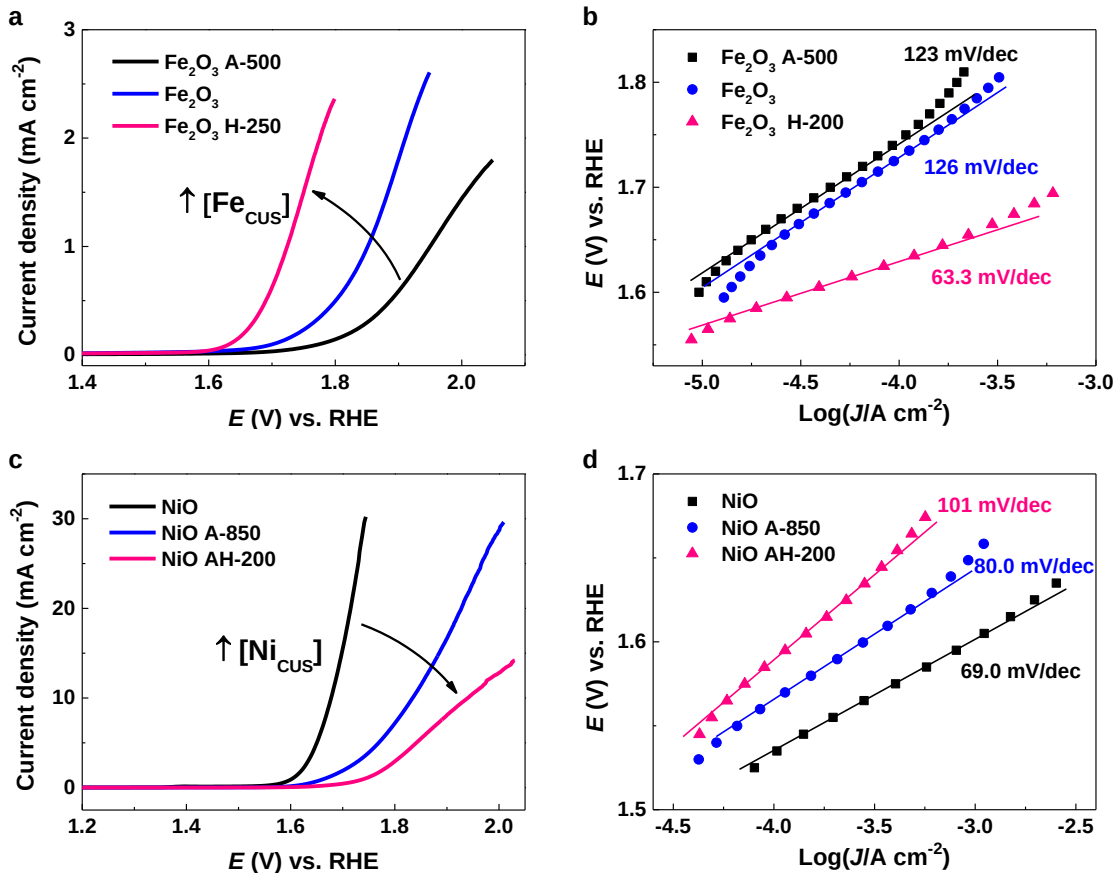

Figure 2-13. Catalytic activity variation of Fe_2O_3 and NiO with the density of M_{CUS}. (a, b) LSV and Tafel plots for Fe_2O_3, where arrow shows the direction of activity optimization by increasing Fe_{cus}. (c, d) LSV and Tafel plots for NiO with varying density of Ni_{cus}. Commercial NiO nanoparticles are black in color, indicative of presence of substantial defects (oxygen excess). The density of Ni_{cus} was first reduced by annealing NiO nanoparticles at 850 °C to remove excess surface oxygen (denoted as NiO A-850).[14] NiO AH-200 refers to the sample of NiO A-850 reduced in H_2/Ar (5%, v/v) at 200 °C to further increase the density of Ni_{cus}. The electrochemical tests for NiO were conducted with specially purified electrolyte as stated in methods to rule out the influence of Fe impurity on the performance of NiO based materials.

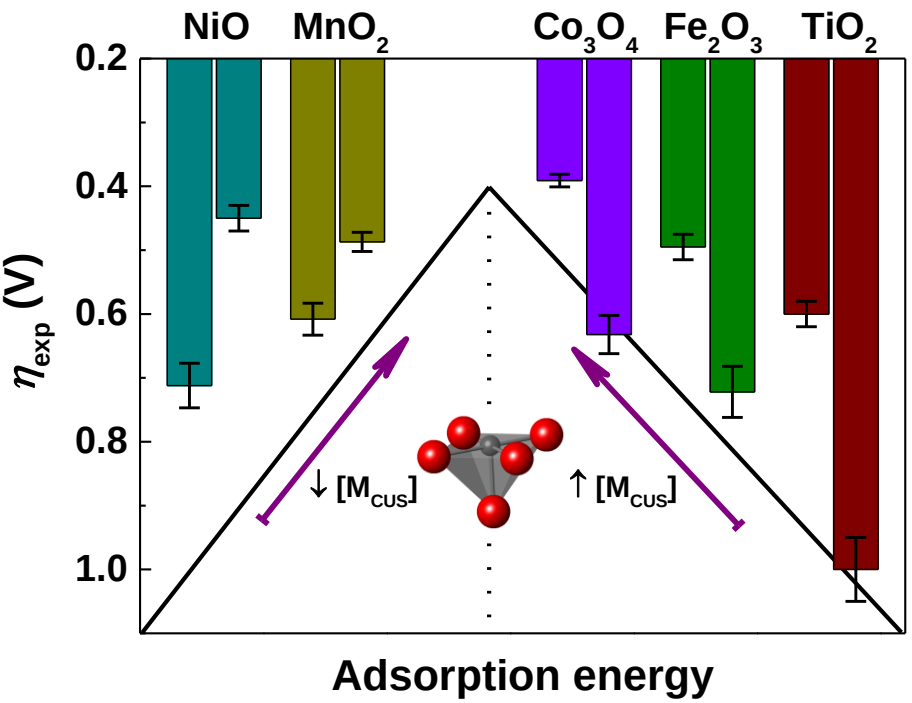

Figure 2-14. Overview of the overpotential dependence on surface M_{CUS} for TMOs. Only the overpotential of TMOs with the highest and the lowest [M_{CUS}] are shown for comparison. The arrows indicate the rational optimization direction: increase [M_{CUS}] for the TMOs on the right (weak binding), while reduce [M_{CUS}] for the TMOs on the left (strong binding). The η_{exp} for Fe_2O_3 refers to *current density* = 1 mA cm^2, while that for the rest TMOs correspond to *current density* = 10 mA cm^{-2}.

2.4.4 Electronic origin of surface reactivity of TMOs.

The surface structure, M_{CUS}, is practically useful in tuning the surface reactivity of TMOs. To further understand the electronic origin of this descriptor, we propose the following model based on the molecular orbital and band structure theory. Bond formation of atomic O, a key intermediate in OER, on the surface of a TMO is schematically illustrated in Figure 2-15. Atomic oxygen, the second highest electronegative element, behaves as an acceptor in bonding with metal cations. Adsorption sites are usually M_{CUS}[69] with only available *d* valence electrons for 3*d* and 4*d* TMOs. Hence we assume that the interaction between O and TMO (restricted to

3*d* and 4*d* TMOs) is mainly contributed from the coupling of O 2*p* to the highest occupied *d*-states (denoted as E_d). As shown in Figure 6, the coupling results in bonding states and antibonding states. The bonding states are generally far below Fermi level (E_F) and fully filled, whereas the filling of antibonding states depends on the relative energy of E_d to E_F (denoted as ($E_d - E_F$)). The higher energy of E_d relative to E_F, the less filling of the antibonding states and the stronger adsorption.

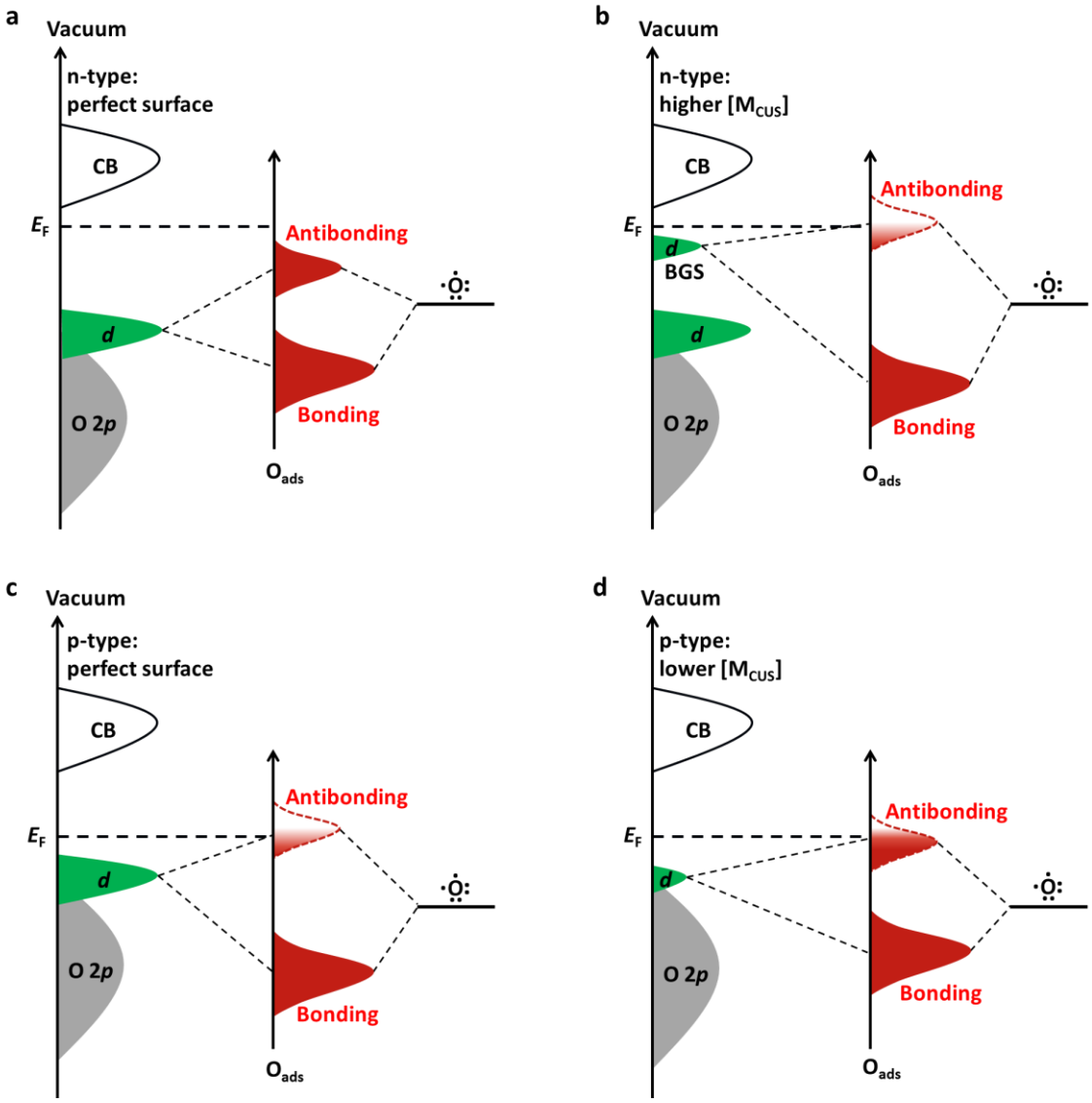

Figure 2-15. Schematic bond formation of atomic oxygen on different types of TMOs through coupling of O 2*p* to the highest occupied *d*-states. Most of the stable TMOs are either semiconductors or insulators, valence band (VB) of which is composed of O 2*p* states and the

d-states of transition metal cation. (a, b) Bonding of O to an n-type TMO. On the stoichiometric surface of an n-type TMO, the antibonding states are usually filled due to the relative low energy of highest occupied *d*-states (E_d) to the Fermi level (E_F). However, surface oxygen deficiency (higher [M_{CUS}]) introduce band gap states (BGS) resulted from unpaired *d*-electrons[19,41]. The generated *d*-states by higher [M_{CUS}] lead to stronger adsorption of O due to upshift of the antibonding states relative to E_F. (c, d) Bonding of O to a p-type TMO. For p-type TMOs, E_d is much closer to E_F, thus antibonding states are less filled as compared to the stoichiometric n-type TMOs. Downshift of E_d relative to E_F results in more filling of the antibonding states, giving rise to weaker bonding. This model implies that not all *d*-states contribute to the bonding strength of adsorbates. Instead, only the highest occupied *d*-states dominate the energy of antibonding states, and together with the Fermi level the filling of antibonding states can be defined. Thus, the (E_d - E_F) should be the electronic origin of surface reactivity for TMOs.

The detailed interpretation of the model is divided into three categories: n-type, p-type and metallic TMOs. For stoichiometric n-type TMOs, E_d in the valence band is far below E_F, which results in lower energy of antibonding states relative to E_F. Thus, the antibonding states are fully filled and the adsorption is very weak. However, a surface with higher [M_{CUS}] than the stoichiometric surface can introduce band gap states (BGS) due to unpaired *d*-electrons (Figure 2-15 b)[70], which can increase E_d and push the antibonding states above E_F, leading to less filling of antibonding states. Therefore, higher [M_{CUS}] gives rise to higher surface reactivity and this can be evidenced by diminished BGS upon adsorption of oxygen[71]. The cases of TiO_2, α-Fe_2O_3, V_2O_5,[72] and MoO_3 can be well described by Figure 2-15 a & b. For stoichiometric p-type TMOs, E_d is close to E_F and thus antibonding states are partially filled as shown in Figure 6c. Therefore, surface reactivity of p-type TMOs is usually higher than that of stoichiometric n-type TMOs, i.e., MnO_2, Co_3O_4 and NiO can adsorb OER intermediates relatively stronger than TiO_2 and α-

Fe_2O_3 (Figure 2-1 b). But some p-type TMOs have different band structures. A typical example is CuO, whose *d*-band in the valence band is lower than the O 2*p* band[73]. Therefore, coupling between Cu 3*d* and O 2*p* results in lower energy of antibonding states relative to E_F and the antibonding states are fully filled, hence bonding of O to CuO is the weakest among all 3*d* TM monoxides[74]. Higher [M_{CUS}] on surface of p-type TMOs also leads to higher surface reactivity in a similar way as shown in Figure 6 b, which has been verified on MnO_2[75] and Co_3O_4. Lower [M_{CUS}] as compared to the stoichiometric surface resulted from extra surface oxygen is also common on p-type TMOs, which leads to lower E_d relative to E_F and thus weakens the adsorption (Figure 6 d). A typical case is NiO[76], which usually present as $Ni_{1-x}O$ due to strong adsorption of oxygen. For metallic TMOs (at room temperature) such as TiO, V_2O_3 and MoO_2, the good electrical conductivity stems from partially occupied *d*-states which extend to E_F[77]. As a result, this group of TMOs shows very high surface reactivity such that they will be oxidized in the presence of O_2.

Some differences and close connections between surface reactivity of TMOs and TMs can be understood by comparing our model with the *d*-band theory. One obvious difference is that the adsorption energy on TMs is contributed from the interaction of adsorbates with both *s* and *d* states of metal atoms, whereas the adsorption energy on TMOs only results from the coupling of adsorbates with the highest occupied *d* states of metal cations. Thus, TMs show much higher surface reactivity than TMOs, which well-explains the reason why TMs cannot work in OER catalysis. Considering the similar electronic descriptor - ($E_d - E_F$) used for describing the surface reactivity for both TMs and TMOs, our model could be regarded as a generalization of the *d*-band theory into TMOs, which showed unsuccessful over the past.

2.5 Conclusion

In summary, we identified a tunable surface structure, M_{CUS}, as an effective surface reactivity descriptor for TMOs in OER. From both computational and experimental results, a

viable design principle to achieve desirable OER activity on TMOs is thus deduced: for better activity, increase [M_{CUS}] for the TMOs with weak intermediates adsorption while reduce [M_{CUS}] for those bind to the intermediates too strongly, and vice versa. The electronic origin of the descriptor can be well interpreted by a new model proposed in this work, wherein the energy of highest occupied *d*-states relative to Fermi level serves as a (electronic structure) descriptor for surface reactivity. Our model well describes the reactivity trends among various TMOs and thus can potentially initiate the development of a universal model for surface chemistry of TMOs.

Chapter 3. A kinetic model for quantitatively resolving elementary surface thermodynamics from kinetic analysis

The most challenging but critical research in the field of catalysis is to identify the rate determining step and associated with elementary thermodynamic origin, based on which one is able to design and develop better catalysts. Sophistication of electrified liquid/solid interface in oxygen electrocatalysis makes it incredibly difficult to identify the elementary surface thermodynamic origin of kinetics by individual research approaches such as traditional kinetic analysis, spectroscopic study and theoretical simulation. Moreover, oxygen evolution (OER) and reduction reaction (ORR) are usually separately studied and hence their mutual intrinsic relation is unclear. Here for the first time, by combining the critical outcome from different research approaches, we developed a new kinetic model for quantitative description of the macroscopic kinetics of the two reactions together as a function of elementary surface thermodynamics. The mechanistic information of elementary surface thermodynamics derived from kinetic data using our model well explains many experimental phenomena in oxygen electrocatalysis. Finally, the predictive power of our method in developing better catalysts was successfully demonstrated on α-MnO_2.

3.1 Introduction

Oxygen evolution reaction (OER) and its reverse reaction – oxygen reduction reaction (ORR) are two of the most important electrochemical reactions that have attracted intensive research interests over the past decades because of their potential imperative implications in many clean energy processes[6,37,78]. Unfortunately, despite of intensive research, OER and ORR still badly limit the commercialization of clean energy conversion technologies due to lack of design principles to guide the development of efficient and stable electrocatalysts from abundant materials. Different approaches have been employed to identify key elementary steps involved in oxygen electrocatalysis so as to develop catalyst design principles[79].

Traditional kinetic model constructed decades ago can give good interpretation of macroscopic kinetics[80]. But, the insufficient understanding on surface chemistry of electrocatalysis badly prohibits researchers from resolving the elementary thermodynamic origin of kinetic limitation. Spectroscopic techniques, especially *in-situ* spectroscopy, adopted in electrocatalysis have greatly promoted understanding of electrocatalysis under working conditions[37,81,82]. However, the information obtained from spectroscopic studies is still very limited owing to the intrinsic complexity of electrified liquid/solid interface – an environment in which many surface science techniques widely applied in gas/solid interfaces cannot apply[83]. On the other hand, theoretical simulation, especially density functional theory (DFT) simulation, could gain surface thermodynamic information of electrocatalysis directly. Recently, Norskov *et al* identified several critical relations such as linear Brønsted–Evans–Polanyi (BEP) relation between activation energy with reaction energy[65,84] and scaling relation between different intermediates[8,12,43]. The relations greatly reduced the difficulty in identifying RDS and its thermodynamic origin. But, the current DFT simulations are mainly used to study model systems to give a qualitative rationale of the experimental kineics[79]. In practice or even lab tests, both catalysts themselves such as structure and composition and the interface are

much more complicated. Therefore, in many cases the simulated results can't give a convincing interpretation of experiment data.

Each approach has its unique strength and limitation in resolving electrocatalysis. Quantitatively combination of different approaches in a comprehensive study should be more fruitful but it requires solid background from all related disciplines and thus such reports are scarce even in more simple hydrogen electrocatalysis[27,85,86]. Therefore, there exists a substantial gap between the current understanding with real reaction mechanisms, which greatly slows down the design of catalysts that could meet for practical requirements. To bridge the gap, a solid relation to link macroscopic kinetics with elementary thermodynamics is urgently needed. Electrocatalysis is a highly interdisciplinary and relative immature field, which requires comprehensive investigation by a deep combination of different approaches. By combining the conceptual outcome from different approaches, here we present a general and quantitative description of the oxygen electrocatalytic kinetics based on the microscopic thermodynamic origin, the binding energies of intermediates on catalysts surface. The results of our model describe experimental kinetics very well and, for the first time, provide a methodology to quantitatively identify elementary surface thermodynamics and give a clear description of mutual relation between OER and ORR. Based on this fundamental advancement, we further demonstrate the predictive power of our model by rationally developing better catalysts based on α-MnO_2 in both OER and ORR.

3.2 Experimental section

3.2.1 Catalyst synthesis and electrodes preparation.

The synthesis methods for Fe_2O_3, Co_3O_4, RuO_2, NiO and α-MnO_2 nanostructures are the same as that used in our previous work[21]. RuO_2 nanoparticles are prepared through a reported method[87]. To prepare a working electrode, the catalysts were first dispersed in an isopropyl

alcohol (IPA)/water (v : v = 1 : 1) solution with a concentration of 2 mg/ml. Since α-MnO_2 nanorods are difficult to be well dispersed in the solution, we mixed α-MnO_2 with multi walled carbon nanotube (MWCNT) with a ratio α-MnO_2 : MWCNT = 4 : 1 to get a well dispersed ink. The mixture was sonicated for 3 h to form a well-dispersed solution. Subsequently, 10 μl of the solution was drop-casted onto a pre-cleaned glassy carbon (GC) rotating disk electrode (0.196 cm^2). The electrode was dried in atmosphere overnight before electrochemical test. Pt and Au electrodes used in this work are purchased from Pine Research Instrumentation and have been cleaned prior to electrochemical tests.

3.2.2 Electrochemical studies.

Electrochemical tests were conducted on an Autolab PGSTAT 30 with a three-electrode configuration. Specially designed glass-free cell, reference and counter electrodes (provided by Hangzhou Saiao Electrochemical Technology Co., LTD) were used in all electrochemical tests to eliminate the influence of glass components on the activity of catalysts.[88] Saturated calomel electrode (SCE, 0.241 V vs. SHE (standard hydrogen electrode)) was used as the reference electrode, while Pt plate (~1 cm^2) was used as the counter electrode only in the OER tests. Considering the severe dissolution of Pt at high potential[89], titanium sheet was selected as the counter electrode in ORR tests to avoid the re-deposition of dissolved Pt on the working electrodes. The electrochemical testing was conducted at a rotating speed of 1600 rpm in 1 M KOH electrolyte (pH = 13.72) to minimize mass transport limit. To reduce the effects of impurities, high purity KOH (semiconductor grade, 99.99% trace metals basis) was used during the electrochemical testing. All polarization curves were corrected by eliminating the *iR* drop in the electrical circuit. Relatively low scan rate (5 mV s^{-1}) was employed to diminish the contribution of non-faradic current to the current of polarization curves. The series resistance (R_s), mainly originating from ionic conduction in the electrolyte, is in the range of 5.5 to 7.0 Ω.

The potentials of polarization curves were compensated based on the following equation: $V_{RHE} = V_{SCE} + 0.241 + 0.059 * pH - R_s * i$.

3.3 Model description

3.3.1 Basic assumptions and relations

Our aim here is to identify the elementary surface thermodynamic origin of reaction kinetics, based on which we will be able to predict how to improve catalytic activity or design new efficient catalysts. Compared with acidic media, alkaline solution offers higher compatibility to most materials, and hence more experimental data are available to test and improve our model. In this work, we mainly concentrate on oxygen electrocatalysis in alkaline solution. Since oxygen electrocatalysis is extremely complicated and here we intend to give an analysis of the two reactions together, we would confine our analysis within the following assumptions to avoid unnecessary obstacles. All potentials in this work are referred to reversible hydrogen electrode (RHE).

1) The reactions take place on clean and perfect surfaces with uniform chemical reactivity.

2) The reactions undergo a general 4 electron-transfer (ET) pathway as shown in equation (3-1) to (3-4). Different reaction pathways may also be proposed, but it essentially does not affect the basic trends in catalytic activity[12,43].

3) Scaling relationship for the binding energy of the intermediates applies in our model but the value is slightly modified (equation 3-8) based on experimental data to give a better quantitative description of the experimental kinetics.

4) The activation energy of each elementary step scales with the reaction energy in the BEP relationship[65,84]. Under this scheme, the RDS and PDS (potential determining step, which is defined by Norskov et. al.[8,12,43]) are identical.

The oxygen electrocatalysis involves the following elementary reactions:

$$M^* + OH^- \rightleftarrows M-OH^* + e^- \quad (3\text{-}1)$$

$$M-OH^* + OH^- \rightleftarrows M-O^* + H_2O + e^- \quad (3\text{-}2)$$

$$M-O^* + OH^- \rightleftarrows M-OOH^* + e^- \quad (3\text{-}3)$$

$$M-OOH^* + OH^- \rightleftarrows M^* + O_2 + H_2O + e^- \quad (3\text{-}4)$$

The overall reaction is:

$$4\,OH^- \rightleftarrows O_2 + 2\,H_2O + 4\,e^- \quad (3\text{-}5)$$

where M^* refers to the adsorption site on catalyst surface. We use reversible reaction arrow to indicate that one reaction such as OER is the back reaction of ORR. This reaction pathway involves three intermediates (OH^*, O^*, OOH^*). Elementary surface thermodynamics determines the equilibrium potential through Nernst equation. In addition to the above ET steps, pure chemical reactions can also take place and sometimes become the RDS. Therefore, we name the chemical reaction after the n_{th} ET step as the $(n+0.5)_{th}$ step as the rate equation for the chemical reaction as the RDS still obeys the general equation obtained from the electron-transfer steps.

$$\Delta G^0 = -FE^0 \quad (3\text{-}6)$$

For the overall reaction, $E^0_{O_2/OH^-}$ = 1.23 V. For each elementary step, its own equilibrium potential is given by the corresponding reaction energy. Therefore, for each elementary reaction, the higher equilibrium potential corresponds to higher energy gap.

The equilibrium potential for (5) is an average of (1) to (4):

$$E^0_{O_2/OH^-} = \frac{E^0_1 + E^0_2 + E^0_3 + E^0_4}{4} = 1.23\ \text{V vs RHE} \quad (3\text{-}7)$$

The distinct equilibrium potential should, in principle, bring about some typical characteristics in the kinetic data. For example, the onset of the overall reaction is controlled by the RDS, and other steps (fast steps) will, in principle, take place at potentials prior to the OER onset and after the ORR onset. These correlate with the adsorption/desorption of intermediates on/from the surface of catalyst to a certain extent depending on surface thermodynamics. Since the solubility of O_2 in aqueous electrolyte is about 3 orders lower than that of OH^-,[90] the signals associated with fast reaction steps to/from O_2 may be too weak to be detected by experiments. This is consistent with the experimental results that OH* adsorption and oxide film formation can be clearly observed in CV (cyclic voltammetry) scans of metals[88]. Therefore, only fast steps from OH^- such as OH* adsorption is explicit in potential sweep measurements. These reactions will form peaks in dynamic potential sweep measurements such as CV and LSV (linear sweep voltammetry), which can be used as a characteristic to identify surface reactivity and RDS.

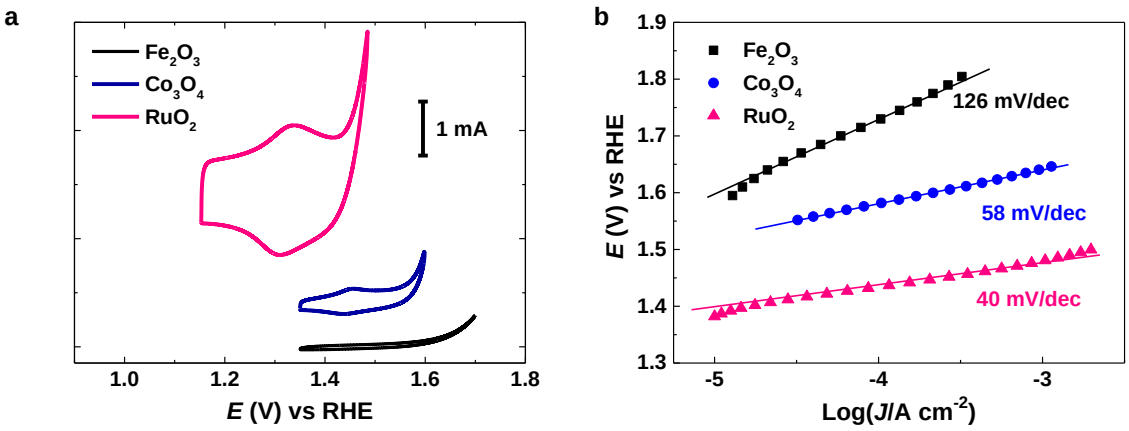

Figure 3-1. CV curves and Tafel plots for typical OER catalysts. With careful comparison one can easily observe that the potential range of peaks is not included in the Tafel region. For example, the anodic peak for RuO_2 ends at about 1.4 V, at which the linear relation just starts. This suggests the OH_{ads} adsorbed under the peaks is unreactive intermediates.

3.3.2 Scaling relationship used for kinetic simulation

Here we provide detailed description of our model and the assumptions used in this work. Basically, there are two major corrections to the Norskov's DFT simulation results. Firstly, the offset in the energy of OOH* relative to OH* in the scaling relationship is 3.2 eV, which predicts the equilibrium potential of RDS for best OER and ORR catalysts are 1.6 V and 0.86 V vs RHE respectively. The thermodynamic overpotential for best catalysts is 370 mV, much higher than experimental overpotential for state-of-the-art catalysts (about 200 mV for RuO_2 in OER and 200-250 mV for Pt_3Ni in ORR[91]). Generally, thermodynamic overpotential predicted from DFT calculations are usually higher than their real value. Take Co_3O_4 as an example, the thermodynamic overpotential is 760 mV[92], whereas measured overpotential at 10 mA/cm^2 is only about 540 mV and onset overpotential is 300 mV. Hence, a lower offset (2.86 eV in this work) in scaling relationship value should be adopted to reproduce the experimental activity trends (equation 3-8). Secondly, the OER activity of some typical materials such as Fe_2O_3 is limited by the first electron-transfer (ET) step predicted by Tafel slope (as shown in Figure 3-7). The slope of the scaling relationship between the energy of O* with that of OH* is corrected to account for experimental trends (equation 3-9).

$$\Delta G_{\mathrm{OOH}^*} - \Delta G_{\mathrm{OH}^*} = 2.86 \text{ eV} \quad (3\text{-}8)$$

$$\Delta G_{\mathrm{O}^*} = 0.54 * \Delta G_{\mathrm{OH}^*} + 0.77 \text{ eV} \quad (3\text{-}9)$$

The relation described by above two equations maybe the major sources of error in simulating kinetics. As so far no more precise relations has been identified by experiments, we tend to use the conceptual relation identified from DFT simulations.

Here the definition of ΔG_{OH^*}, ΔG_{O^*}, and $\Delta G_{\mathrm{OOH}^*}$ follows that of Norskov's DFT simulation work[12]. With the two equations one can get the energy of O* and OOH* for a given energy of

OH*. Then the reaction energy for each elementary step can be deduced (shown in Figure 3-2).

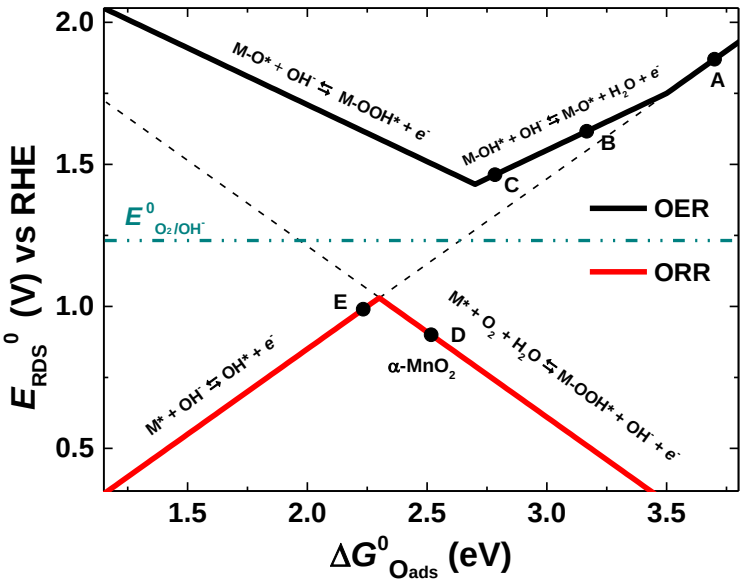

Figure 3-2. Activity volcano plots for oxygen electrocatalysis. Which elementary ET step is RDS is shown in the volcano plots. The overall thermodynamic information of a catalyst can be deduced once we know its location in the activity volcano plot.

3.3.3 Adsorption model

If the adsorption step of a reactive intermediate is too much faster than subsequent step, the intermediate adsorption could be treated as equilibrium step. Due to the interaction between adsorbed intermediate, the adsorption free energy also vary with coverage, especially at high coverage[93].

$$\Delta G^{0\prime} = \Delta G^0 + c\theta \qquad (3\text{-}10)$$

Where c is a constant that describes the rate of change of adsorption free energy with coverage[94]. This equation is a general description of intermediate adsorption. When c is small enough (approaching 0), it becomes Langmuir adsorption isotherm; when c is significantly

higher than 0, it becomes Temkin isotherm. The coverage of intermediate can only be calculated by numerical methods for Temkin adsorption.

3.3.4 Reaction rate law based on elementary thermodynamics

Since both OER and ORR are highly irreversible reactions, we directly omit the back reaction in RDS in reaction rate equations. This simplification is reasonable as back reaction only significantly influences overall kinetics at very low reaction rate, whereas the current density measured in experiments at this reaction rate usually exceed the sensitivity of electrochemical equipment. Under this treatment, the surface coverage of the reactive intermediates generated from RDS and steps after RDS is zero.

We firstly present the reaction rate equations for OER, based on which that of ORR can be easily derived. According to our description in article, n = 1, 2, 3 refers to RDS is first, second, third electron-transfer (ET) step for OER. Besides, we use n = 1.5, 2.5 to describe the chemical reaction RDS between ET steps to formulate a general description. n = 4 is least possible in OER, thus we do not deduce its kinetics here.

For n = 1 in OER, velocity of the RDS is given by:

$$v_1 = k_1\, \theta_{\mathrm{M}^*} a_{\mathrm{OH}^-} \qquad (3\text{-}11)$$

where θ_{M^*} represent the surface coverage of empty catalytic sites, which is 1 for this case. a_{OH^-} is activity of OH^- in electrolyte, taken as 1 in this work. k_1 is rate constant for reaction (1) and is given by:

$$k_1 = k_1^0 * e^{\frac{\alpha F(E - {E_1}^0)}{RT}} \qquad (3\text{-}12)^{95}$$

Where k_1^0 is reaction rate constant under $E = {E_1}^0$ vs RHE. α, usually taken as 0.5 in rough analysis, is the transfer coefficient whose influence on Tafel slope is discussed in the main context. F is Faradic constant of 96485 C mol^{-1}. Here the equilibrium potential of RDS is unambiguously used as refence potential to derive kinetics. On this basis, we can quantitatively

simulate the experimental kinetics of proposed elementary surface thermodynamics and, in turn, quantitatively identify elementary thermodynamic information from experimental kinetics.

For n = 2 and 3, velocity of the RDS is given by:

$$v_2 = k_2\ \theta_{\mathrm{OH}^*} a_{\mathrm{OH}^-} \tag{3-13}$$

$$v_3 = k_3\ \theta_{\mathrm{O}^*} a_{\mathrm{OH}^-} \tag{3-14}$$

θ_{OH^*} and θ_{O^*} represent the surface coverage of OH* and O*. k_2, k_3 are given by:

$$k_2 = k_2^0 * e^{\frac{\alpha F(E-E_2{}^0)}{RT}} \tag{3-15}$$

$$k_3 = k_3^0 * e^{\frac{\alpha F(E-E_3{}^0)}{RT}} \tag{3-16}$$

For n = 1.5 and 2.5, velocity of the RDS is given by:

$$v_{1.5} = k_{1.5}\ \theta_{\mathrm{OH}^*} \tag{3-17}$$

$$v_{2.5} = k_{2.5}\ \theta_{\mathrm{O}^*} \tag{3-18}$$

Where $k_{1.5}$ and $k_{2.5}$ are reaction rate constants for the chemical reaction. Different from the reaction rate constants of ET steps, that for pure chemical reaction are independent on potential. From equation (3-17) and (3-18) we can understand that, for the catalysts whose RDS is chemical reaction, the kinetics is only determined by the surface coverage of intermediates with a given reaction rate constant.

For n = 1.5 and 2, the active sites are either empty or occupied by OH*.

$$\theta_{\mathrm{M}^*} + \theta_{\mathrm{OH}^*} = 1 \tag{3-19}$$

Since adsorption of OH is equilibrium step, reaction (1) is in equilibrium.

$$\frac{\theta_{\mathrm{OH}^*}}{\theta_{\mathrm{M}^*} a_{\mathrm{OH}^-}} = K_1^0 e^{\frac{F(E-E_1^{0\prime})}{RT}} \tag{3-20}$$

Where K_1^0 is equilibrium constant of reaction (1), $E_1^{0\prime}$ is equilibrium potential of reaction (1), given by:

$$E_1^{0\prime} = (\Delta G_{\mathrm{OH}^*} + c_1\theta_{\mathrm{OH}^*} - \Delta G_{\mathrm{OH}^-})/F \quad (3\text{-}21)$$

From equation (3-19) and (3-20) we can get:

$$\theta_{\mathrm{OH}^*} = 1 - \frac{1}{1+K_1^0 e^{\frac{F(E-E_1^{0\prime})}{RT}}} \quad (3\text{-}22)$$

Since $E_1^{0\prime}$ on the right side of equation (3-22) also contains θ_{OH^*} for Temkin isotherm, the equation can only be solved numerically.

For n = 2.5 and 3, the active sites can be empty, occupied by OH or O.

$$\theta_{\mathrm{M}^*} + \theta_{\mathrm{OH}^*} + \theta_{\mathrm{O}^*} = 1 \quad (3\text{-}23)$$

Reaction (2) is also in equilibrium.

$$\frac{\theta_{\mathrm{O}^*}}{\theta_{\mathrm{OH}^*} a_{\mathrm{OH}^-}} = K_2^0 e^{\frac{F(E-E_2^{0\prime})}{RT}} \quad (3\text{-}24)$$

and

$$\theta_{\mathrm{O}^*} = \frac{K_1^0 K_2^0 e^{\frac{F(2E-E_1^{0\prime}-E_2^{0\prime})}{RT}}}{1+K_1^0 e^{\frac{F(E-E_1^{0\prime})}{RT}} + K_1^0 K_2^0 e^{\frac{F(2E-E_1^{0\prime}-E_2^{0\prime})}{RT}}} \quad (3\text{-}25)$$

The derived formula for kinetics of OER can be easily used for ORR by substituting the reactants. In this work, we believe that only the first and last ET step can be the RDS in ORR and these two steps are much slower than the rest steps. In this scenario, the middle two ET steps have little influence on the overall reaction rate as the intermediate from the first ET (OOH*) would rapidly evolve to OH*. Therefore, we can use n = 1.5 or 2 to simulate the ORR kinetics if the last ET has the most unfavourable thermodynamics.

For n = 1 in ORR,

$$v_1^{\mathrm{ORR}} = k_1^{\mathrm{ORR}}\ \theta_{\mathrm{M}^*} a_{\mathrm{O}_2} \tag{3-26}$$

In addition to reaction rate constant that vary with potential, the kinetics also depend on surface coverage of available active sites and the concentration of O_2.

$$k_1^{\mathrm{ORR}} = k_1^{\mathrm{ORR},0} * e^{\frac{-\alpha F(E-{E_4}^0)}{RT}} \tag{3-27}$$

For n = 1.5 and 2,

$$v_{1.5}^{\mathrm{ORR}} = k_{1.5}^{\mathrm{ORR}}\ \theta_{\mathrm{OH}^*} \tag{3-28}$$

$$v_2^{\mathrm{ORR}} = k_2^{\mathrm{ORR}}\ \theta_{\mathrm{OH}^*} \tag{3-29}$$

k_2^{ORR} is determined by equilibrium potential $({E_1}^0)$ of reaction (1).

$$k_2^{\mathrm{ORR}} = k_2^{\mathrm{ORR},0} * e^{\frac{-\alpha F(E-{E_1}^0)}{RT}} \tag{3-30}$$

The surface coverage of reactive intermediate θ_{OH^*} is given by:

$$\theta_{\mathrm{OH}^*} = 1 - \frac{1}{1+K_4^0 e^{\frac{-F(E-E_4^{0\prime})}{RT}}} \tag{3-31}$$

For both OER and ORR, the steady state current density of the overall reaction is described by:

$$J_{\mathrm{ET}} = 4Fv_i \tag{3-32}$$

The above formulation only considers pure kinetic limitation. When reaction rate increases, mass transport limitation will become increasingly significant. The overall reaction rate is proportional to the steady state current density (J) that can be readily measured by potentiostat equipment. J is given by:

$$\frac{1}{J} = \frac{1}{J_{\mathrm{MT}}} + \frac{1}{J_{\mathrm{ET}}} \tag{3-33}$$[95]

Note: J_{MT} is constant at a given reaction condition such as reactant concentration, active catalyst surface area and rotating rate for RDE tests. For example, the simulated LSV curves

for both typical OER and ORR catalysts well reproduced the experimental trends as shown in Figure 3 and 4.

In the simulation, the coverage of intermediates that appear in above equations refers to the "reactive intermediates", which should be distinguished from "unreactive intermediates" that will be discussed next. Here we define "unreactive intermediates" as the adsorbed intermediates that only involve in adsorption but do not participate in complete catalytic cycle, such as the case of underpotential deposited hydrogen on Pt in hydrogen evolution reaction (HER).

When the reaction rate is slow enough ($J = J_{ET}$), the reaction of RDS could be taken as irreversible, which means the back reaction can be neglected. The Tafel slope (b) can be calculated from the following equation at 25°C[96]:

$$b = 59\ /(n - 1 + \alpha)\ \ \mathrm{mV/dec} \qquad (3\text{-}34)$$

where α is the transfer coefficient with a generally assumed value of 0.5, meaning that 50% of the applied overpotential goes toward lowering the activation barrier for the reaction. n refers to the n_{th} ET as the RDS. But for ORR, n = 1.5 or 2 when last ET step is RDS. It has to be noted that the above equation holds only at the condition where the surface coverage of the produced intermediates from the steps prior to the RDS, if any, is very low and the change in coverage doesn't induce variation in reaction energy, corresponding to the Langmuir adsorption isotherm[97].

Table 3-1. Kinetic characteristics for different cases and typical examples

n	Tafel slope/ (mV/dec)	Typical example	Dominated reactive intermediate

		OER	ORR	OER	ORR
1	118.2	α-Fe_2O_3	α-MnO_2	none	none
1.5	59.1	Co_3O_4	Pt/C	OH*	OH*
2	39.4	RuO_2	-	OH*	OH*
2.5	29.6	α-MnO_2	-	OH* and O*	-
3	23.6	-	-	OH* and O*	-

Note: Different Tafel slope for a material could take place as the surface property is sensitive to preparation and subsequent treatment condition.

Here we describe the basic process of kinetic fitting to quantitatively resolve elementary surface thermodynamics. Firstly, we can use well-developed Tafel slope analysis (Table 3-1) to gain a preliminary reaction mechanism, particularly RDS and thermodynamic origin. As Tafel slope mainly consider the kinetics at low reaction rate, the information of kinetics at higher reaction rate need to be solved from LSV fitting to gain a conclusive result.

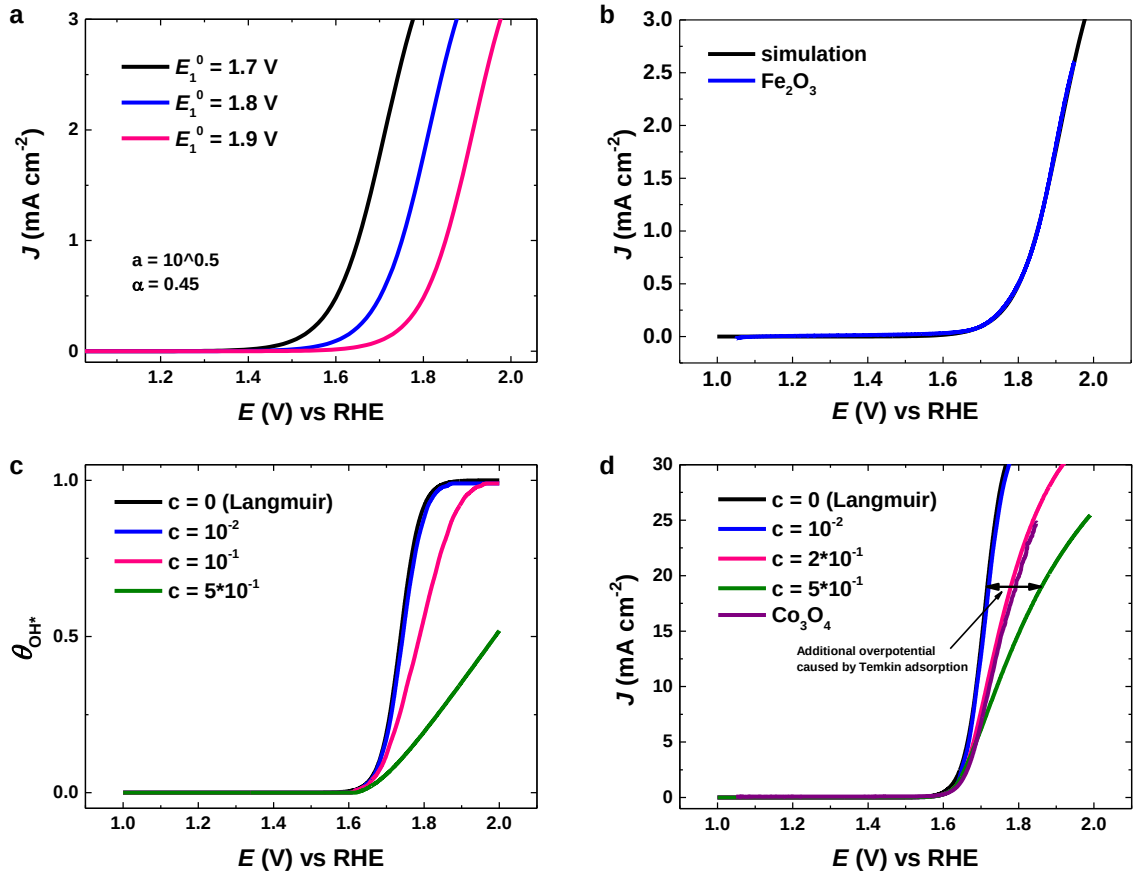

Figure 3-3. a, Simulated LCV curves of OER catalysts whose activity is limited by first step, showing the influence of equilibrium potential of E_1^0. **b,** Comparison of fitting result with experimental kinetics of a typical catalyst Fe_2O_3. Detailed value of constants used: J_{MT} = 5 mA/cm^2, a = $10^{0.5}$, α = 0.45. **c,** Simulated θ_{OH^*} for n = 1.5 and 2 as a function of potential, showing the influence of coverage induced change of adsorption free energy. **d,** Simulated LCV curves of OER catalysts (n = 1.5) and comparison with experimental kinetics of Co_3O_4. The influence of θ_{OH^*} on kinetics is clearly shown: the stronger dependence of adsorption free energy on θ_{OH^*}, the higher additional overpotential. Detailed value of constants used: $E_1^0 = 1.56\ V$, $K_1^0 = 10^{-3}$, $k_{1.5} = 100$, J_{MT} = 5 mA/cm^2. Through this simulation, we can deduce a conclusion, the kinetics for the catalysts with adsorbed reactive intermediates are also significantly influenced by adsorption isotherm.

3.4 Results and Discussion

3.4.1 Relation and difference between OER and ORR

Based on the above descriptions, the relation between OER and ORR is schematically illustrated in Figure 3-4. Figure 3-4a shows that at $U = 0$, all steps in OER is uphill in free energy with the largest step as the RDS, whereas all steps in ORR is downhill and the smallest step is the RDS. As a result, the RDS of OER is the fastest step in ORR and vice versa. Therefore, to improve the catalytic activity, one should work on its own RDS to tune the reaction energy toward the optimal value in OER or ORR.

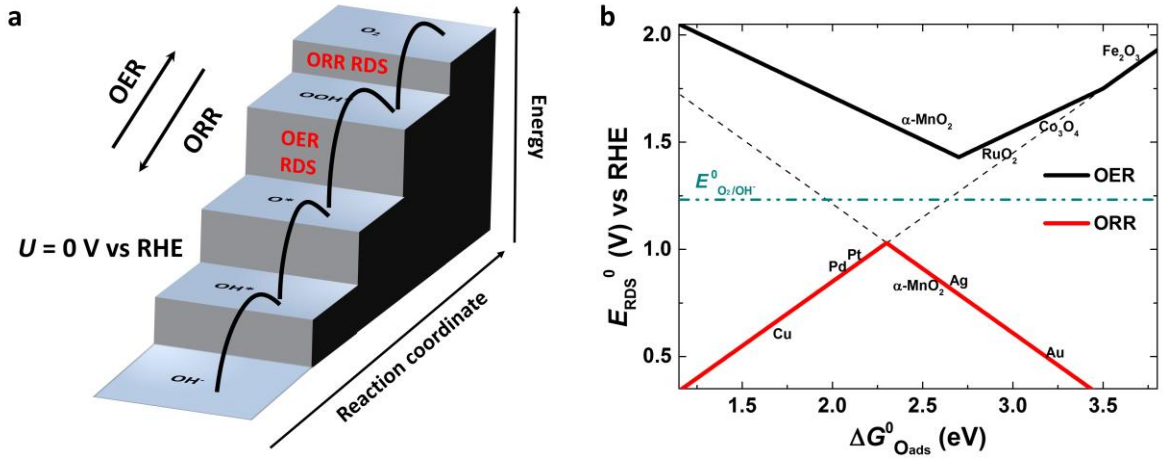

Figure 3-4. Schematic illustration of the elementary steps in oxygen electrocatalysis together with the activity volcano plots. **a,** The potential energy diagram of a typical catalyst whose surface reactivity is too high for OER but too low for ORR. **b,** Activity volcano plot for OER and ORR derived from modified scaling relationship. The positions of representative catalysts are shown. Simulated kinetics of representative catalysts (dotted points) and comparison with their experimental data will be presented in the discussion of Figure 3 and 4. The definition of the activity descriptor follows that defined by Norskov[9,12]. The higher free energy of O_{ads} means the lower surface reactivity, thus the surface reactivity increases from the right side to the left side. The activity for OER is most probably limited by reaction (2) or (3). Reaction (1) becomes

the RDS if surface reactivity is too low, and the last step has the lowest probability to be the RDS. For ORR, first or last step has the highest probability to be the RDS, which means that the activity of ORR is either limited by O_2 activation or by H_2O formation from adsorbed OH*.

Figure 3-4b provides a comprehensive overview of the activity trends in OER and ORR. In principle, the catalysts sitting on one volcano plot should exhibit the predicted activity for the reverse reaction by vertically shifting them to the intersection with the other volcano plot. For example, transition metal oxides (TMOs) mostly fall on the right side of the ORR activity volcano plot, indicating that the activation of O_2 is difficult (Figure 3-5a). Based on the above analysis, the ORR activity trends should follow the order of $Fe_2O_3 < Co_3O_4 < RuO_2 < \alpha\text{-}MnO_2$, which have been well-reproduced by our electrochemical tests as shown in Figure 3-5b. However, the inverse prediction encounters a problem for metals because of the high surface reactivity. Transition metals, even noble metals, will undergo serious surface reconstruction or oxide formation at high positive potentials, which is a typical phenomenon showing that electrochemical environment exerts hasher modification of materials as compared to regular heterogeneous catalysis[22,34,79]. This phenomenon not only makes it difficult to straightforwardly predict OER activity of metals from ORR activity volcano plot, but also accounts for the undesired metal dissolution, which is a major concern for activity loss in fuel cells[81].

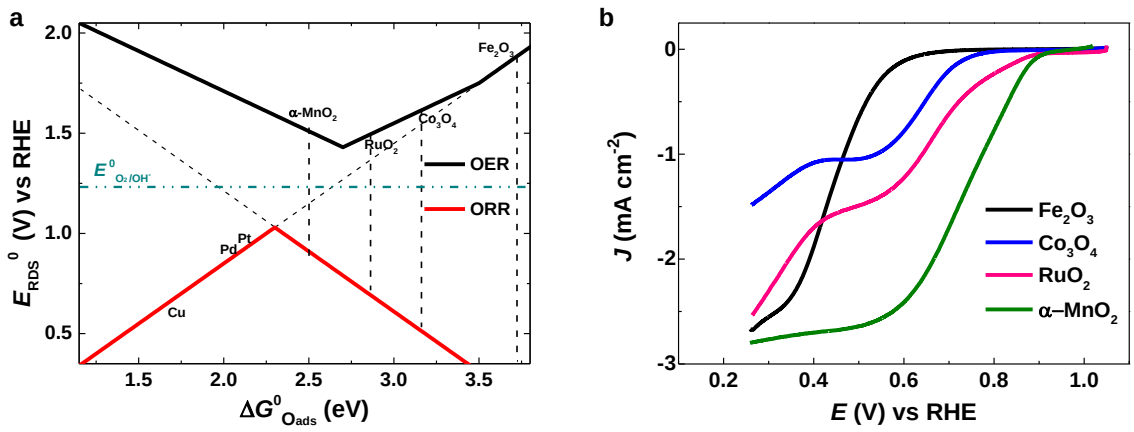

Figure 3-5. Predicted and experimental ORR activity of common transition metal oxides. **a,** Predicted ORR activity from OER activity volcano plot. The intersection points for all the TMOs are located on the right leg of ORR activity volcano plot, indicating the RDS of the TMOs in ORR should be the activation of O_2. Therefore, the higher surface reactivity, the higher catalytic activity in ORR. **b,** Measured ORR kinetics. The activity increases in the order: $Fe_2O_3 < Co_3O_4 < RuO_2 < \alpha\text{-}MnO_2$, consistent with the predication from our model.

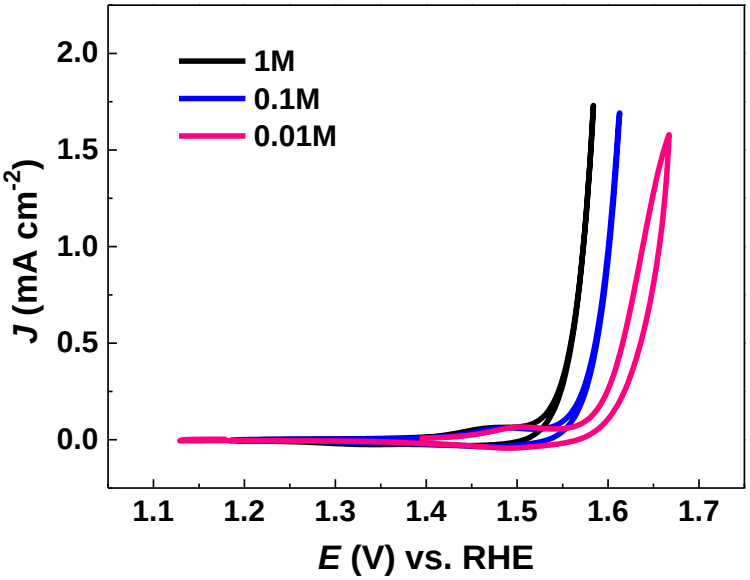

Figure 3-6. CV curves for Co_3O_4 obtained in varying concentration of OH^-. The influence of reactant concentration on OER kinetics is remarkable: the overpotential increases significantly with decrease in OH^- concentration. As the concentration of reactants has such a significant influence on overpotential, it is not difficult to understand that experimentally measured overpotential for the best catalysts in OER is usually smaller than that in ORR. The reactant concentration for OER (typically 1 mol/L) is usually much higher than that for ORR due to the lower solubility of O_2 (on the order of 10^{-3} mol/L)[90]. Moreover, the low solubility of O_2 also means that the signals associated with fast reaction steps to/from O_2 may be too weak to be detected by experiments. This is consistent with the experimental results that adsorption/desorption peaks in CV usually can be seen in OER but not common in ORR.

3.4.2 Kinetic analysis with the new model

In electrocatalysis, potential is the driving force, which is similar to temperature or pressure in heterogeneous catalysis[79]. Therefore, voltammetry methods, including LSV, CV and Tafel analyses are widely used in the evaluation of electrocatalytic kinetics. Here, through comparison between simulated LSV and Tafel plots with experimental data, we manage to test the validity of our model. If the simulated kinetics could quantitatively describe the experimental kinetics, the parameters in the model would provide valuable elementary surface thermodynamic information. With this information, we will be able to predict the way to improve the catalytic activity of the resultant catalysts.

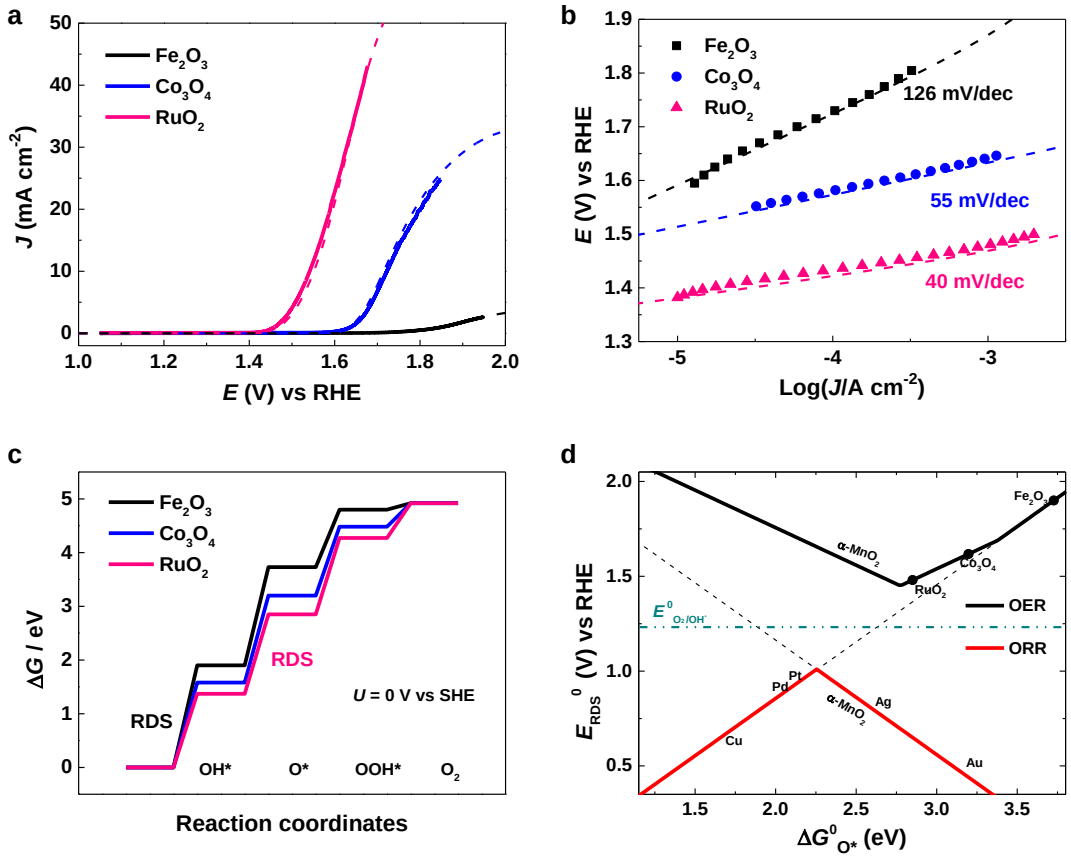

Figure 3-7. Fitting of experimental kinetics of the representative OER catalysts and the identified elementary surface thermodynamics. **a, b,** Comparison of simulated LSV and Tafel

plots with the experimental data. Simulated kinetics are presented in dashed lines. Here we show the kinetic data of Fe_2O_3, Co_3O_4 and RuO_2 to represent poor, medium and good OER catalysts. The reaction mechanism for the three catalysts are different, which can be used to test applicability of our kinetic model in describing different reaction mechanisms. **c,** Potential energy diagram derived from kinetic fitting. The RDS of Fe_2O_3 and RuO_2 are shown, whereas RDS of Co_3O_4 is the chemical reaction step which has been shown in Figure 2c. **d,** The positions of the catalysts in simulated activity volcano plot.

Figure 3-7 a & b show clearly that the experimental kinetics of the representative OER catalysts can be well fitted by our kinetic model. Both LSV curves and Tafel plots show quantitative consistency between experimental and simulated data, which suggests that our kinetic model well describes the kinetics of OER catalysts regardless of activity and reaction mechanism. In the process of fitting, several features in experimental kinetics can be used as hints to derive elementary thermodynamic information. From Tafel slope we can propose a preliminary judgement of RDS and reaction rate law according to Table 3-1. The OER onset for the three classes of catalysts differs greatly, which is associated with equilibrium potential of RDS. Onset potential is close to equilibrium potential of RDS, which means that this feature could be used to deduce thermodynamic information of RDS. In addition, for the cases that involve intermediate adsorption prior to RDS, the increase rate of current density with potential in LSV is determined by the adsorption isotherm of the intermediates (section 3.3.3). If the adsorption energy of intermediate decreases significantly with the intermediate coverage (Temkin adsorption), the current density increases slowly with potential, resulting in higher overpotential at high current density condition compared with Langmuir adsorption. Since our kinetic model is based on elementary surface thermodynamics, the kinetic fitting results could provide the detailed information of elementary reactions as shown in Figure 3-7 c & d, where the thermodynamic origin of RDS for the three catalysts are clearly shown. Compared with

optimal OER catalyst, the surface reactivity of Fe_2O_3 and Co_3O_4 should be significantly increased to achieve higher activity, which has been demonstrated as an effective method in our previous work[21]. The excellent consistence between simulation and experiments in OER not only proves the validity of our model, but also provides a methodology to deduce elementary surface thermodynamic information of any catalysts from electrochemical data.

Based on previous description, our model should also apply in ORR. Similar kinetic simulation and experimental data for representative ORR catalysts are given in Figure 3-8. Here we present the kinetics for the case of n = 1, 1.5 and 2. For the catalysts with low surface reactivity, O_2 activation becomes the RDS, for which n = 1 well describes the reaction kinetics. Owing to the scaling relationship, the energy barrier for O_2 activation and OH* desorption to form H_2O in ORR would be much higher than the rest steps. Thus, the steps other than O_2 activation and OH* desorption should have little influence on kinetics except for adding two electrons per O_2 reduction[93]. As a result, if the last step becomes the RDS in ORR, the reaction rate cannot be simply described by equation (3-6) using n = 4[98]. Instead, n = 1.5 or 2 should be used to predict the Tafel slope because the middle two steps are much faster than the first and last step in ORR, which gives a Tafel slope of 60 mV/dec (chemical reaction within OH* to produce H_2O as the RDS) or 40 mV/dec. A Tafel slope of around 60 mV/dec at the low overpotential region (120 mV/dec can also be detected at the high overpotential region) is frequently observed on Pt and Pt based catalysts in ORR[99,100], which can be well described by our simulation.

Detailed comparison in Figure 3-8c shows that the macroscopic kinetics for Pt/C and α-MnO_2, two representative catalysts in ORR, can be well described by our kinetic model. In turn, we can assign these two materials in the activity volcano plot as shown in Figure 3-8b. The high surface reactivity of Pt is manifested by its strong OH* adsorption peak and the oxide

formation peak in the CV curve as shown in Figure 4d. On the contrary, α-MnO_2 has weak electrochemical response, consistent with the identified surface reactivity as shown in Figure 4b. Considering metal oxidation and the subsequent dissolution have been identified as the major cause for the activity loss in the long term electrochemical tests[17,101], we can now predict that the most efficient ORR catalyst will not only exhibit better catalytic activity (with smaller Tafel slope about 40 mV/dec) than Pt but also have much improved stability. The improved stability originates from the higher oxidation potential and thus stronger resistance to dissolution.

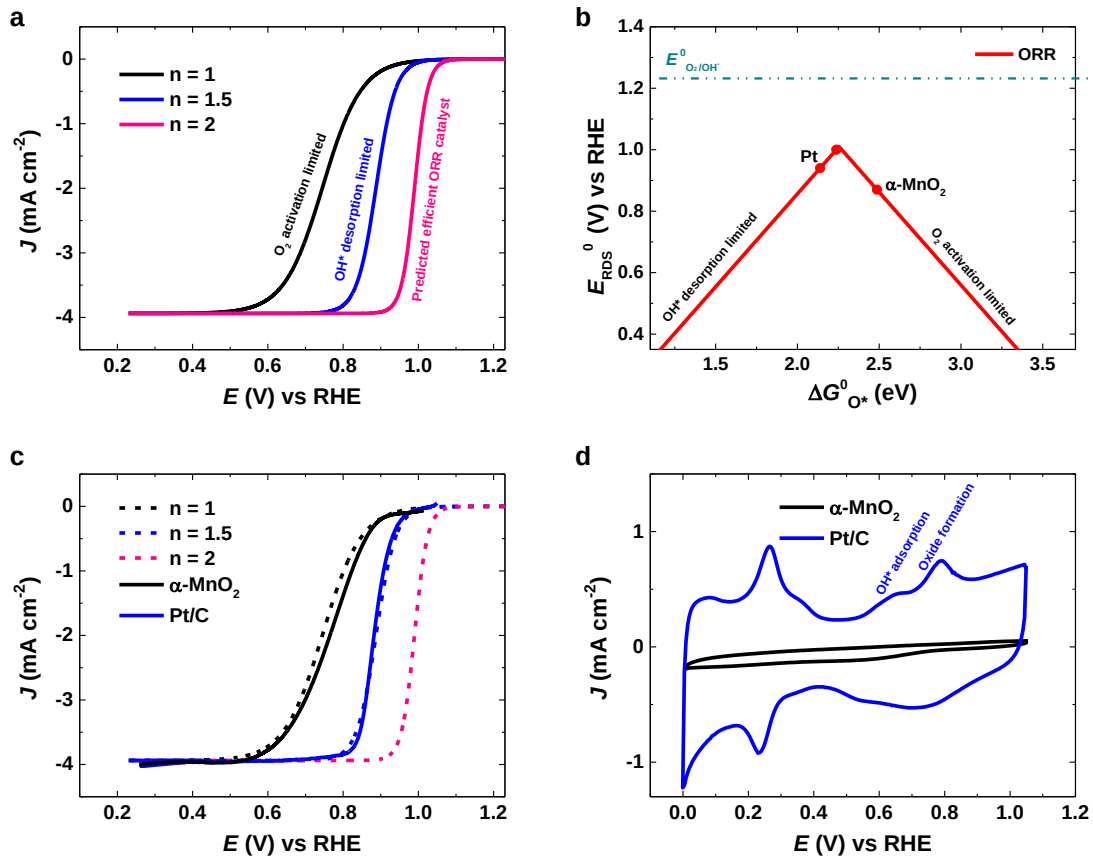

Figure 3-8. Comparison of simulated kinetics with the experimental data for representative ORR catalysts. **a,** Simulated LSV of three representative points as shown in **b**. **c,** Measured LSV of typical Pt/C and α-MnO_2 in ORR. **d,** CV curves of Pt/C and α-MnO_2 in N_2 saturated solution.

Based on interpretation of individual OER and ORR, we give our analysis toward their mutual relationship. As discussed previously, the fastest step in ORR should be the RDS of OER assuming RDS is identical to PDS. As illustrated in Figure 1b, OER activity of metal catalysts with high surface reactivity cannot be simply predicted by shifting the position from the ORR volcano plot to the OER volcano plot due to changed surface property in OER working condition. The specific surface reactivity of the corresponding oxide should take into consideration if one intends to derive a good predication. Different from their metal counterparts, transition metal oxides are stable in the usual potential range for both ORR and OER. Thus ORR activity of transition metal oxides can be well predicted by Figure 3-4 through simple shifting, and Figure 3-5b displays the experimental data of common transition metal oxides. Although TMOs show lower ORR activity as compared to the noble metal catalysts e.g., Pt, their intrinsic stability and potential role in stabilizing metals during ORR are attractive[102].

3.4.2 New interpretation of "redox peaks" in CV curves

For CV curves, no special feature for n = 1 in both OER and ORR is expected due to the solely influence of double layer capacitance charging current, which can be visualized from the CV curve of Fe_2O_3 in Figure 3-1. Moreover, very few cases give a redox peak prior to the onset of ORR. The case for n = 3 (should not exist in ORR as analysed in the article) is very complicated and should be based on the case of n = 2. Therefore, we give a detailed interpretation of typical CV curves of n = 2 (or 1.5) in OER, which typically manifest a peak (sometimes multiple split peaks) prior to the onset of OER.

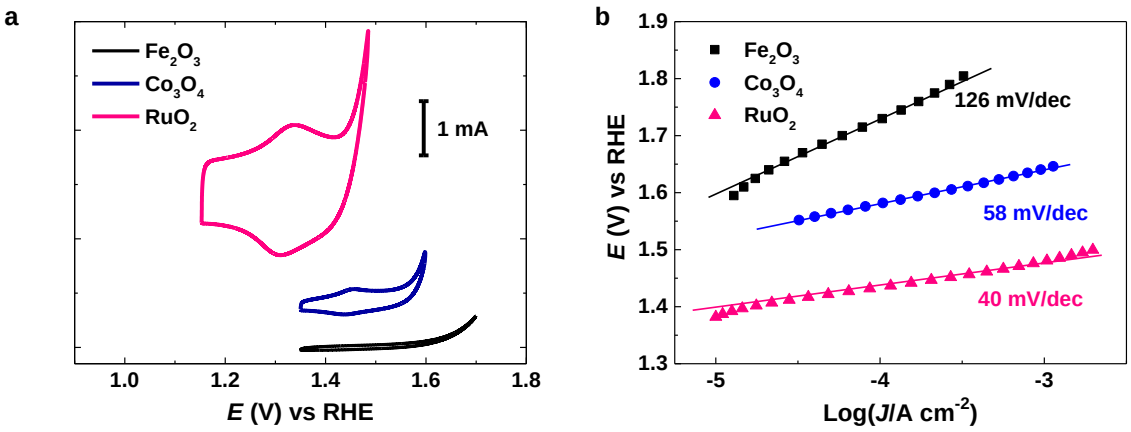

Figure 3-9. CV curves and Tafel plots for typical OER electrocatalysts. With careful comparison, it can be easily observed that the potential range of peaks is not included in the Tafel region. For example, the anodic peak for RuO_2 ends at about 1.4 V vs RHE, at which the linear relation just starts, suggesting that the OH_{ads} under this peak is unreactive intermediates.

In our previous work, we ascribed the peak(s) prior to the onset of OER to the adsorption/desorption of OH* due to its strong correlation with surface reactivity and catalytic activity[21]. Recently, we found more and more evidences suggesting that the OH* is the unreactive intermediates under this potential. Strictly speaking, a surface is spatially different in atomic scale regarding to the chemical reactivity[103,104]. Owing to the existence of different adsorption sites[93], which bind to intermediates with different energy, the intermediates could be adsorbed at different potential range. Peaks associated with underpotential intermediate adsorption/desorption has been extensively reported in hydrogen electrocatalysis on Pt, Pd, and etc[16,80,105]. However, many research works suggest that UPD intermediates are not reactive intermediates in the overall reaction. For example, Markovic and co-workers observed a strong inhibition, instead of strong correlation, of hydrogen oxidation kinetics in the H_{upd} region on Pt surface[16].

Since the surface chemistry of intermediates adsorption/desorption is incredibly complicated, detailed description of all characteristics as observed in the experimental CV curve is beyond the scope of this work. A following work to quantitatively describe the features will be published elsewhere. In this work, we briefly and qualitatively interpreted some typical CV curves based on our understanding. We propose the peaks are associated with adsorption of unreactive intermediates (Figure 3-10). Therefore, under the potential, no net reaction occurs. The overall reaction can only take place at higher overpotential. But we still believe that the CV peaks offer valuable signals of surface reactivity, which can be used as a descriptor to identify surface reactivity of unfamiliar materials. Obviously, the higher the surface reactivity is, the lower potential occurs for OH* adsorption (Figure 3-1 and 3-11). Moreover, the reversibility of OH* adsorption/desorption reflects surface reactivity. For materials with weak surface reactivity, the potential difference between the anodic peak and the cathodic peak is small and the paired peaks show good symmetry (3-1). On the contrary, the materials with high surface reactivity usually manifest asymmetric peaks with large potential difference (Figure 3-11).

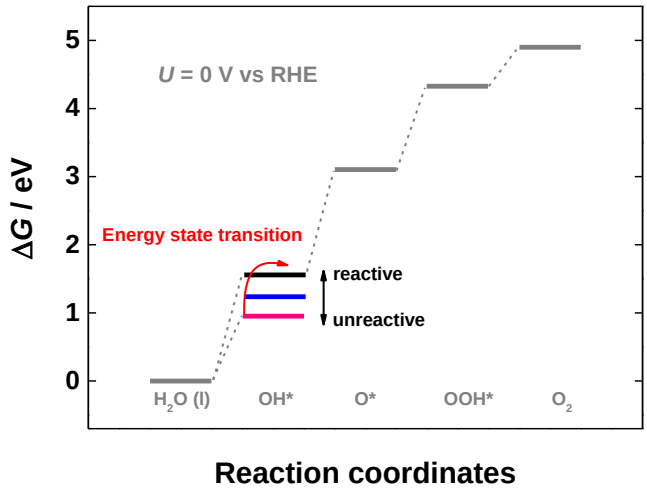

Figure 3-10. Illustration of influence of "unreactive intermediates" on reaction pathway. The intermediate (OH*) will first adsorb on favourite adsorption sites, which prohibits its

evolution to O* due to the strong binding of OH*. But when adsorption of OH* on such favourite sites reaches saturation, the subsequent adsorption of OH* will take the relatively unfavourite sites that have higher energy, or the pre-adsorbed OH* will be transformed into the higher energy state. Then the overall reaction will be energetically feasible to turn over on modified surfaces. But for very reactive surfaces, the adsorption of OH* will induce surface reconstruction or phase transformation as shown in Figure 3-11.

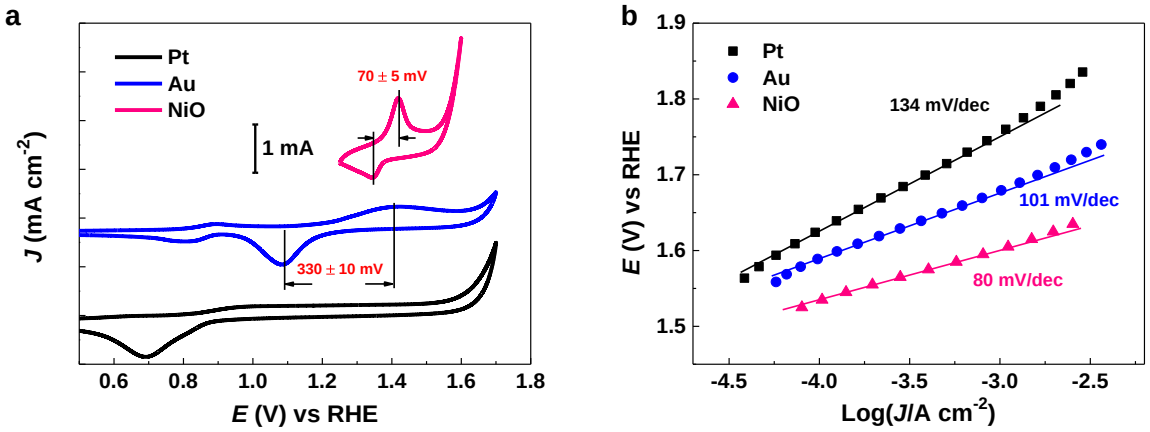

Figure 3-11. Kinetic features for catalysts that undergo serious surface reconstruction or phase transformation. **a, b,** CV and Tafel plots for typical catalysts with high surface reactivity. One obvious characteristic is that the shape of CV curve changes significantly after the first several cycles due to irreversible phase transformation such as NiO[106,107]. Moreover, the peak difference is quite large.

The kinetic behaviour of the materials with high surface reactivity, including some oxides, hydroxides and most transition metals, is no longer simple in OER due to the high positive applied bias. These materials will undergo serious surface reconstruction or oxide formation at high applied potentials. Therefore, the measured activity of transition metals in OER usually reflects the activity of oxidized metal surfaces. This result suggests that not all adsorbed species detected by experiments are reactive intermediates. Inappropriate interpretation of reaction

mechanism with such detected unreactive intermediates could be misleading. Therefore, to get a conclusive reaction mechanism, one need to quantitatively combine spectroscopic investigation with other approaches such as kinetic study and theoretical simulation.

3.4.3 A surface reactivity descriptor

Based on the above analysis, the signals of OH* adsorption/desorption could be used as a surface reactivity descriptor. Figure 3-12 shows the CV curves of some well-studied metals and α-MnO_2, whose adsorption property is uncertain.

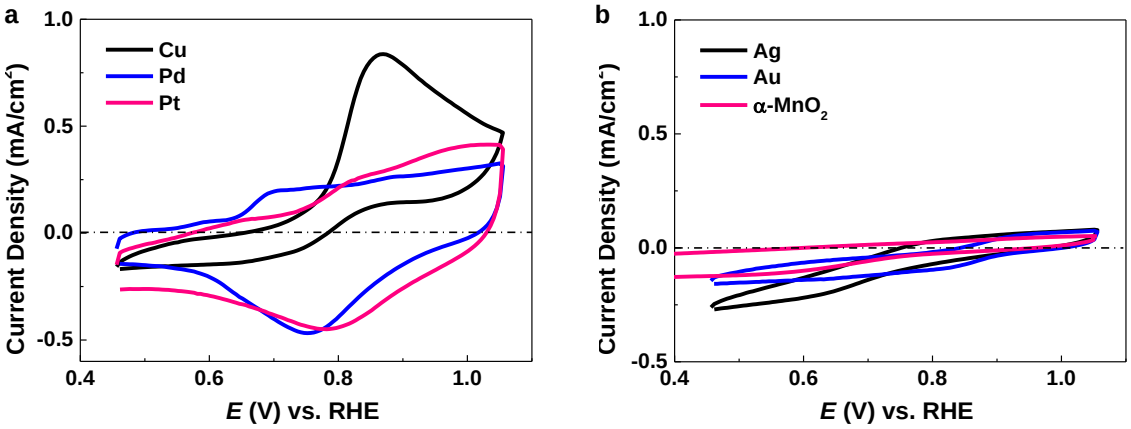

Figure 3-12. CV curves of various materials with different surface reactivity in N_2 saturated solution. The electrodes were prepared by electrodeposition method. The precursor solution for electrodeposition, which contains 0.01 M metal cation such as Cu^{2+}, Pd^{2+}, Ag^{+}, and etc, was prepared by dissolving analytical reagent copper chlorine, palladium(II) chloride, silver nitrate, potassium hexachloroplatinate, and chloroauric acid in ultrapure water (18.2 MΩ, EMD Millipore). Electrocatalyst films were electrodeposited galvanostatically on pre-cleaned substrate such as glassy carbon electrode and fluorine-doped tin oxide (FTO) with a current density of 0.5 mA cm^{-2} for 0.1 μM metal film.

OH* adsorption decreases in the order of Cu > Pd > Pt > Ag > Au, which matches well with the surface reactivity trends reported in the literature[12]. Among the five metals tested, Cu has

the highest surface reactivity and the surface is irreversibly oxidized during the anodic scan. α-MnO_2 shows adsorption property like Ag and Au. Therefore, the surface reactivity of α-MnO_2 should be similar as that of Ag and Au, with activation of O_2 as the RDS in ORR. This prediction is in good consistency with the analysis in the article (see discussion of Figure 3-5).

3.5 Predictive power in developing better catalysts

The basic laws obtained from this work make it possible to uncover the elementary surface thermodynamics of real catalysts. Based on the information, one can anticipate ways to reduce the kinetic barrier to achieve better catalytic activity, which is the ultimate goal of fundamental research in catalysis. A prerequisite to developing better catalysts lies in the capability of rationally tuning the surface thermodynamics. As discovered in our previous work, the surface reactivity of transition metal oxides could be controlled by changing the surface density of coordinatively unsaturated metal (M_{CUS}) cations.[21] This knowledge was developed as an effective method to tune the surface thermodynamics. In this section we present example (α-MnO_2 nanorods) to show how to use the identified elementary thermodynamic information to develop better oxygen electrocatalysts.

With the aid of OER kinetics of α-MnO_2, we successfully identified its associated thermodynamic origin. The Tafel slope (~30 mV/dec)[21] manifests that the RDS of OER for α-MnO_2 with low density of Mn_{CUS} is the chemical reaction between reaction (2) and (3), or the direct recombination of O* to generate O_2. Additionally, the dynamic voltammetry of α-MnO_2 in OER does not show any adsorption peaks of intermediates prior to the OER onset, suggesting that the reaction energy of the steps prior to the RDS on α-MnO_2 is not too much lower than that of the RDS. Based on the above analysis, we proposed the most possible potential energy profile for α-MnO_2 as schematically shown in Figure 3-13a (the corresponding position in activity plot is shown in Figure 3-13b). This model gives the following prediction: to achieve

better catalytic activity in OER, we should reduce the energy gap of step (3); on the other hand, increase in energy gap of step (4) is needed to realize improved ORR activity.

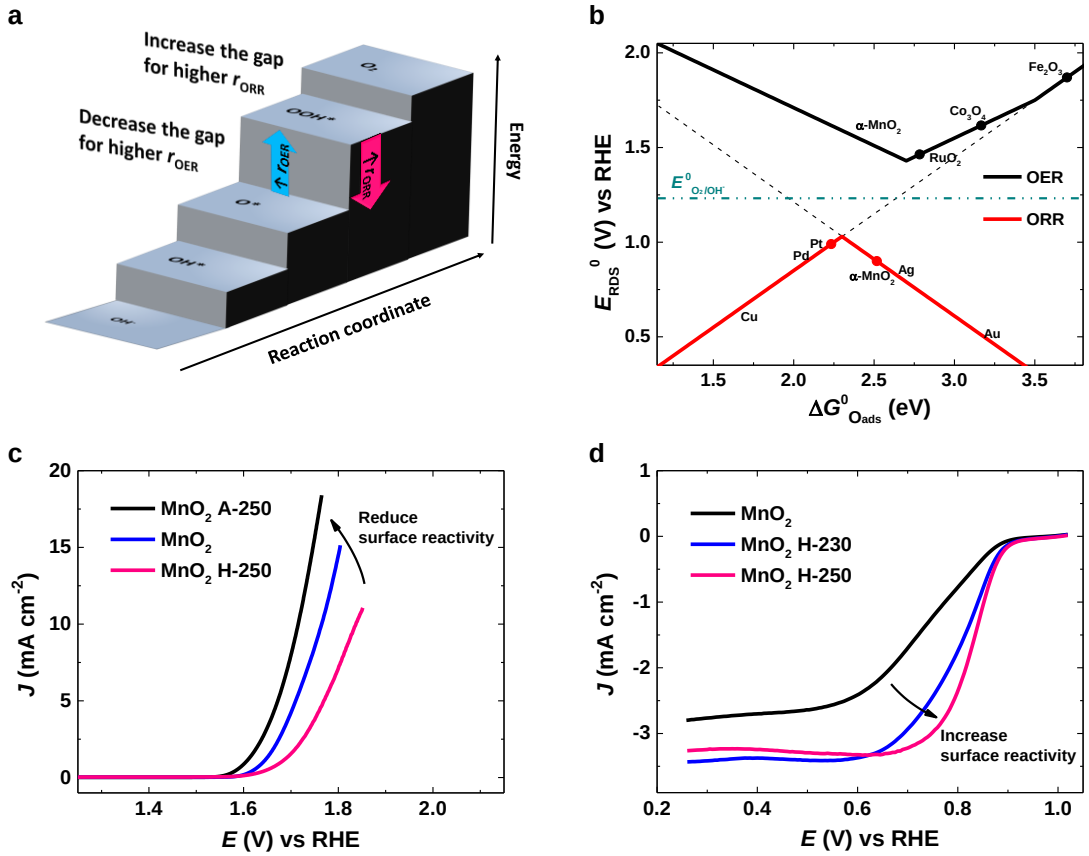

Figure 3-13. Rationally developing better catalysts for oxygen electrocatalysis on nanostructured α-MnO_2 through surface thermodynamic engineering. **a,** Surface thermodynamics of α-MnO_2 nanorods in oxygen electrocatalysis Identified from OER kinetics. **b,** Proposed position of α-MnO_2 in activity volcano plots of OER and ORR. **c,** Rationally developing better OER catalysts based on α-MnO_2. **d,** Rationally developing better ORR catalysts based on α-MnO_2. The samples are named with treatment environment and temperature. Specifically, A and H represent the samples annealed in air and 5% H_2/Ar, respectively, and numbers are the treatment temperature.

Our previous study shows that, by decreasing surface reactivity of α-MnO_2, the OER kinetics can be significantly improved (Figure 3-13c)[21]. As predicted from Figure 3-13 a & b, reaction (4) is the fastest step in OER for α-MnO_2 because of the lowest reaction energy. Hence, it is deduced that the RDS in ORR for α-MnO_2 would be the adsorption (activation) of O_2. In order to break the surface thermodynamic limitation, it is necessary to increase the energy gap between OOH* and O_2. Since O_2 is the reactant, whose energy is constant, it is only possible to decrease the energy of OOH* (by increasing surface reactivity). By doing that, although all other intermediates also bind more strongly on the catalyst surface, the most significant effect on the overall kinetics is the increase of the rate of RDS. Our experiments well verified the prediction from our model. The ORR activity for α-MnO_2 can be remarkably improved by increasing surface reactivity. The significantly improved performance of α-MnO_2 through our prediction and the subsequent experimental verification demonstrate the predictive power of our theoretical model.

3.6 Conclusion

In order to acquire more complete and conclusive elementary thermodynamic information for catalyst design, we need not only combine the study of OER and ORR together, but also integrate the valuable outcome of kinetic study, spectroscopic detection and theoretical simulation. This work offers the first attempt to quantitively resolve the elementary surface thermodynamic information of oxygen electrocatalysis from kinetic data. Predictive power of the mechanistic information derived from our model has been proved on α-MnO_2 as an example to develop better oxygen electrocatalysts. However, we should say the model/methodology developed in this work is far from perfect. Instead, this is a starting point of quantitatively resolving underneath elementary processes for catalyst design. Subsequent work is necessary

to improve the description of experimental data and make more instructive predictions for the design of better catalysts.

Chapter 4. Origin of inconsistence between exchange current density with activity in oxygen electrocatalysis

Exchange current density has been used to represent activity in hydrogen electrocatalysis. However, in oxygen electrocatalysis, including both oxygen evolution reaction (OER) and oxygen reduction reaction (ORR), exchange current density usually does not correlate with catalytic activity. Here we present a detailed study on this issue to identify the origin of the anomalistic phenomena. Through comparison with kinetic behaviour of hydrogen electrocatalysis we prove that kinetics of oxygen electrocatalysis and other highly irreversible reactions are predominantly dependent on Tafel slope, instead of exchange current density. Low Tafel slope of good catalysts originates from the collective contribution from RDS and pre-adsorbed intermediates prior to RDS, which also causes orders decrease in exchange current density predicted from Tafel plots.

4.1 Introduction

One primarily goal in electrocatalyst design is to minimize overpotential, which is determined by exchange current density and Tafel slope[93]. An ideal electrocatalyst should be equipped with exchange current density as high as possible and Tafel slope as low as possible at the same time (see Tafel equation)[108]. The case is simple in hydrogen electrocatalysis, where a better catalyst usually has higher exchange current density and lower Tafel slope. The consistence between the two determining factors of activity makes it feasible to use exchange current density to represent overall catalytic activity. Therefore, the well-known activity volcano plots of hydrogen electrocatalysis based on this descriptor gives a good rationale of experimental trends and still serve as a basic principle in catalyst design of hydrogen electrocatalysts[109,110].

Tafel equation: $\eta = b[\log(J) - \log(J_0)]$

where J_0 is exchange current density, J is current density at overpotential η, b is Tafel slope.

However, in oxygen electrocatalysis, only Tafel slope usually correlate with overall catalytic activity, where good catalysts have low Tafel slope[21]. But an obviously better catalyst (with much lower overpotential) may manifest orders of magnitude lower exchange current density and this trend is general in both OER and ORR. This anomalous phenomenon makes it inappropriate to use exchange current density to describe activity trends in oxygen electrocatalysis. Thus, the activity volcano plots in OER and ORR are based on the overpotential at a certain current density[25,111] or thermodynamic overpotential[9,12]. The inconsistence between exchange current density with catalytic activity was firstly depicted by Conway *et al* as early as 1987 and a suggestion was proposed that Tafel slope is more suitable to describe catalytic activity[112]. But the origin of the inconsistence still remains elusive, which leaves an unanswered question: how to balance exchange current density and Tafel slope in designing a new catalyst?

4.2 Experimental details

4.2.1 Catalyst synthesis and electrode preparation

The synthesis methods for Fe_2O_3, Co_3O_4, NiO and α-MnO_2 catalysts are the same as those used in our previous work[21]. RuO_2 nanoparticles were prepared according to a reported method[87]. Pt/C (20% Pt on Vulcan XC-72) was purchased from Premetek. To prepare a working electrode, the catalysts were first dispersed in an isopropyl alcohol (IPA)/water (v : v = 1 : 1) solution with a concentration of 2 mg/ml. The mixture was sonicated for 3 h, and subsequently, 10 μl of the solution was drop-casted onto a pre-cleaned glassy carbon (GC) rotating disk electrode (0.196 cm^2). The electrode was dried in atmosphere overnight before electrochemical test. The metal electrodes used in ORR (Figure 2) were prepared by electrodeposition method. The

precursor solution for electrodeposition, which contains 0.01 M metal cation was prepared by dissolving analytical reagent copper chlorine, palladium(II) chloride, silver nitrate, and potassium hexachloroplatinate in ultrapure water (18.2 MΩ, EMD Millipore). Electrocatalyst films were electrodeposited galvanostatically on pre-cleaned glassy carbon electrode with a current density of 0.5 mA cm^{-2} for 0.1 μM metal film assuming 100% faradaic efficiency.

4.2.2 Electrochemical studies

Electrochemical tests were conducted on an Autolab PGSTAT 30 with a three-electrode configuration. Specially designed glass-free cell, reference and counter electrodes (provided by Hangzhou Saiao Electrochemical Technology Co., LTD) were used in all electrochemical tests to eliminate the influence of glass components on the activity of catalysts[88]. Saturated calomel electrode (SCE, 0.241 V vs. SHE (standard hydrogen electrode)) was used as the reference electrode, while polished high surface Titanium plate (~10 cm^2) was applied as the counter electrode. The electrochemical tests were conducted at a rotating speed of 1600 rpm in 1 M KOH electrolyte (pH = 13.72) to minimize mass transport limit. To reduce the effects of impurities, high purity KOH (semiconductor grade, 99.99% trace metals basis) was used throughout the electrochemical tests. All polarization curves were corrected by eliminating the *iR* drop in the electrical circuit. Relatively low scan rate (1 mV s^{-1}) was employed to reduce the contribution of non-faradic current to the current of polarization curves. The series resistance (R_s), mainly originated from ionic conduction in the electrolyte, is in the range of 5.5 to 7.0 Ω. The potentials of polarization curves were compensated based on the following equation: $V_{RHE} = V_{SCE} + 0.241 + 0.059 * pH - R_s * i$.

4.3 Results and discussion

Here we explore in detail the origin of the general inconsistence between exchange current density and catalytic activity in oxygen electrocatalysis. We start with a glance of the

phenomena by a simple comparison between hydrogen electrocatalysis and oxygen electrocatalysis on their representative catalysts. Linear sweep voltammetry (LSV) curves in Figure 1 (a, b) show the kinetics of best catalysts in hydrogen and oxygen electrocatalysis. HER and HOR (hydrogen oxidation reaction) kinetics on Pt/C is quite fast as the current density reaches appreciable value within just several tens of mV, suggesting the hydrogen electrocatalysis on Pt/C is approaching reversible. However, the overpotential in both OER and ORR is much higher, more than 250 mV is needed to drive oxygen electrocatalysis even on the best catalysts. Another frustrating result is that best catalysts in oxygen electrocatalysis are only good in one specific reaction such as Pt/C efficient in just ORR but sluggish in OER, inverse activity is found on RuO_2. The high specificity together with high overpotential make oxygen electrocatalysis highly irreversible.

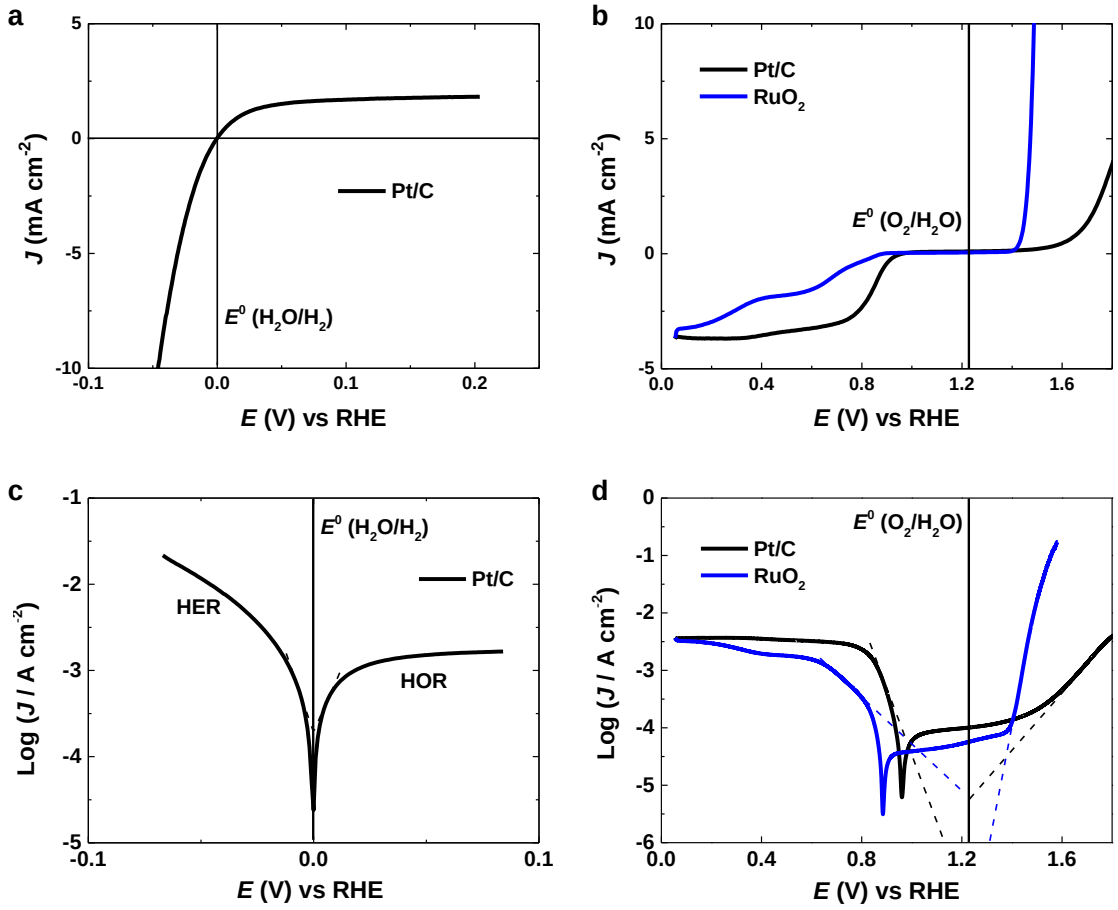

Figure 4-1. Electrochemical kinetics of the best catalysts in hydrogen and oxygen electrocatalysis. (a) LSV of Pt/C in hydrogen electrocatalysis. (b) LSV of Pt/C and RuO_2 in oxygen electrocatalysis. (c) Tafel plot of Pt/C in hydrogen electrocatalysis. (d) Tafel plot of Pt/C and RuO_2 in oxygen electrocatalysis. Electrochemical tests of hydrogen (oxygen) electrocatalysis were done in 1 M KOH purged with H_2 (O_2). All the LSV curves were collected by scanning from negative to positive potential with a scan rate 1 mV/s on RDE, 1600 rpm.

The high catalytic activity on Pt/C stem from high exchange current density (on the order of 10^{-4} A/cm^2) and low Tafel slope (35~45 mV/dec). However, the contribution from exchange current density and Tafel slope in oxygen electrocatalysis is inconsistent on the two representative catalysts. Relatively fast kinetics in oxygen electrocatalysis are positively contributed by low Tafel slope, but negatively contributed by low exchange current density. For example, good activity of RuO_2 in OER is positively contributed by low Tafel slope (~ 40 mV/dec), but negatively contributed by very low exchange current density (~10^{-9} A/cm^2). Although RuO_2 has 4 orders of magnitude higher exchange current density in ORR (~10^{-5} A/cm^2), the high Tafel slope in ORR (160 mV/dec) renders its overall low activity in ORR. Same trend is found on Pt/C. the inconsistence between overall catalytic activity with exchange current density means that overall catalytic activity in oxygen electroctalysis is predominantly influenced by Tafel slope, which should overcome the overpotential cost by low exchange current density to ensure the overall good activity. The inconsistence has been observed on representative catalysts in oxygen electrocatalysis, but is this phenomenon general in oxygen electrocatalysis? The trend on more catalysts is examined as shown in Figure 2.

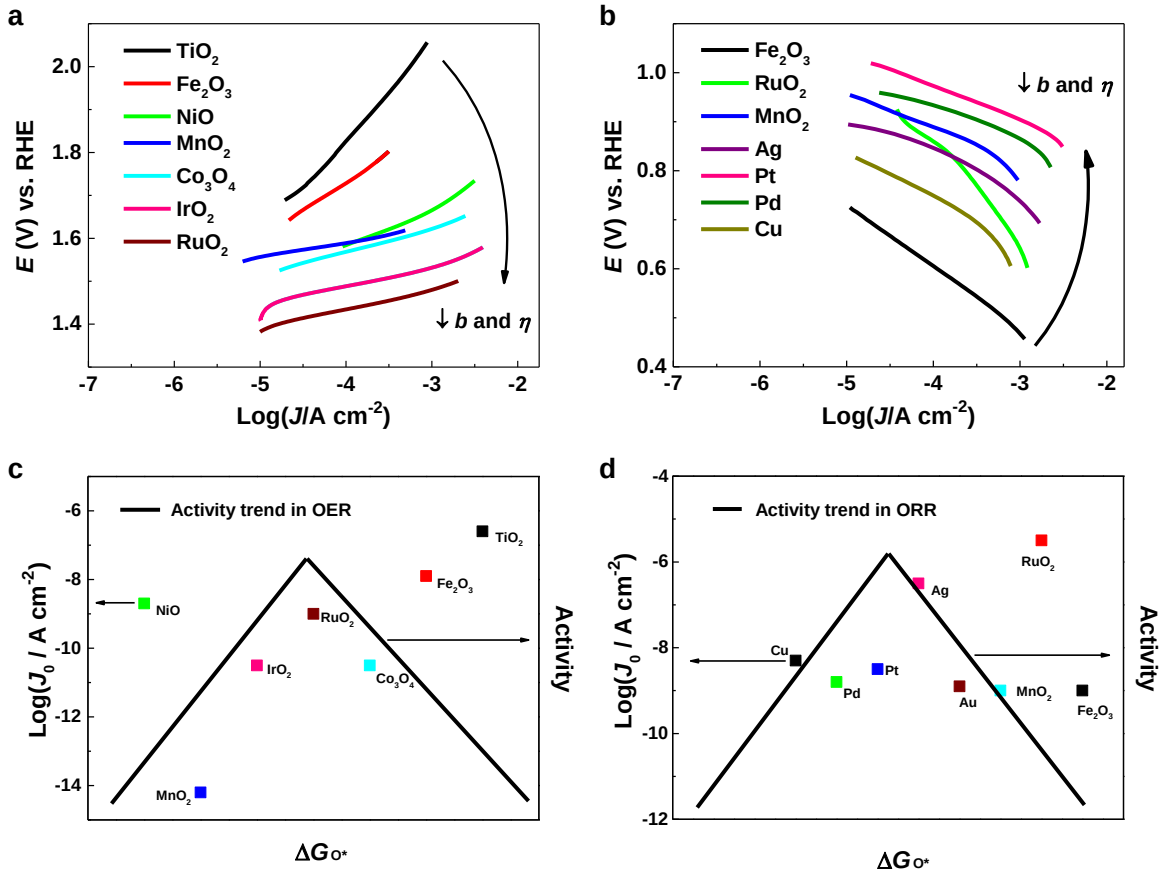

Figure 4-2. Collection of Tafel plots and derived exchange current density of representative catalysts in oxygen electrocatalysis. (a) Tafel plots of representative catalysts, mainly metal oxides, in OER. (b) Tafel plots of representative catalysts, mainly consist of metals and some metal oxides, in ORR. Arrows in (a, b) show the consistent trends of decreasing Tafel slope and overpotential. (c, d) Trend comparison between exchange current density with activity of representative catalysts in oxygen electrocatalysis.

Firstly, we can obtain basic activity trends and kinetic features in oxygen electrocatalysis from Tafel plots in Figure 2 (a, b). The equilibrium potential of oxygen electrocatalysis is 1.23 V vs RHE, higher than which is the region that OER take place and lower than which is the overpotential region that ORR happen. Unfortunately, almost no catalysts show significant current density at overpotential within 200 mV in neither OER, nor ORR, which accounts for

the major efficiency loss in electrochemical energy conversion devices that involve oxygen electrocatalysis as half reaction. Lowest overpotential in OER is only achieved on precious metal oxides such as RuO_2 and IrO_2, whereas earth abundant transition metal oxides either manifest medium activity (Co_3O_4, MnO_2 and NiO) or very low activity (Fe_2O_3 and TiO_2). Precious metals such as Pt and Pd can catalyse ORR reactions at highest potential region (lowest overpotential). Less expensive metals and metal oxides usually show significantly higher overpotential in ORR. An obvious kinetic feature of both OER and ORR in general is that better catalysts have lower Tafel slope, demonstrating the clear positive contribution from Tafel slope to overall kinetics. The trends of exchange current density should be separately presented to distinguish its contribution to overall kinetics.

Considering activity volcano plots based on adsorption free energy of oxygen intermediate (ΔG_{O*}) give an excellent rationale of experimental trends of catalytic activity in oxygen electrocatalysis[9,12], we plot the exchange current density with ΔG_{O*} in Figure 2 (c, d) to distinguish its contribution to overall activity. However, exchange current density of the representative catalysts in both reactions are disorderly distributed compared with volcano trend of catalytic activity, suggesting exchange current density fails to describe the activity in oxygen electrocatalysis in general. The only trend in general is that the relatively low exchange current density is usually obtained on catalysts with relatively low Tafel slope. The anomalous trends in exchange current density means that it is not appropriate to use exchange current density to describe activity trends in oxygen electrocatalysis.

Since the overall kinetics are contributed by the two parameters inconsistently, the specific contribution should be clearly and strictly distinguished from its original form, Tafel equation. Based on Tafel equation we give a strict mathematical analysis to identify the individual contribution to overpotential from exchange current density and Tafel slope. Here we consider three typical Tafel slope: 120, 60, and 40 mV/dec to represent poor, medium and good catalysts

respectively. According to experimental trends in exchange current density, exchange current density is inversely proportional with their catalytic activity, say, 10^{-5}, 10^{-7}, 10^{-9} A/cm^2 for the poor, medium and good catalysts respectively. From Tafel equation we can distinguish the specific contribution of exchange current density and Tafel slope to overall electrochemical kinetics as shown in Figure 3.

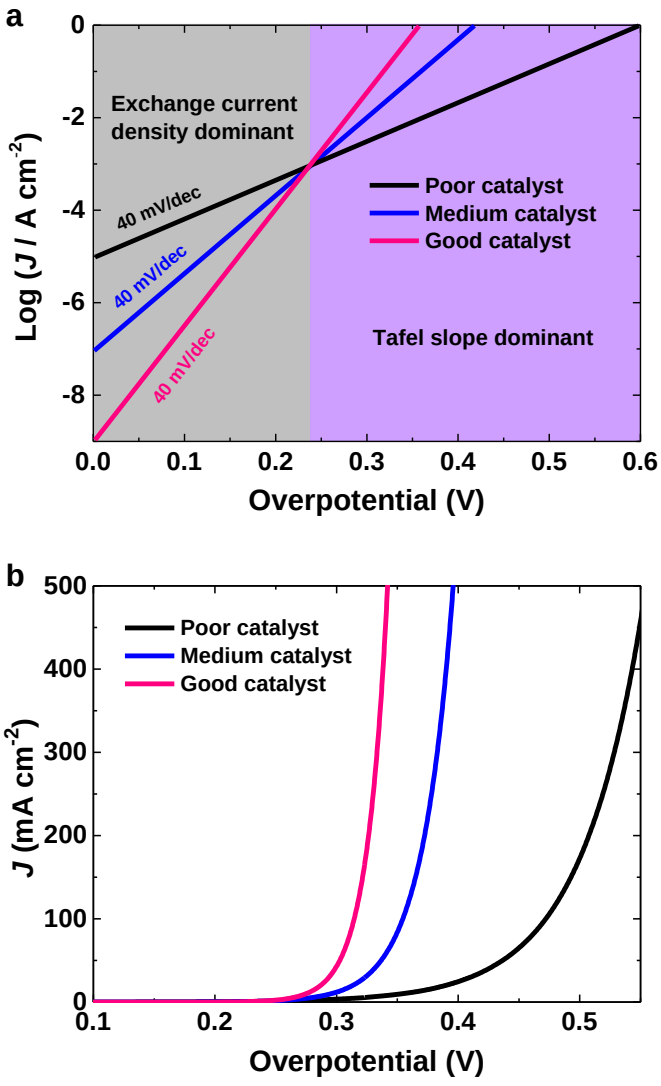

Figure 4-3. Mathematical analysis of the overpotential contribution from exchange current density and Tafel slope. (a) Simulated Tafel plots and (b) Simulated LSV curves for the three typical catalysts with different exchange current density and Tafel slope. Mass transport

influence has not been taken into consideration in the kinetic simulation as it has same influence on three kinds of catalysts.

Obviously, the intersection point (240 mV) in Tafel plots (Figure 3 (a)) divides the kinetics into two regions: at low overpotential range the current density are dominated by exchange current density, whereas at high overpotential region overall kinetics are dominated by Tafel slope. For irreversible reactions such as oxygen electrocatalysis, significant reaction rate could only be achieved at relatively high overpotential range than 240 mV. Thus, the overall kinetics are dominated by Tafel slope, which can be clearly observed from simulated LSV in Figure 3 (b) where current density at visible range only positively depends on Tafel slope. Unlike oxygen electrocatalysis, hydrogen electrocatalysis and other relatively reversible catalytic reactions usually need operate at much lower overpotential range, say, 100 mV. Thus, the overall kinetics of the relatively reversible reactions are exclusively dominated by exchange current density, demonstrating the validity of using exchange current density to describe overall activity.

So far, we have proven the overall kinetics of oxygen electrocatalysis and hydrogen electrocatalysis are dominated by different parameters from mathematical respect. But a mechanistic question arises: why exchange current density is in general inconsistent with overall activity? This question could only be clearly answered by combining the traditional kinetic model[80] with latest thermodynamic information on elementary steps from Density Functional Theory (DFT) simulation[12,43,110].

The DFT simulation by Norskov and Rossmeisl *et al* suggests that the irreversibility of oxygen electrocatalysis stem from the substantial deviation of thermodynamic potential of elementary step from ideal value (1.23 V vs RHE for each electron-transfer step). The best catalysts such as RuO_2 in OER and Pt in ORR all have more than 300 mV deviation in potential determining step (PDS) from this ideal value[9,12]. Moreover, the scaling relationship between

adsorbed intermediates renders it impossible to tune thermodynamics of each elementary step independently[78]. The scaling relationship results in the optimal adsorption energy for OER catalyst is significantly higher than that for ORR catalyst. Therefore, the best catalysts in OER and ORR should have quite different surface reactivity. That's why good OER catalysts are mainly metal oxides whose surface reactivity is in general lower than metals that usually used in ORR. So, within the constraint of the scaling relationship it is impossible for a catalyst to reach highest activity in both reactions, which is the origin of the specificity in oxygen electrocatalysis.

Although DFT simulation straightforwardly provide thermodynamics information of elementary steps, which is hard to obtain from traditional kinetic modelling or experimental techniques, many experimental kinetic features still can't be directly interpreted with DFT simulation results such as Tafel slope and predicted rate determining step (RDS)[98]. Traditional kinetic model describes kinetics on overall equilibrium potential, thus it can't resolve how each elementary step contributes overall kinetics. Here we combine the outcomes from two approaches to identify the influence of the thermodynamics of elementary steps on overall kinetics. Assuming the activation energy of each elementary step scales with the reaction energy in the linear Brønsted–Evans–Polanyi (BEP) relationship[45,65]. Thus, our analysis is simplified as PDS also becomes RDS.

Using OER as an example we can clearly identify the origin of low exchange current density for good catalysts. Firstly, we define catalyst I and catalyst II to represent typical good and poor catalysts in OER respectively. From traditional kinetic respect, catalyst I has high Tafel slope and catalyst II has low Tafel slope. From thermodynamic respect, catalyst I has high equilibrium potential of PDS, whereas that of catalyst II should be low. Combining above kinetic and thermodynamic features we can specify the details of the representative catalysts. For catalyst I, Tafel slope is 120 mV/dec and $E_1^0 = 1.75$ V vs RHE. For catalyst II, Tafel slope

is 40 mV/dec, and $E_2^0 = 1.45$ V vs RHE and its first step $E_1^{0\prime} = 1.40$ V vs RHE. The reason why first step as PDS should have much higher equilibrium potential than second step has been well illustrated by Koper in a theoretical analysis[43].

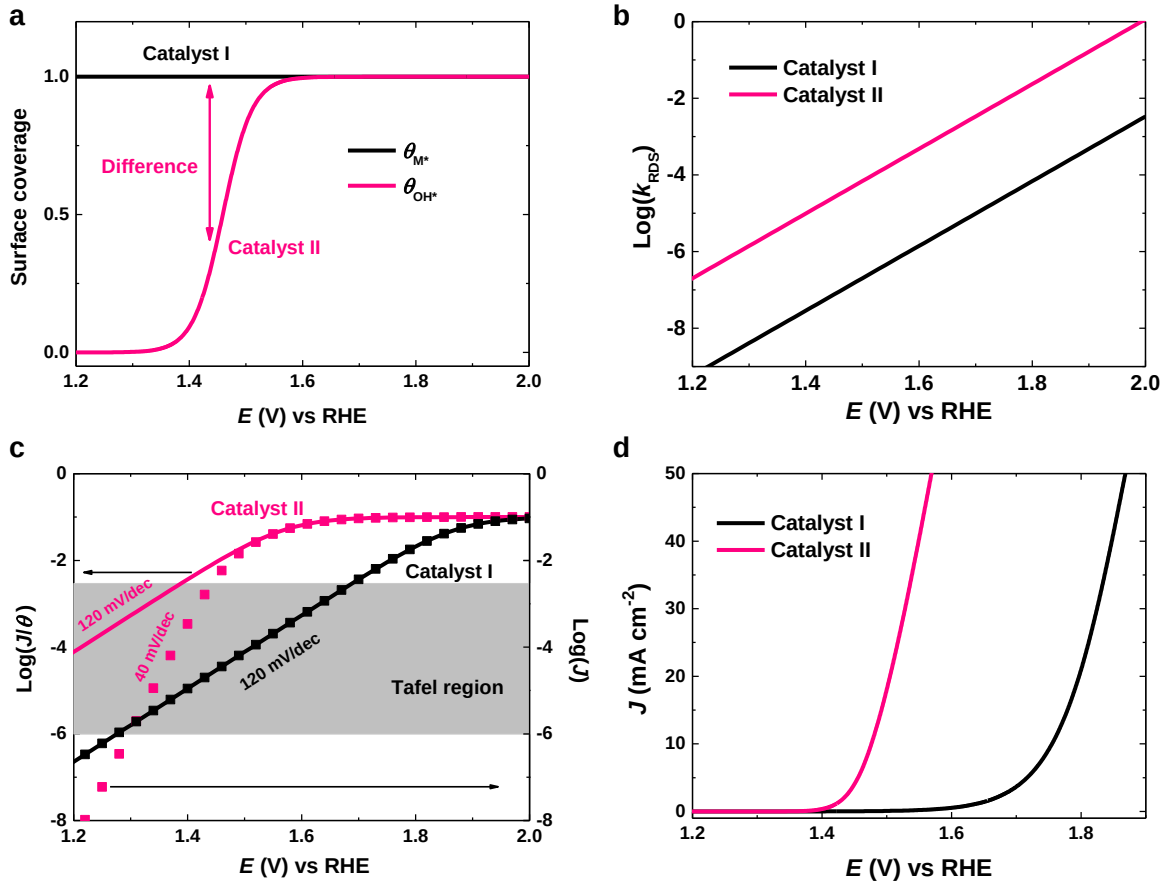

Figure 4-4. Influence of surface coverage of adsorbed intermediate on Tafel plots. (a) Surface coverage of adsorption sites and OH* with potential. (b) Variation of rate constant for RDS (k_{RDS}) with potential. (c) Simulated kinetics showing the influence of the surface coverage. Solid lines are log(J/θ) and scatters are log(J) for the catalysts. Tafel region is shown according to experimental data. The mass transport influence on overall kinetics in the simulation has been taken into consideration[97]. The value of slope (dE/dlog(J/θ) and Tafel slope, dE/dlog(J)) for each catalyst is shown for comparison. (d) Simulated LSV curves.

Considering a general reaction pathway in OER, the first two steps are:

$$M^* + OH^- \quad \rightleftarrows \quad M - OH^* + e^- \tag{1}$$

$$M - OH^* + OH^- \quad \rightleftarrows \quad M - O^* + H_2O + e^- \tag{2}$$

If the first step as RDS, the velocity of RDS is given by:

$$v_1 = k_1 \, \theta_{M^*} a_{OH^-} \tag{3}$$

Where a_{OH^-} is activity of reactant (OH^-), taken as 1 for 1 M KOH solution, θ_{M^*} is unity for this case[96].

If the second step as RDS, the velocity of RDS is given by:

$$v_2 = k_2 \, \theta_{OH^*} a_{OH^-} \tag{4}$$

Where θ_{OH^*} can be solved from quasi-equilibrium treatment of first step as it is much faster than RDS[96,97].

$$\theta_{OH^*} = 1 - \frac{1}{1 + K_1^0 e^{\frac{F(E - E_1^0)}{RT}}} \tag{5}$$

The rate constants depend on the overpotential of individual elementary steps:

$$k_i = k_i^0 * e^{\frac{\alpha F(E - E_i{}^0)}{RT}} \tag{6}$$

Assuming $k_1^0 = k_2^0$ for strict comparison, then the rate constants are exclusively dependent on the difference between applied potential with equilibrium potential (overpotential of elementary step) of the RDS as shown in Figure 4 (b).

At low current density range that mass transport limitation has neglectable influence on overall kinetics, the steady state current density of the overall reaction is described by:

$$J = 4Fv_i \tag{7}$$

Simulated surface coverage in Figure 4 (a) shows that θ_{OH^*} increases rapidly with applied potential before saturation ($\theta_{OH^*} = 1$). The difference between θ_{OH^*} and 1 causes deviation

between log(J) and log(J/θ) for catalyst II, whereas that for catalyst I are well overlapped due to unity value of θ_{M^*} (Figure 4 (c)). The comparison between log(J) and log(J/θ) clearly shows that the Tafel slope for good catalysts is contributed by RDS and fast step prior to RDS, which means it is a collective effect. In fact, rate constant for RDS (k_{RDS}) is the primary factor in defining catalytic activity as the low coverage of OH* at low potential region actually reduces current density of catalyst II. But exchange current density predicted from Tafel plot of catalyst II shifts to several orders lower, which results even lower exchange current density than catalyst I. Therefore, the influence of pre-adsorbed intermediates for good catalysts is that the Tafel slope becomes lower, whereas exchange current density also shifts to lower value. However, the overall current density at high overpotential region is still dominated by reaction rate of RDS (Figure 4(d)). This is the origin of the inconsistence between exchange current density and catalytic activity.

4.4 Conclusion

Therefore, for oxygen electrocatalysis and other highly irreversible reactions, directly compare exchange current density for different catalysts that have different Tafel slope couldn't provide any conclusive physical meaning. This is because pre-adsorbed intermediates greatly reduce the exchange current density predicted from Tafel plots. Tafel slope is a good activity descriptor because low Tafel slope usually correlate with low overpotential of PDS. Thus, we could safely conclude a better catalyst in irrerversible reactions such as oxygen electrocatalysis should have lower Tafel slope, developing a catalyst with such kinetic features should start from the surface property to control the thermodynamics of elementary steps.

Chapter 5. Conclusion

5.1 M_{CUS} as a surface reactivity descriptor for TMOs in OER

What's the major problem for the rational catalyst design in OER?

Known as the Sabatier principle in heterogeneous catalysis, surface reactivity determines catalytic performance, which has been accepted over a century. But for transition metal oxides (TMOs), the fundamental relation between surface reactivity and the structure and composition remains elusive. TMOs constitute a major group of catalysts for a number of important reactions, such as the oxygen evolution reaction (OER), one of the most intensively studied electrochemical reactions, which can be found in numerous energy related applications. As a result, rational catalyst design in OER is hampered by undiscovered surface reactivity descriptor for TMOs.

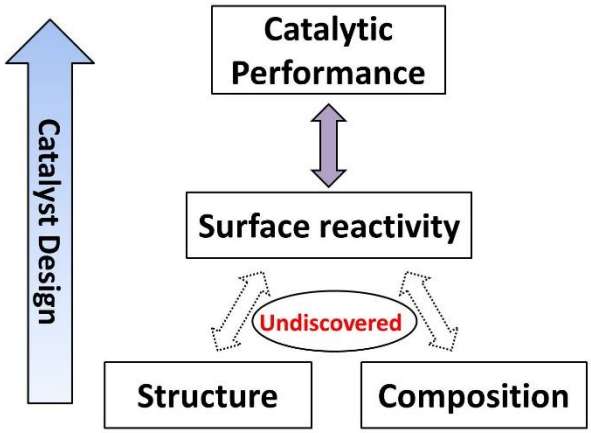

Scheme 5-1. A general outline of catalyst design.

Then why the identification of surface reactivity descriptor is so difficult?

The identification of surface reactivity descriptor for TMOs is primarily prohibited by vast divergence in electronic structure of TMOs[47]. Many TMOs usually could be stably existed in different phases. For example, TiO_2 has rutile, anatase and brookite structure. Moreover, due

to the intrinsic property of d electrons, the metal cations can manifest different oxidation states. For instance, the oxidation state of Mn in manganese oxides can be +2, +3, +4, +6, and +7. Such a divergence makes the property of one oxide to the next very different. Therefore, comparison between oxides to get conclusive trends becomes almost impossible. In our reseach, we identified a general and tunable surface structure, coordinatively unsaturated metal cation (M_{CUS}), could be used to continuously tune electronic structure of a TMO. The strong dependence of surface reactivity on M_{CUS} suggests it can be a good surface reactivity descriptor for TMOs. Surface reactivity of a TMO increases monotonically with the density of M_{CUS} ($[M_{CUS}]$) at the surface; hence increase $[M_{CUS}]$ improves the catalytic activity for weak-binding oxides but impairs that for strong-binding oxides. Based on this surface reactivity descriptor, a rational catalyst design principle is proposed in Figure 5-1.

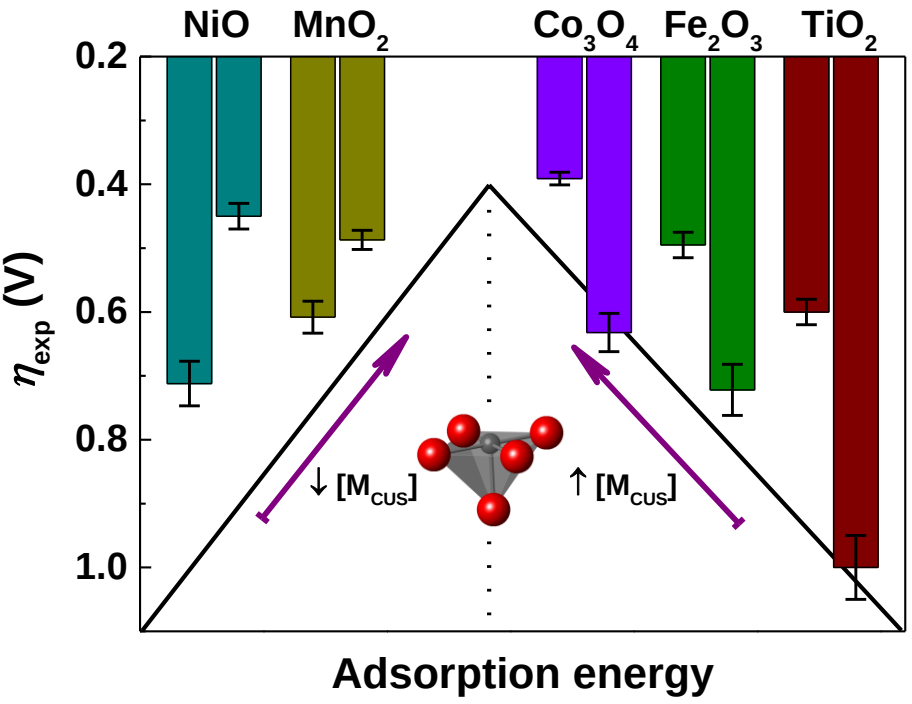

Figure 5-1. Rational catalyst design principle in OER by tuning $[M_{CUS}]$ on TMOs surfaces. To highlight the influence of M_{CUS} on catalytic activity, only the overpotential of TMOs with the highest and the lowest $[M_{CUS}]$ are shown for comparison. The arrows indicate the rational

optimization direction: increase [M_{CUS}] for the TMOs on the right (weak binding), while reduce [M_{CUS}] for the TMOs on the left (strong binding). The η_{exp} for Fe_2O_3 refers to *current density* = 1 mA cm^2, while that for the rest TMOs correspond to *current density* = 10 mA cm^{-2}.

5.2 Electronic structural origin of the surface reactivity descriptor

What's the electronic origin of the surface reactivity descriptor? Why could M_{CUS} well describes surface reactivity trends for TMOs?

The success in identification of the descriptor is attributed to the predictable variation of the electronic structure that determines reactivity through tuning [M_{CUS}] on a TMO surface, which makes it easier to identify the origin of surface reactivity. Thus, an electronic structure model is proposed to describe the observed trends. In this model, the energy of the highest occupied d-states of TMOs relative to Fermi level determines the bonding strength of adsorbates by affecting the filling of antibonding states. In other words, the energy gap between the highest occupied d-states with Fermi level could be the origin of surface reactivity. As illustrated in Scheme 5-2, the larger the energy gap, the higher filling of antibonding states in the bond of adsorption.

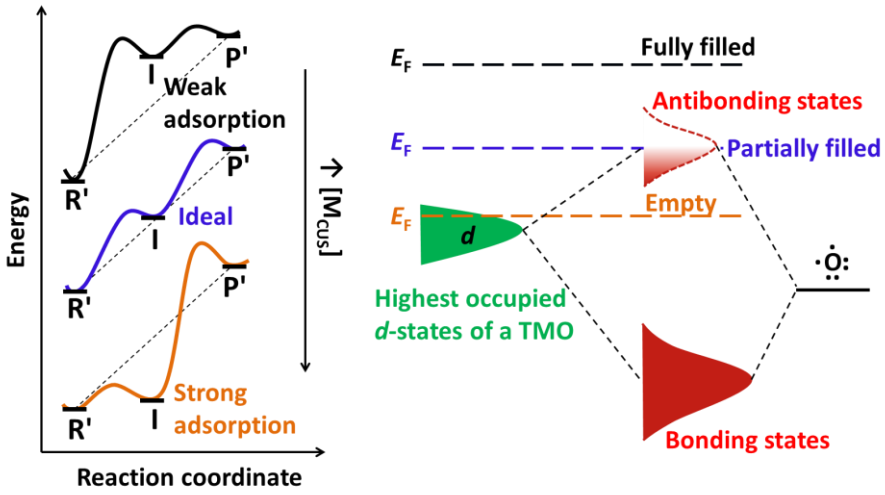

Scheme 5-2. A general outline of catalyst design.

Our model not only well-describes the reactivity trends caused by [M_{CUS}], but also successfully rationalizes the surface reactivity of various TMOs for the first time. For example, a surface with higher [M_{CUS}] correspond to the lower energy gap between the highest occupied d-states with Fermi level, thus the antibonding states are less filled and the bonding is stronger. For the surface reactivity difference between TMOs, our model also gives a good rationale of why p-type TMOs usually have higher surface reactivity than n-type TMOs. The exploration of electronic origin would greatly promote current understanding of surface chemistry for TMOs.

5.3 An electrochemical method for evaluating surface reactivity

Different from heterogenous catalysis that happen on gas-solid interfaces, in which the adsorption of intermediates could be detected by many *in-situ* methods, the adsorption energy of the intermediates in electrocatalysis is very difficult to measure as the catalyst surface is buried in liquid. Therefore, until today there is still no direct methods to measure the bond strength between adsorbates with catalyst surface in electrocatalysis.

In this project, we also developed a method to evaluate the surface reactivity of a material by electrochemical methods. As shown in equation 5-1, the difference in adsorption energy would result in difference in the coverage of adsorbates. Thus, we can use surface coverage as a descriptor for adsorption energy and surface reactivity. Surface reactivity determined coverage of intermediate is illustrated in Scheme 5-3.

$$\theta \propto \exp(\frac{\Delta H_{ads}}{RT}) \qquad (5\text{-}1)$$

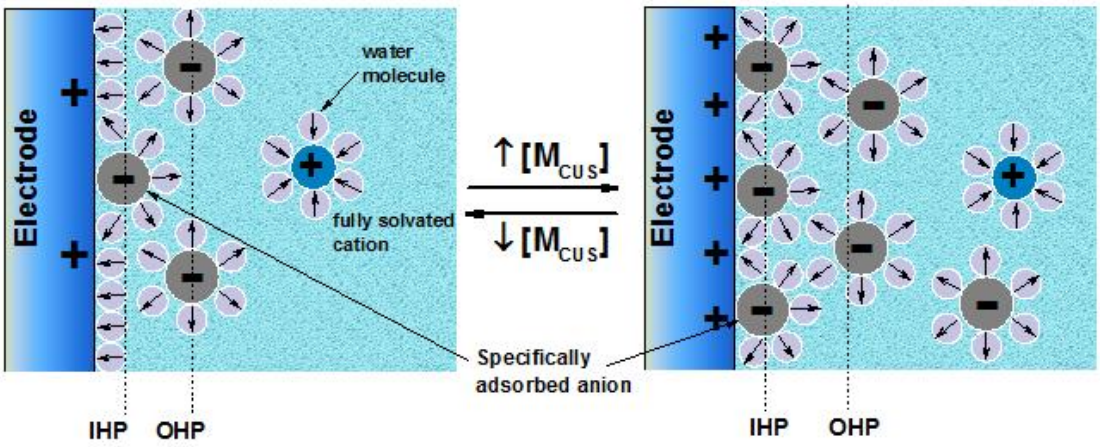

Scheme 5-3. Schematic illustration of surface reactivity determined surface coverage of intermediates.

The coverage of intermediates in electrocatalysis can be decoupled from the adsorption associated capacitance by quantitatively resolving electrochemical impedance spectroscopy (EIS)[94]. The electrical equivalent circuit is shown in Figure 5-2 and the basic relations used in calculation the coverage of intermediates are equation 5-2 and 5-3.

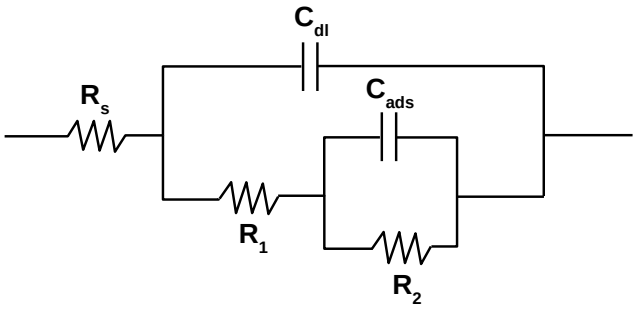

Figure 5-2. Electrical equivalent circuit (EEC) for characterization of intermediates adsorption. R_s refers to the series resistance in the circuit. C_{dl} and C_{ads} are the capacitance from double layer and intermediates adsorption, respectively, whereas the physical significance of R_1 and R_2 are still under debate but with a general viewpoint that overall charge transfer resistance $R_{ct} = R_1 + R_2$[12]. To account for the deviation of capacitance from ideal capacitive behavior, constant

phase elements are adopted in the specific fitting to replace pure capacitors in the equivalent circuit.

$$C_{\text{ads}}(E) = q\,(^{d\theta(E)}/_{dE}) \tag{5-2}$$

$$\theta(E) = \frac{1}{\sigma}\int_{E0}^{E} C_{ads}(E)dE \tag{5-3}$$

This method is quite powerful in evaluating surface reactivity and continuously help my research in electrocatalysis. It has been continuously used in our group as an important characterization method of surface reactivity at working conditions of catalysts. For example, it has also been adopted as a fundamental analysis method in revealing the underneath mechanism of adsorption energy difference in modified carbon based electrocatalysts[113]. Since the adsorption associated capacitance can also be analyzed from CV curves, recently we are developing this method into CV based analysis, which shows excellent consistence of surface reactivity for transition metals and TMOs.

5.4 A new kinetic model for quantitatively resolving elementary surface thermodynamics for catalyst design

The increasing pressure from energy and environment forces human being to search for clean and renewable energy technologies such as water splitting and fuel cells. However, the efficiency of these technologies is primarily limited by oxygen electrocatalysis, including oxygen evolution (OER) and reduction reaction (ORR), due to slow kinetics. To rationally design/develop better catalysts, it is essential to identify and control the elementary surface thermodynamics as it determines catalytic activity (Sabatier principle). Both tasks are highly challenging due to the intrinsic sophistication of electrified solid-liquid interface in electrocatalysis. Therefore, rationally design a catalyst to meet for the practical demand is still very challenging. Previously, we reported a general strategy to rationally control surface

thermodynamics of OER on transition metal oxides through surface structure engineering[21]. Here for the first time, we manage to develop a method to quantitatively resolve elementary surface thermodynamics for the catalyst design.

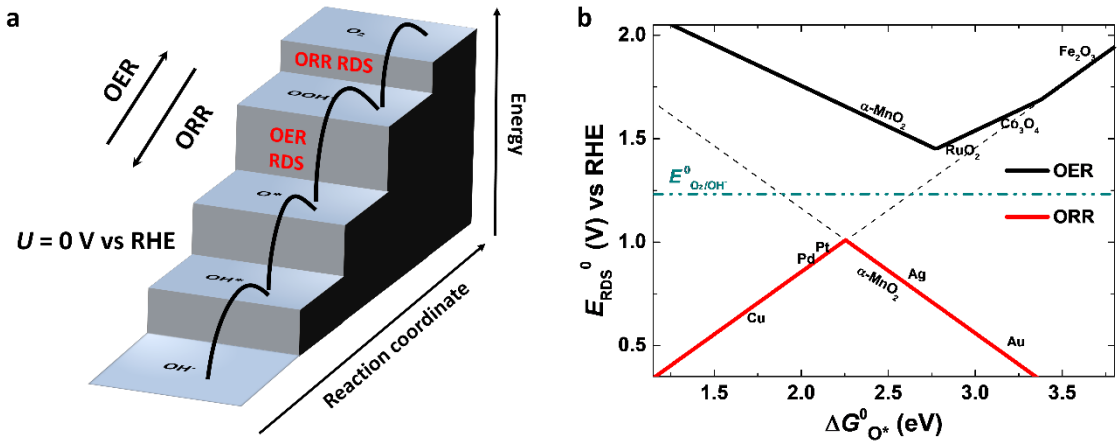

Figure 5-3. (a) Schematic illustration of the elementary steps involved in oxygen electrocatalysis and **(b)** the activity volcano plots (activity map). For the first time, we describe the activity trends of OER and ORR in a same activity map. The intrinsic relation between OER and ORR is clearly addressed, that is, the rate-determing step (RDS) in OER is the fastest step in ORR and vice versa. To rationally design a better catalyst based on a material, the elementary surface thermodynamics should be quantitatively resolved as shown in **(a)**. Then, direction to improve activity can be derived from its location in activity map in **(b)**.

By combining the latest conceptual outcomes from different approaches, here we present a general and quantitative description of the oxygen electrocatalytic kinetics based on the elementary thermodynamic origin, the binding energies of intermediates on catalysts surface. Our model describes experimental kinetics very well and gives a clear interpretation of mutual relation between OER and ORR. One primary difference of our kinetic model from the traditional kinetic model is that our model is based on surface thermodynamics of elementary steps and thus offers predictive power in catalyst design. Therefore, our model for the first time

provides a methodology to quantitatively identify elementary surface thermodynamics from electrochemical kinetics. Based on the identified elementary surface thermodynamic information, we will be able to predict how to improve kinetics of an arbitrary catalyst, which is demonstrated using α-MnO_2 as an example to rationally develop better catalysts in both OER and ORR.

To facilitate the use of our model in catalyst design by other researchers, we are now developing a user friendly online App that integrates the detailed calculations. The first version will be published for free upon the publish of this work. As for the copyright, users will be required to cite this work in their publications that use the online APP as an analysis tool. With the assistance of the online App, we hope more researchers will benefit from our model in developing more efficient catalysts.

5.5 Origin of inconsistence between exchange current density with activity in oxygen electrocatalysis

Exchange current density has been used to represent activity in hydrogen electrocatalysis. However, in oxygen electrocatalysis, including both oxygen evolution reaction (OER) and oxygen reduction reaction (ORR), exchange current density usually does not correlate with catalytic activity. Here we present a detailed study on this issue to identify the origin of the anomalistic phenomena. Through comparison with kinetic behaviour of hydrogen electrocatalysis we prove that kinetics of oxygen electrocatalysis and other highly irreversible reactions are predominantly dependent on Tafel slope, instead of exchange current density. Low Tafel slope of good catalysts originates from the collective contribution from RDS and pre-adsorbed intermediates prior to RDS, which also causes orders decrease in exchange current density predicted from Tafel plots.

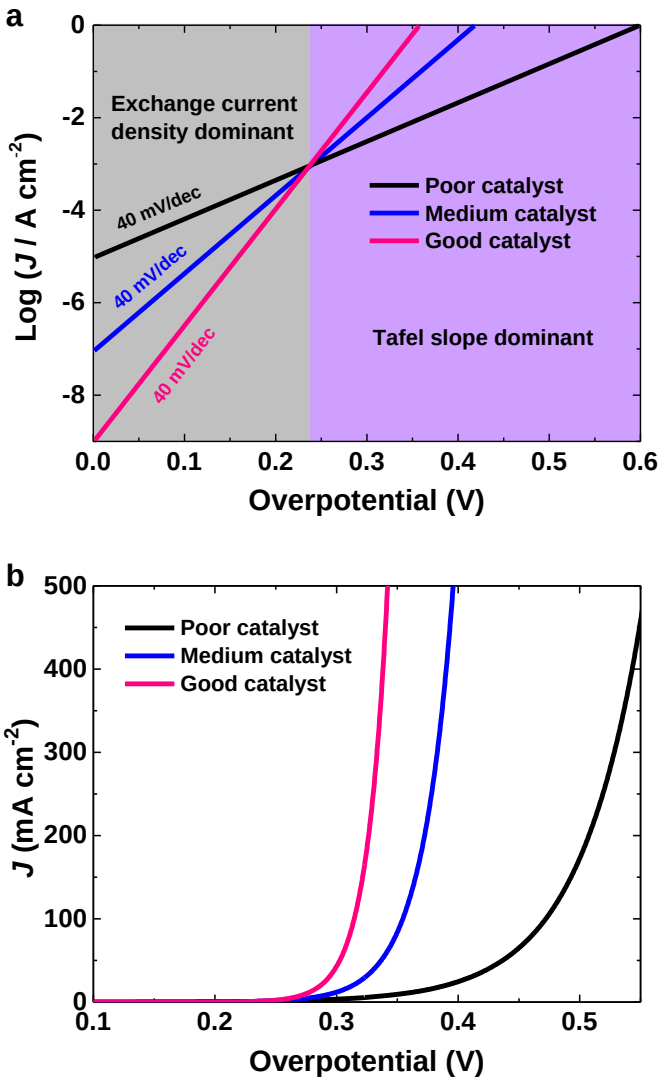

Figure 5-4. Mathematical analysis of the overpotential contribution from exchange current density and Tafel slope. (a) Simulated Tafel plots and (b) Simulated LSV curves for the three typical catalysts with different exchange current density and Tafel slope. Mass transport influence has not been taken into consideration in the kinetic simulation as it has same influence on three kinds of catalysts.

References

1 Tripković, A. V. *et al.* Methanol electrooxidation on supported Pt and PtRu catalysts in acid and alkaline solutions. *Electrochim. Acta* **47**, 3707-3714, (2002).

2 Honkala, K. *et al.* Ammonia Synthesis from First-Principles Calculations. *Science* **307**, 555-558, doi:10.1126/science.1106435 (2005).

3 Freund, H. J., Meijer, G., Scheffler, M., Schlögl, R. & Wolf, M. CO oxidation as a prototypical reaction for heterogeneous processes. *Angew. Chem. Int. Ed.* **50**, 10064-10094 (2011).

4 Somorjai, G. A. & Li, Y. *Introduction to surface chemistry and catalysis*. 5-30 (John Wiley & Sons, 2010).

5 Nørskov, J. K., Abild-Pedersen, F., Studt, F. & Bligaard, T. Density functional theory in surface chemistry and catalysis. *Proc. Natl Acad. Sci. USA* **108**, 937-943, doi:10.1073/pnas.1006652108 (2011).

6 Katsounaros, I., Cherevko, S., Zeradjanin, A. R. & Mayrhofer, K. J. J. Oxygen Electrochemistry as a Cornerstone for Sustainable Energy Conversion. *Angew. Chem. Int. Ed.* **53**, 102-121, doi:10.1002/anie.201306588 (2014).

7 Jens, K., Studt, F., Abild-Pedersen, F. & Bligaard, T. *Fundamental concepts in heterogeneous catalysis*. 4 (John Wiley & Sons, 2014).

8 Man, I. C. *et al.* Universality in Oxygen Evolution Electrocatalysis on Oxide Surfaces. *ChemCatChem* **3**, 1159-1165 (2011).

9 Rossmeisl, J., Qu, Z. W., Zhu, H., Kroes, G. J. & Nørskov, J. K. Electrolysis of water on oxide surfaces. *J. Electroanal. Chem.* **607**, 83-89 (2007).

10 Hong, W. T. *et al.* Toward the rational design of non-precious transition metal oxides for oxygen electrocatalysis. *Energy Environ. Sci.*, doi:10.1039/C4EE03869J (2015).

11 O'Brien, T. F., Bommaraju, T. V. & Hine, F. *Handbook of Chlor-Alkali Technology: Volume I: Fundamentals, Volume II: Brine Treatment and Cell Operation, Volume III: Facility Design and Product Handling, Volume IV: Operations, Volume V: Corrosion, Environmental Issues, and Future Developments*. Vol. 1 (Springer Science & Business Media, 2007).

12 Nørskov, J. K. *et al.* Origin of the Overpotential for Oxygen Reduction at a Fuel-Cell Cathode. *The Journal of Physical Chemistry B* **108**, 17886-17892, doi:10.1021/jp047349j (2004).

13 McNaught, A. D. & McNaught, A. D. *Compendium of chemical terminology*. Vol. 1669 (Blackwell Science Oxford, 1997).

14 Trasatti, S. Adsorption—volcano curve. *Handbook of fuel cells* (2003).

15 Yates, J. T. & Campbell, C. T. (National Acad Sciences, 2011).

16 Schmidt, T. J., Ross Jr, P. N. & Markovic, N. M. Temperature dependent surface electrochemistry on Pt single crystals in alkaline electrolytes: Part 2. The hydrogen evolution/oxidation reaction. *J. Electroanal. Chem.* **524–525**, 252-260, (2002).

17 Lopes, P. P. *et al.* Relationships between Atomic Level Surface Structure and Stability/Activity of Platinum Surface Atoms in Aqueous Environments. *ACS Catalysis* **6**, 2536-2544, doi:10.1021/acscatal.5b02920 (2016).

18 Metiu, H., Chrétien, S., Hu, Z., Li, B. & Sun, X. Chemistry of Lewis Acid–Base Pairs on Oxide Surfaces. *J. Phys. Chem. C* **116**, 10439-10450, doi:10.1021/jp301341t (2012).

19 Ertl, G. in *Reactions at Solid Surfaces* 1-17 (John Wiley & Sons, Inc., 2010).

20 Bligaard, T. & Nørskov, J. K. in *Chemical Bonding at Surfaces and Interfaces* (ed A. Nilsson, Pettersson, L. G. M. & Nørskov, J. K.) 257-275 (Elsevier, 2008).

21 Tao, H. B. *et al.* Identification of Surface Reactivity Descriptor for Transition Metal Oxides in Oxygen Evolution Reaction. *J. Am. Chem. Soc.* **138**, 9978-9985, doi:10.1021/jacs.6b05398 (2016).

22 Ertl, G., Knözinger, H., Schüth, F. & Weitkamp, J. *Handbook of heterogeneous catalysis: 8 volumes*. Vol. 3 1271-1273 (wiley-vch, 2008).

23 Ertl, G. in *Reactions at Solid Surfaces* 105-109 (John Wiley & Sons, Inc., 2010).

24 Medford, A. J. *et al.* From the Sabatier principle to a predictive theory of transition-metal heterogeneous catalysis. *J. Catal.* **328**, 36-42, (2015).

25 Trasatti, S. Electrocatalysis by oxides — Attempt at a unifying approach. *J. Electroanal. Chem. Interfacial Electrochem.* **111**, 125-131 (1980).

26 Ertl, G., Knözinger, H. & Weitkamp, J. Handbook of heterogeneous catalysis. 960 (1997).

27 Jaramillo, T. F. *et al.* Identification of active edge sites for electrochemical H2 evolution from MoS2 nanocatalysts. *science* **317**, 100-102 (2007).

28 Malko, D., Kucernak, A. & Lopes, T. In situ electrochemical quantification of active sites in Fe–N/C non-precious metal catalysts. *Nature Communications* **7**, 13285, doi:10.1038/ncomms13285

(2016).

29 Friebel, D. *et al.* Identification of Highly Active Fe Sites in (Ni,Fe)OOH for Electrocatalytic Water Splitting. *J. Am. Chem. Soc.* **137**, 1305-1313, doi:10.1021/ja511559d (2015).

30 Schaub, R. *et al.* Oxygen vacancies as active sites for water dissociation on rutile TiO 2 (110). *Phys. Rev. Lett.* **87**, 266104 (2001).

31 Haber, F. Nobel Prize Lecture 1918. *Nobel Lectures, Chemistry 1901-1921* (1901).

32 Bosch, F. Nobel Prize Lecture 1931. *Nobel Lectures, Chemistry 1922-1941* (1922).

33 Logadóttir, Á. & Nørskov, J. K. Ammonia synthesis over a Ru(0001) surface studied by density functional calculations. *J. Catal.* **220**, 273-279, (2003).

34 Ertl, G. in *Reactions at Solid Surfaces* 21-22 (John Wiley & Sons, Inc., 2010).

35 Nilsson, A. *et al.* The electronic structure effect in heterogeneous catalysis. *Catal. Lett.* **100**, 111-114, doi:10.1007/s10562-004-3434-9 (2005).

36 Besenbacher, F. *et al.* Design of a Surface Alloy Catalyst for Steam Reforming. *Science* **279**, 1913-1915, doi:10.1126/science.279.5358.1913 (1998).

37 Stamenkovic, V. R. *et al.* Improved Oxygen Reduction Activity on Pt₃Ni(111) via Increased Surface Site Availability. *Science* **315**, 493-497, doi:10.1126/science.1135941 (2007).

38 Subbaraman, R. *et al.* Enhancing Hydrogen Evolution Activity in Water Splitting by Tailoring Li+-Ni(OH)2-Pt Interfaces. *Science* **334**, 1256-1260, doi:10.1126/science.1211934 (2011).

39 Stamenkovic, V. R. *et al.* Trends in electrocatalysis on extended and nanoscale Pt-bimetallic alloy surfaces. *Nat Mater* **6**, 241-247, (2007).

40 Bard, A. J. & Fox, M. A. Artificial photosynthesis: solar splitting of water to hydrogen and oxygen. *Acc. Chem. Res.* **28**, 141-145 (1995).

41 Weber, M. F. & Dignam, M. J. Efficiency of splitting water with semiconducting photoelectrodes. *J. Electrochem. Soc.* **131**, 1258-1265 (1984).

42 Karlsson, R. K. B. & Cornell, A. Selectivity between Oxygen and Chlorine Evolution in the Chlor-Alkali and Chlorate Processes. *Chem. Rev.* **116**, 2982-3028, doi:10.1021/acs.chemrev.5b00389 (2016).

43 Koper, M. T. M. Thermodynamic theory of multi-electron transfer reactions: Implications for electrocatalysis. *J. Electroanal. Chem.* **660**, 254-260 (2011).

44 Hammer, B. & Norskov, J. Why gold is the noblest of all the metals. *Nature* **376**, 238-240 (1995).

45 Greeley J. *et al.* Alloys of platinum and early transition metals as oxygen reduction electrocatalysts. *Nature Chem.* **1**, 552-556, (2009).

46 Calle-Vallejo, F. *et al.* Number of outer electrons as descriptor for adsorption processes on transition metals and their oxides. *Chem. Sci.* **4**, 1245-1249, doi:10.1039/C2SC21601A (2013).

47 Cox, P. *The surface science of metal oxides*. 1-7, 158-200, and 264-266 (Cambridge university press, 1996).

48 Suntivich, J. *et al.* Design principles for oxygen-reduction activity on perovskite oxide catalysts for fuel cells and metal–air batteries. *Nature Chem.* **3**, 546-550, (2011).

49 Suntivich, J., May, K. J., Gasteiger, H. A., Goodenough, J. B. & Shao-Horn, Y. A perovskite oxide optimized for oxygen evolution catalysis from molecular orbital principles. *Science* **334**, 1383-1385 (2011).

50 García-Mota, M., Vojvodic, A., Abild-Pedersen, F. & Nørskov, J. K. Electronic Origin of the Surface Reactivity of Transition-Metal-Doped TiO2(110). *J. Phys. Chem. C* **117**, 460-465, doi:10.1021/jp310667r (2012).

51 Xu, Z. & Kitchin, J. R. Relationships between the surface electronic and chemical properties of doped 4d and 5d late transition metal dioxides. *The Journal of Chemical Physics* **142**, 104703, (2015).

52 Liu, B. & Aydil, E. S. Growth of Oriented Single-Crystalline Rutile TiO2 Nanorods on Transparent Conducting Substrates for Dye-Sensitized Solar Cells. *J. Am. Chem. Soc.* **131**, 3985-3990, doi:10.1021/ja8078972 (2009).

53 Chen, H. M., Liu, R. S., Li, H. & Zeng, H. C. Generating Isotropic Superparamagnetic Interconnectivity for the Two-Dimensional Organization of Nanostructured Building Blocks. *Angew. Chem. Int. Ed.* **45**, 2713-2717 (2006).

54 Liu, X. *et al.* Single crystal α-Fe 2 O 3 with exposed {104} facets for high performance gas sensor applications. *RSC Adv.* **2**, 6178-6184 (2012).

55 Su, D., Ahn, H.-J. & Wang, G. Hydrothermal synthesis of α-MnO 2 and β-MnO 2 nanorods as high capacity cathode materials for sodium ion batteries. *J. Mater. Chem. A* **1**, 4845-4850 (2013).

56 Trotochaud, L., Young, S. L., Ranney, J. K. & Boettcher, S. W. Nickel–Iron Oxyhydroxide Oxygen-Evolution Electrocatalysts: The Role of Intentional and Incidental Iron Incorporation. *J. Am. Chem. Soc.* **136**, 6744-6753, doi:10.1021/ja502379c (2014).

57 Pang, C. L., Lindsay, R. & Thornton, G. Structure of clean and adsorbate-covered single-crystal rutile TiO2 surfaces. *Chem. Rev.* **113**, 3887-3948 (2013).

58 Papageorgiou, A. C. *et al.* Electron traps and their effect on the surface chemistry of TiO2 (110). *Proc. Natl Acad. Sci. USA* **107**, 2391-2396 (2010).

59 Wendt, S. *et al.* The Role of Interstitial Sites in the Ti3d Defect State in the Band Gap of Titania. *Science* **320**, 1755-1759, doi:10.1126/science.1159846 (2008).

60 Krüger, P. *et al.* Defect States at the TiO2(110) Surface Probed by Resonant Photoelectron Diffraction. *Phys. Rev. Lett.* **100**, 055501 (2008).

61 Kowalski, P. M., Camellone, M. F., Nair, N. N., Meyer, B. & Marx, D. Charge Localization Dynamics Induced by Oxygen Vacancies on the ${\mathrm{TiO}}_{2}(110)$ Surface. *Phys. Rev. Lett.* **105**, 146405 (2010).

62 Epling, W. S., Peden, C. H. F., Henderson, M. A. & Diebold, U. Evidence for oxygen adatoms on TiO2(110) resulting from O2 dissociation at vacancy sites. *Surface Science* **412–413**, 333-343, (1998).

63 Lira, E. *et al.* Dissociative and molecular oxygen chemisorption channels on reduced rutile TiO 2 (110): an STM and TPD study. *Surface Science* **604**, 1945-1960 (2010).

64 Deskins, N. A., Rousseau, R. & Dupuis, M. Distribution of Ti3+ Surface Sites in Reduced TiO2. *J. Phys. Chem. C* **115**, 7562-7572, doi:10.1021/jp2001139 (2011).

65 Nørskov, J. K. *et al.* Universality in heterogeneous catalysis. *J. Catal.* **209**, 275-278 (2002).

66 Wang, Y. *et al.* Reduced Mesoporous Co3O4 Nanowires as Efficient Water Oxidation Electrocatalysts and Supercapacitor Electrodes. *Adv. Energy Mater.* **4** (2014).

67 Tung, C.-W. *et al.* Reversible adapting layer produces robust single-crystal electrocatalyst for oxygen evolution. *Nature Commun.* **6**, doi:10.1038/ncomms9106 (2015).

68 Somorjai, G. A. *Introduction to surface chemistry and catalysis*. 303 (John Wiley & Sons, 1994).

69 García-Mota, M. *et al.* Tailoring the Activity for Oxygen Evolution Electrocatalysis on Rutile TiO2 (110) by Transition-Metal Substitution. *ChemCatChem* **3**, 1607-1611 (2011).

70 Sánchez-Sánchez, C. *et al.* Valence band electronic structure characterization of the rutile TiO2 (110)-(1 × 2) reconstructed surface. *Surface Science* **608**, 92-96, (2013).

71 Zhang, W. *et al.* Electronic structures of bare and terephthalic acid adsorbed TiO2(110)-(1 [times] 2) reconstructed surfaces: origin and reactivity of the band gap states. *Phys. Chem. Chem. Phys.* **17**, 20144-20153, doi:10.1039/C5CP01298H (2015).

72 Zhang, Z. & Henrich, V. E. Surface electronic structure of V2O5(001): defect states and chemisorption. *Surface Science* **321**, 133-144, (1994).

73 Ghijsen, J. *et al.* Electronic structure of ${\mathrm{Cu}}_{2}$O and CuO. *Physical Review B* **38**, 11322-11330 (1988).

74 Xu, Z. & Kitchin, J. R. Relating the electronic structure and reactivity of the 3d transition metal monoxide surfaces. *Catal. Commun.* **52**, 60-64, (2014).

75 Cheng, F. *et al.* Enhancing Electrocatalytic Oxygen Reduction on MnO2 with Vacancies. *Angew. Chem. Int. Ed.* **52**, 2474-2477, doi:10.1002/anie.201208582 (2013).

76 Kotsev, N. K. & Ilieva, L. I. Determination of non-stoichiometric oxygen in NiO by temperature-programmed reduction. *Catal. Lett.* **18**, 173-176 (1993).

77 Greiner, M. T. *et al.* Universal energy-level alignment of molecules on metal oxides. *Nat Mater* **11**, 76-81, (2012).

78 Seh, Z. W. *et al.* Combining theory and experiment in electrocatalysis: Insights into materials design. *Science* **355**, doi:10.1126/science.aad4998 (2017).

79 Wieckowski, A. & Neurock, M. Contrast and Synergy between Electrocatalysis and Heterogeneous Catalysis. *Advances in Physical Chemistry* **2011**, 18, doi:10.1155/2011/907129 (2011).

80 Conway, B. E. & Tilak, B. V. Behavior and Characterization of Kinetically Involved Chemisorbed Intermediates in Electrocatalysis of Gas Evolution Reactions. *Advances in Catalysis* **38**, 1-147, (1992).

81 Zhang, J., Sasaki, K., Sutter, E. & Adzic, R. R. Stabilization of Platinum Oxygen-Reduction Electrocatalysts Using Gold Clusters. *Science* **315**, 220-222, doi:10.1126/science.1134569 (2007).

82 Shao, M. H. & Adzic, R. R. Spectroscopic Identification of the Reaction Intermediates in Oxygen Reduction on Gold in Alkaline Solutions. *The Journal of Physical Chemistry B* **109**, 16563-16566, doi:10.1021/jp053450s (2005).

83 Skúlason, E. *et al.* Density functional theory calculations for the hydrogen evolution reaction in an electrochemical double layer on the Pt(111) electrode. *Phys. Chem. Chem. Phys.* **9**, 3241-3250 (2007).

84 Bligaard, T. *et al.* The Brønsted–Evans–Polanyi relation and the volcano curve in heterogeneous catalysis. *J. Catal.* **224**, 206-217, (2004).

85 Strmcnik, D. *et al.* Improving the hydrogen oxidation reaction rate by promotion of hydroxyl adsorption. *Nature Chem.* **5**, 300-306, (2013).

86 Kunimatsu, K., Senzaki, T., Tsushima, M. & Osawa, M. A combined surface-enhanced infrared and electrochemical kinetics study of hydrogen adsorption and evolution on a Pt electrode. *Chemical Physics Letters* **401**, 451-454, (2005).

87 Cruz, J. *et al.* Preparation and characterization of RuO2 catalysts for oxygen evolution in a solid polymer electrolyte. *Int J Electrochem Sci* **6**, 660 (2011).

88 Subbaraman, R. *et al.* Origin of Anomalous Activities for Electrocatalysts in Alkaline Electrolytes. *J. Phys. Chem. C* **116**, 22231-22237, doi:10.1021/jp3075783 (2012).

89 Chen, R. *et al.* Use of Platinum as the Counter Electrode to Study the Activity of Nonprecious Metal Catalysts for the Hydrogen Evolution Reaction. *ACS Energy Letters*, 1070-1075, doi:10.1021/acsenergylett.7b00219 (2017).

90 Davis, R. E., Horvath, G. L. & Tobias, C. W. The solubility and diffusion coefficient of oxygen in potassium hydroxide solutions. *Electrochim. Acta* **12**, 287-297, (1967).

91 Stamenkovic, V. R., Strmcnik, D., Lopes, P. P. & Markovic, N. M. Energy and fuels from electrochemical interfaces. *Nat Mater* **16**, 57-69, doi:10.1038/nmat4738 (2017).

92 Garcia-Mota, M. *et al.* Importance of correlation in determining electrocatalytic oxygen evolution activity on cobalt oxides. *J. Phys. Chem. C* **116**, 21077-21082 (2012).

93 Bard, A. J. & Faulkner, L. R. *Electrochemical methods: fundamentals and applications*. 91-115 (John Wiley & Sons, Inc, 2001).

94 Gileadi, E. & Conway, B. E. Kinetic Theory of Adsorption of Intermediates in Electrochemical Catalysis. *The Journal of Chemical Physics* **39**, 3420-3430, (1963).

95 Surendranath, Y. & Nocera, D. G. Oxygen Evolution Reaction Chemistry of Oxide-Based Electrodes. *Progress in Inorganic Chemistry, Volume 57*, 505-560 (2011).

96 Doyle, R. L. & Lyons, M. E. G. in *Photoelectrochemical Solar Fuel Production: From Basic Principles to Advanced Devices* (eds Sixto Giménez & Juan Bisquert) 54-58 and 64-65 (Springer International Publishing, 2016).

97 Surendranath, Y. & Nocera, D. G. Oxygen Evolution Reaction Chemistry of Oxide-Based Electrodes. *Progress in Inorganic Chemistry, Volume 57*, 533-540 (2011).

98 Koper, M. T. Analysis of electrocatalytic reaction schemes: distinction between rate-determining and potential-determining steps. *J Solid State Electr* **17**, 339-344 (2013).

99 van der Vliet, D. *et al.* On the importance of correcting for the uncompensated Ohmic resistance in model experiments of the Oxygen Reduction Reaction. *J. Electroanal. Chem.* **647**, 29-34, (2010).

100 Paulus, U. A., Schmidt, T. J., Gasteiger, H. A. & Behm, R. J. Oxygen reduction on a high-surface area Pt/Vulcan carbon catalyst: a thin-film rotating ring-disk electrode study. *J. Electroanal. Chem.* **495**, 134-145, (2001).

101 Pizzutilo, E. *et al.* Palladium electrodissolution from model surfaces and nanoparticles. *Electrochim. Acta* **229**, 467-477, (2017).

102 Hu, J. *et al.* Increasing Stability and Activity of Core–Shell Catalysts by Preferential Segregation of Oxide on Edges and Vertexes: Oxygen Reduction on Ti–Au@Pt/C. *J. Am. Chem. Soc.* **138**, 9294-9300, doi:10.1021/jacs.6b04999 (2016).

103 Gómez, E. d. V., Amaya-Roncancio, S., Avalle, L. B., Linares, D. H. & Gimenez, M. C. DFT study of adsorption and diffusion of atomic hydrogen on metal surfaces. *Appl. Surf. Sci.* **420**, 1-8, (2017).

104 Huang, B., Xiao, L., Lu, J. & Zhuang, L. Spatially Resolved Quantification of the Surface Reactivity of Solid Catalysts. *Angew. Chem.* **128**, 6347-6351 (2016).

105 Pronkin, S. N., Bonnefont, A., Ruvinskiy, P. S. & Savinova, E. R. Hydrogen oxidation kinetics on model Pd/C electrodes: Electrochemical impedance spectroscopy and rotating disk electrode study. *Electrochim. Acta* **55**, 3312-3323, (2010).

106 Yeo, B. S. & Bell, A. T. In situ Raman study of nickel oxide and gold-supported nickel oxide catalysts for the electrochemical evolution of oxygen. *J. Phys. Chem. C* **116**, 8394-8400 (2012).

107 Lyons, M. E. & Brandon, M. P. The oxygen evolution reaction on passive oxide covered transition metal electrodes in aqueous alkaline solution. Part 1-Nickel. *Int. J. Electrochem. Sci* **3**, 1386-1424 (2008).

108 Walter, M. G. *et al.* Solar Water Splitting Cells. *Chem. Rev.* **110**, 6446-6473 (2010).

109 Trasatti, S. Work function, electronegativity, and electrochemical behaviour of metals. *J. Electroanal. Chem. Interfacial Electrochem.* **39**, 163-184, (1972).

110 Nørskov, J. K. *et al.* Trends in the exchange current for hydrogen evolution. *J. Electrochem. Soc.* **152**, J23-J26 (2005).

111 Trasatti, S. Electrocatalysis in the anodic evolution of oxygen and chlorine. *Electrochim. Acta* **29**, 1503-1512 (1984).

112 Conway, B. E., Bai, L. & Sattar, M. A. Role of the transfer coefficient in electrocatalysis: Applications to the H2 and O2 evolution reactions and the characterization of participating adsorbed intermediates. *Int J Hydrogen Energ* **12**, 607-621, (1987).

113 Li, L. *et al.* Unraveling Oxygen Evolution Reaction on Carbon-based Electrocatalysts: Effect of Oxygen Doping on Oxygenated Intermediates Adsorption. *ACS Energy Letters* (2017).

Publications

Tao, H. B., Chen, J., Xu, Y., Huang, X. & Liu, B. Quantitative Description of Kinetics of Oxygen Electrocatalysis with Elementary Surface Thermodynamics for Catalyst Design. *in preparation*.

Tao, H. B., Zhang, J., Huang, X. & Liu, B. Origin of inconsistence between exchange current density with activity in oxygen electrocatalysis. *in preparation*.

Tao, H. B. *et al.* Identification of Surface Reactivity Descriptor for Transition Metal Oxides in Oxygen Evolution Reaction. *J. Am. Chem. Soc.* **138**, 9978-9985, (2016).

Tao, H. B., Yang, H. B., Chen, J., Miao, J. & Liu, B. Biomolecule-assisted synthesis of carbon nitride and sulfur-doped carbon nitride heterojunction nanosheets: An efficient heterojunction photocatalyst for photoelectrochemical applications. *Beilstein journal of nanotechnology* **5**, 770-777 (2014).